PhD Thesis / Tesi Doctoral

-

INTRATHECAL ADMINISTRATION OF AAVrh10 CODING FOR β-GLUCURONIDASE CORRECTS BIOCHEMICAL AND HISTOLOGICAL HALLMARKS OF MUCOPOLYSACCHARIDOSIS TYPE VII MICE AND IMPROVES BEHAVIOR AND SURVIVAL

Author / Autora:

Gemma Pagès i Pi

Director / Directora:

Assumpció Bosch Merino

Doctorat en Bioquímica, Biologia Molecular i Biomedicina
Departament de Bioquímica i Biologia Molecular
Universitat Autònoma de Barcelona

2015

CONCLUSIONS

CONCLUSIONS

1. Intravenous administration of AAV9 and AAVrh10 in mice can transduce sensory neurons in DRG but not motor neurons in spinal cord.

2. AAV9 is more efficient than AAVrh10 in transducing brain and liver after intravenous administration in mice.

3. AAV9 raises more IgG than AAVrh10 after intravenous administration in immunologically naïve mice, which correlates to a rise in NAbs.

4. Intrathecal administration of AAVrh10 by lumbar puncture leads to widespread transduction in the brain, mainly infecting neurons but also some astrocytes and oligodendrocytes.

5. In C57BL/6 mice, intrathecal administration of AAVrh10 also transduces cells of brain blood vessels.

6. Intrathecal administration of AAVrh10 achieves transduction of somatic organs after drainage of AAV vector to the bloodstream.

7. Transduction of brain and liver can be achieved by lumbar intrathecal delivery of AAVrh10 with a dose 20 times lower than by intravenous delivery of AAV9 with comparable efficiency.

8. The intrathecal delivery of AAVrh10 coding for β-glucuronidase to MPS VII mice leads to a better outcome when mice are injected at a younger age and after a longer treatment duration.

9. A dose of 8.75×10^{11} vg/kg of AAVrh10-GUSB administered intrathecally to 8-week-old MPS VII mice can transduce the CNS and somatic organs of MPS VII mice and attain β-glucuronidase activity levels that provide therapeutic benefit.

10. The therapeutic benefit of intrathecal AAVrh10-GUSB delivery is evidenced by the decrease and even normalization of the pathological biochemical hallmarks of the disease of MPS VII mice in the CNS and somatic organs. These include LAMP-1 accumulation, lysosomal vesicle enlargement, astrogliosis and secondary elevation of lysosomal enzymatic activity.

11. In brain, there is a correlation trend between the level of β-glucuronidase activity and the biochemical correction attained.

12. The improvement of the physical, cognitive and emotional characteristics of MPS VII mice provided by the treatment allowed a general improvement in the mouse ethogram and a gain of function in their ability to swim.

13. Intrathecal AAVrh10-GUSB treatment attained a 105% increase in MPS VII mice life span, from median survival of 4.2 months to 8.6 months.

MATERIALS AND METHODS

MATERIALS AND METHODS

1. MATERIALS

1.1. VIRAL VECTORS

The AAV vectors used in this work were produced by the Viral Vector Production Unit (UPV) of the *Centre de Biotecnologia Animal i Teràpia Gènica* in the *Universitat Autònoma de Barcelona* (*sct.uab.cat/upv*), following standard operating procedures (Zolotukhin et al. (1999)).

The AAV vectors were produced by triple transfection with the following plasmids:

1. **pXX6:** the plasmid that contains the adenoviral genes required for AAV replication.
2. **rep2capX**: this plasmid contains the *rep* gene of AAV2 and the *cap* gene of the desired serotype. We used the plasmids rep2cap9 and rep2cap10, kindly provided by James Wilson at University of Pennsylvania, Philadelphia, USA.
3. The plasmid with the **expression cassette** flanked by the **ITR** sequences of AAV2.

The different AAV vectors produced are not strictly serotypes but pseudotypes, because the ITR and the *rep* sequences are from the AAV serotype 2, while the *cap* sequence is from a different AAV serotype. However, since the tropism depends on the capsid proteins, this does not influence the characteristics of the vector.

Briefly, the production procedure consists in a triple transfection of HEK293 cells, using polyethileneimine as the transfection reagent. After 48 hours, the cellular pellet and the cell culture medium are separated by centrifugation. Both samples are used to isolate the AAV particles produced. The subsequent purification steps are freeze-thaw cycles to lyse the cells, centrifugation to eliminate cellular debris, and the addition of polyethylene glycol to favor the precipitation of AAV particles. Then, AAV vector particles are purified by ultracentrifugation in an iodixanol gradient (based on Zolotukhin et al. (1999)). The titration of the viral vector preps is performed using Quant-iT™ PicoGreen® dsDNA Assay Kit (Life Technologies, Carlsbad, CA, USA), an

intercalating agent that allows the vector DNA quantification by fluorescence detection (Piedra et al. (2015)).

Table 7 shows the characteristics of the expression cassettes of the vectors used, as well as the quantifications, in viral genomes (vg) per ml, of the vector preparations used in this work.

Table 7: AAV vector stocks used in this work

vector name	promoter	transgene	post-transcriptional regulatory element	stock titration (vg/ml)
AAV9-GFP	CAG*	GFP	WPRE**	1.12×10^{12}
AAVrh10-GFP	CAG	GFP	WPRE	Different stocks. Range: 4.2×10^{12} - 1.6×10^{13}
AAVrh10-GUSB	CAG	GUSB	-	3.50×10^{12}
AAVrh10-mock	CAG	-	WPRE	1.70×10^{12}
AAV9-Luciferase	CMV	Luciferase	-	5.03×10^{12}
AAVrh10-Luciferase	CMV	Luciferase	-	4.33×10^{12}

***CAG** is a synthetic promoter with strong and ubiquitous expression in mammalian cells constructed using the cytomegalovirus (CMV) early enhancer element, the promoter and the first exon and intron of the chicken β-actin gene, and the splice acceptor of the rabbit β-globin gene (Miyazaki et al. (1989)).

****WPRE** is a sequence placed in cis at 3' of the transgene in AAV vector constructs. When it is transcribed, WPRE sequence enhances the expression of the transgene (Loeb et al. (1999)). The GUSB cassette (Bosch et al. (2000)) does not contain this sequence because the expression cassette would be larger than what is recommended for efficient encapsidation of AAV vectors.

1.2. MICE

All the mice used in this work were bred in the SPF animal facility of the CBATEG in the *Universitat Autònoma de Barcelona,* with the exception of the mice used for intravenous injection, which were bred in the *Servei d'Estabulari* of the *Universitat Autònoma de Barcelona.* In both cases, mice were fed *ad libitum* with a standard diet (2018S Teklad Global; Harlan Laboratories Inc., Indianapolis, IN, USA) and kept under temperature and light controlled conditions (12 h light and 12 h dark).

In the first part of the work, we used two different standard mouse strains: ICR (CD-1®) Outbred Mice and C57BL/6 Inbred Mice. In the second part of the work, we used a MPS VII mouse model tolerant to human β-glucuronidase (Sly et al. (2001)), with a C57BL/6 genetic background. Heterozygote MPS VII mice were kindly provided by

Dr. William S. Sly (St. Louis University School of Medicine, St. Louis, MO, USA). Heterozygote mice were bred in the CBATEG SPF animal facility. At 1 month of age, weaning and mouse identification were performed. Using a tail clip homogenate, β-glucuronidase activity was analyzed in order to identify the mice as mutant (MPS VII), heterozygote (HTZ) or wild type (WT). The procedure for β-glucuronidase activity quantification is explained later on in this work.

1.3. ANTIBODIES AND COUNTERSTAINING REAGENTS

Antibodies were used as specific detection reagents in different experiments of this work. **Table 8** specifies all the different antibodies used, and also two counterstaining reagents used in immunofluorescence staining.

1.4. BUFFER SOLUTIONS

The following standard buffer solutions were used in different techniques. Unless specified, all reagents purchased to Panreac, Castellar del Vallès, Barcelona, Spain.

Phosphate buffer: 0.1 M phosphate buffer pH 7.4, prepared by equilibration of NaH_2PO_4 and Na_2HPO_4. For 100 ml of phosphate buffer we used 2.565 g of $NaH_2PO_4 \cdot 1\ H_2O$ and 13.502 g of $Na_2HPO_4 \cdot 2\ H_2O$.
Carbonate buffer: 0.1 M carbonate buffer pH 9.2, prepared by mixing 1 volume of Na_2CO_3 0.1 M and 9 volumes of $NaHCO_3$ 0.1 M.
D-PBS (Dulbecco's Phosphate Buffer Saline) pH 7.4: 137 mM NaCl, 3 mM KCl, 10 mM Na_2HPO_4 and 1.7 mM KH_2PO_4. Adjust pH using HCl 37%.
50 mM Tris-HCl pH 7.4: 50mM Trizma® base (Sigma-Aldrich, St. Louis, MO, USA). Adjust pH using HCl 37%.

1.5. IMAGING EQUIPMENT

Magnification with zoom stereomicroscope: Nikon SMZ800 zoom stereomicroscope with Nikon Coolpix 5400 camera (Nikon Corp., Tokyo, Japan).
Bright-field and epifluorescence microscopy: Nikon Eclipse E-800 microscope with Nikon Digital Camera DXM 1200F and ACT-1 software package.
Confocal microscopy: Leica TCS-SP2 AOBS (Leica Microsystems GmbH, Heidelberg, Germany).

Table 8: Antibodies and counterstaining reagents

WESTERN BLOT			
PRIMARY ANTIBODIES	**name**	**comercial**	**dilution**
LAMP-1 (90 kDa)	Monoclonal Rat anti-mouse CS107a (clone 1D4B)	BD Pharmingen, BD Biosciences, San Jose, CA, USA	1:4000
GFAP (52 kDa)	Monoclonal Mouse anti-GFAP (clone G-A-5)	Sigma-Aldrich, St. Louis, MO, USA	1:500
Tubulin (48 kDa)	Monoclonal Mouse anti-gamma-tubulin (clone GTU-88)	Sigma-Aldrich, St. Louis, MO, USA	1:5000
Actin (42 kDa)	Polyclonal Rabbit anti-actin	Sigma-Aldrich, St. Louis, MO, USA	1:1000
SECONDARY ANTIBODIES			
anti-rat HRP	Polyclonal Sheep anti-Rat IgG, HRP conjugated	LifeSpan Biosciences, Seattle, WA, USA	1:10000
anti-mouse HRP	Polyclonal Sheep anti-Mouse IgG, HRP conjugated	GE Healthcare, Waukesha, WI, USA	1:10000
anti-rabbit HRP	Polyclonal Swine anti-Rabbit IgG, HRP conjugated	Dako, Agilent Technologies, Glostrup, Denmark	1:10000
IMMUNOFLUORESCENCE			
PRIMARY ANTIBODIES	**name**	**comercial**	**dilution**
NeuN	Monoclonal Mouse anti-NeuN (clone A60)	Merck-Millipore, Merck KGaA, Darmstadt, Germany	1:200
GFAP	Polyclonal Rabbit anti-GFAP	Dako, Agilent Technologies, Glostrup, Denmark	1:500
APC	Monoclonal Mouse anti-APC (Ab7) (clone CC-1)	Merck-Millipore, Merck KGaA, Darmstadt, Germany	1:400
Collagen IV	Polyclonal Rabbit anti-collagen type IV	Merck-Millipore, Merck KGaA, Darmstadt, Germany	1:200
LAMP-1	Monoclonal Rat anti-mouse CS107a (clone 1D4B)	BD Pharmingen, BD Biosciences, San Jose, CA, USA	1:100
SECONDARY ANTIBODIES			
anti-mouse 568	Alexa Fluor® 568 Goat anti-Mouse IgG (H+L) Antibody	Molecular Probes, Life Technologies, Carlsbad, CA, USA	1:200
anti-rabbit 405	Alexa Fluor® 405 Goat anti-Rabbit IgG (H+L) Antibody	Molecular Probes, Life Technologies, Carlsbad, CA, USA	1:200
anti-rabbit 488	Alexa Fluor® 488 Goat anti-Rabbit IgG (H+L) Antibody	Molecular Probes, Life Technologies, Carlsbad, CA, USA	1:200
anti-rabbit 568	Alexa Fluor® 568 Goat anti-Rabbit IgG (H+L) Antibody	Molecular Probes, Life Technologies, Carlsbad, CA, USA	1:200
anti-rat 488	Alexa Fluor® 488 Goat anti-Rat IgG (H+L) Antibody	Molecular Probes, Life Technologies, Carlsbad, CA, USA	1:200
COUNTERSTAINING REAGENTS			
Hoechst	Hoechst Stain Solution	Sigma-Aldrich, St. Louis, MO, USA	1:1
Nissl	NeuroTrace® 530/615 Red Fluorescent Nissl Stain	Molecular Probes, Life Technologies, Carlsbad, CA, USA	1:150
ELISA			
REAGENTS	**name**	**comercial**	**dilution**
Mouse IgG	IgG from mouse serum, reagent grade	Sigma-Aldrich, St. Louis, MO, USA	serial dil.
anti-mouse HRP	Polyclonal Sheep anti-Mouse IgG, HRP conjugated	GE Healthcare, Waukesha, WI, USA	1:80000

2. METHODS

2.1. MOUSE HANDLING

All the experimental procedures with mice were approved by the Comitè d'Ètica en Experimentació Animal i Humana of the Universitat Autònoma de Barcelona.

2.1.1. Surgical procedures

2.1.1.1.Intravenous injection

The intravenous administration of AAV vectors to 8-week-old ICR mice was performed by tail vein injection. Mice were immobilized into a restrainer and the AAV vector was injected by hand using a 1 ml plastic syringe with a 27 Gauge needle to a lateral tail vein in a single bolus. The injection volume was 475 μl in the tropism experiments and 150 μl in the immune response experiments.

2.1.1.2. Intrathecal injection

The intrathecal injection allows the delivery of the viral vectors to the CSF. It was performed to mice previously anesthetized by intraperitoneal administration of ketamine/xylacine. Then, the dorsum of the mouse was shaved and sterilized with 70% ethanol. An incision was made to visualize the lumbar vertebral column at the region of L3 and L4. The AAV vector was delivered manually, using a Hamilton syringe (Hamilton Company, Bonaduz, GR, Switzerland) and a 33 Gauge needle. The tip of the needle was introduced into the intervertebral foramen between L3 and L4 and the proper position of the needle was confirmed by a tail flick reflex. Then, AAV vector was slowly delivered into the CSF by manual injection. The needle was removed 30 seconds after the end of the vector delivery in order to favor spread through the CSF and avoid efflux to periphery. After injection, the epaxial muscles were sutured using absorbable sutures (Safil 5/0; B.Braun Medical SA, Rubí, Barcelona, Spain) and the skin was closed using Michel suture clips (Fine Science Tools GmbH, Heidelberg, Germany). Mice were surveilled until they recovered from anesthesia.

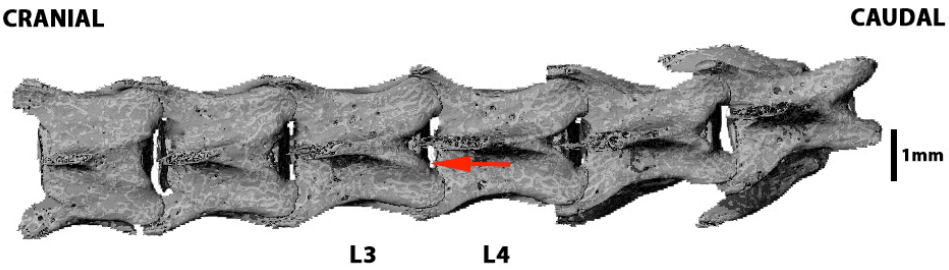

Figure 58: Intrathecal injection. Dorsal view of a mouse lumbar spine. The red arrow represents the site and direction of the injection. (Adapted from *www.ucalgary.ca/microct/*)

2.1.1.3. Anesthesia and euthanasia

For surgery procedures and before perfusion, mice were anesthetized by intraperitoneal injection of a mix of ketamine (Imalgene 50 mg/ml; Merial Laboratorios, Tarragona, Spain) and xylacine (Rompun; Bayer AG, Leverkusen, Germany) diluted in 0.9% saline solution (B.Braun Medical S.A.). The dosage for ICR mice was 100 mg/kg of ketamine and 10 mg/kg of xylacine, whereas the dosage for C57BL/6 mice, including MPS VII mice, was 120 mg/kg of ketamine and 12 mg/kg of xylacine.

Euthanasia of the mice was performed by different means, depending on the subsequent use of the mouse samples. In order to obtain fresh tissue samples, mice were first anesthetized by inhalation of isoflurane (Isoflo; ESTEVE, Barcelona, Spain) in a closed chamber, and decapitation was performed using scissors. When required, blood samples were taken at the moment of euthanasia. Then, organs and tissue samples were dissected and introduced into 1.5 ml eppendorf tubes, which were flash frozen into liquid nitrogen and preserved at -80ºC until they were required.

In order to obtain fixed tissue samples, mice were perfused with 4% paraformaldehyde (PFA). First, the mouse was anesthetized with ketamine/xylacine. The heart was exposed and 5 ml of phosphate buffer were injected to the left ventricle followed by 20 ml of 4% PFA. Organs and tissues were dissected and kept in 4% PFA at 4ºC until processing.

4% PFA: PFA in powder (Sigma-Aldrich) diluted in phosphate buffer 0.1 M pH 7.4. Overnight stirring at 60ºC was required for proper dilution, followed by filtration.

2.1.2. Behavioral analysis

Mice behavior was assessed by an abbreviated SHIRPA three-stage protocol (Giménez-Llort et al. (2002); adapted from Rogers et al. (1997)), with direct observation in the home-cage and several sensorimotor and behavioral tests.

2.1.2.1 Sensorimotor tests

Reflexes (visual reflex and posterior legs extension reflex) were tested by holding the mouse by its tail and gently lowering it to a black surface. With the aim to assess motor coordination and equilibrium, distance covered and latency to fall off were recorded when mice were placed onto a horizontal wooden rod (1.3 cm wide) divided into 10 segments. In order to increase the difficulty of the task, the test was repeated on a metal wire rod (1 cm diameter). The wire rod test was used to assess the prehensility and motor coordination of mice. It consists in allowing the mouse to cling with its forepaws from the middle of a horizontal wire (diameter: 2 mm; length: 40 cm; divided into five segments) for two trials of 5 s and a third trial of 60 s. Muscle strength was measured as the time until falling off the wire in the 60 s trial. Coordination was assessed as the number of segments covered before falling, and prehensility was revealed by the number of elements of support used (i.e. one hindpaw, both hindpaws, both hindpaws and the tail). All the apparatus were suspended 40 cm above a padded table.

2.1.2.2. Corner test

Corner test was used to assess neophobia to a new home-cage. The mouse was placed in the center of a standard cage (Makrolon, 35 x 35 x 25 cm) and its behavior was recorded during 30 s: number of visited corners, number of rearings, and latency of the first rearing.

2.1.2.3. Open-field test

A 5-minute open-field test was performed using a platform with walls (wooden, white, 50 x 50 cm surface, 20 cm high walls) with 10 x 10 cm squares drawn on the surface. The test started by placing the mouse in the center of the open-field (a 10 x 10 cm square) and lasted for 5 minutes, while several different events were recorded. The latency of the behavioral events that take place sequentially when mice are placed in the center of the open-field was recorded: latency of initial movement was used to record initial freezing; thigmotaxis (discrimination of unprotected/protected areas in the test) was assessed by the latency of leaving the central square and that of entering in the peripheral ring (5 cm to the walls); latency of the first rearing and that of the first rearing on the wall recorded the initiation of vertical activities; and the self-grooming behavior was the last event recorded in the sequence of behavioral events. In addition to the latency, the assessment of self-grooming behavior included the number of events and the total duration of groomings. Horizontal and vertical locomotor activities were recorded for each minute of the test, quantified as the number of crossings of squares, and the number of rearings, respectively. In addition, defecation and urination during the test were recorded.

2.1.2.4. T-maze test

T-maze test was used to assess the spontaneous exploratory behavior of the mice in a non-exposed environment using a T-shaped maze (wooden, black, one long arm 50 cm long, two short arms 25 cm long, 20 cm high walls). Animals were placed in the end of the long arm with their head facing the end wall. They were supposed to turn, travel up to the intersection and decide to explore one of the short arms, then go back and explore the second arm. The test finished when they had explored the whole maze, or after 180 s. The sequence of behavioral events until they crossed the maze intersection was recorded: latency to move, to turn, to arrive to the maze intersection and to cross it with the four paws. In addition, for the mice that completed the test exploring the three arms of the maze, the exploratory efficiency was recorded as the total time required for the exploration.

2.1.2.5. 2-Day water maze test

Mice were tested for spatial learning and memory in the 2-day water maze test (adapted from Gulinello et al. (2009)). The test was performed using a pool (90 cm diameter, 30 cm high) filled with water at 25ºC that contained white non-toxic paint to make it opaque, and a platform (7 cm diameter) placed into the pool. The pool was located in the center of a room with asymmetric distribution of the furniture, which provided visual orientation cues. The first day consisted in four trials (*Vis1* to *Vis4*) of 60 s with a visible platform (1 cm above the water surface, indicated by a visible 5 x 8 cm striped flag). On the second day, 24 hours after the visible platform task, the hidden platform task was performed by three 60 s trials (*Hid1* to *Hid3*), with 20 minutes between trials, where mice had to find a hidden platform (1 cm below the water surface, without flag) located at the opposite side of the pool than the previous day. Mice that failed to find the platform within 60 s were manually guided to the platform and placed on it for 5-10 s, the same period as successful animals. All the trials were video-recorded, and a computerized tracking system (SMART, Panlab, Barcelona, Spain) was used for the measurement of the escape latency and swimming distance before reaching the platform. Mean swimming speed was calculated using the distance and latency data of each trial.

2.2. BIOCHEMICAL TECHNIQUES

2.2.1. Protein extraction and quantification

Fresh tissue samples were flash frozen in liquid nitrogen immediately after dissection and kept at -80ºC until processing.

Samples were homogenized in RIPA lysis buffer by sonication at 40 Hz with an ultrasonic processor (Vibra-cell™; Sonics & Materials Inc, Newtown, CT, USA) until they were completely homogenized. Homogenization was followed by centrifugation to eliminate cellular membranes and debris (10-15 min, 12000 rcf, 4ºC using Eppendorf 5415R; Eppendorf AG, Hamburg, Germany). Protein homogenates were kept at -20ºC. Protein quantification was performed by Pierce BCA Protein Assay Kit

(Thermo Fisher Scientific, Waltham, MA, USA) following manufacturer's instructions. Briefly, 10 μl of a 1:10 dilution of each protein sample were mixed with 200 μl of the protein assay reagents, and incubated at 37ºC for 30 min. Absorbance reading at 520 nm was carried out with a microplate reader and the associated software. All samples were analyzed in duplicate.

RIPA lysis buffer: 50 mM Tris-HCl pH 7.4, 150 mM NaCl (Panreac), 1 mM EDTA (USB, Affymetrix, Santa Clara, CA, USA), 1% NP-40 (Sigma-Aldrich), 0,25% sodium deoxycholate (Sigma-Aldrich), 50 mM sodium fluoride (Sigma-Aldrich), 1 mM sodium ortovanadate (Sigma-Aldrich), 10 mM β-glycerophosphate disodium salt hydrate (Sigma-Aldrich), 5 mM sodium pirophosphate decahydrate (Sigma-Aldrich) and a protease inhibitor cocktail (concentration following manufacturer's instructions; Calbiochem, Merck-Millipore, Merck KGaA, Darmstadt, Germany).

2.2.2. β-Glucuronidase and β-hexosaminidase activity

The quantification of enzymatic activities on fresh tissue protein extracts was performed using substrates that, after the enzymatic reaction, give rise to fluorescent products. Ten μl containing 1 to 20 μg of the protein extract were placed into opaque white 96-well plates (Corning Inc, Corning, NY, USA). The total quantity of protein depended on the intrinsic enzymatic activity of the sample (e.g. 1 μg for liver samples, 20 μg for cortex samples). The addition of 50 μl of substrate started the reaction, which was carried out at 37ºC during 1 hour, and stopped with the addition of 200 μl of stop buffer per well. The product fluorescence was detected with Wallac 1420 Victor3 (Perkin Elmer, Waltham, MA, USA) using F335-excitation and F460-emission filters. The fluorescence raw data of the reaction were normalized by the total amount of protein in each sample and expressed as relative light units (RLU) per mg of total protein.

Substrates:
β-glucuronidase: 10 mM 4-methylumbelliferyl-β-D-glucuronide (Sigma-Aldrich)
β-hexosaminidase: 0.01 mM 4-methylumbelliferyl-N-acetyl-β-D-glucosaminide (Sigma-Aldrich)
Stop buffer: 0.2 M Na_2CO_3

2.2.3. In toto β-glucuronidase activity staining

β-Glucuronidase activity was assessed on fixed tissue in order to visualize the extent of the transduction and enzyme spreading achieved throughout different organs.

2.2.3.1. Sample processing

Mice were anesthethized and perfused with 4% PFA as previously described. Organs were dissected, postfixed in 4% PFA for 30 min at 4ºC and then kept in phosphate buffer until required. Samples were cut in 100 μm slices using a vibratome (Leica VT 1000S, Leica Microsystems GmbH). Due to their small size, spinal cord and dorsal root ganglia samples were embedded in 6% agarose (Amresco, Solon, OH, USA) to allow the slicing with the vibratome.

2.2.3.2. β-Glucuronidase staining

The staining procedure started with two 15-min incubations at 4ºC with equilibration buffer followed with two 30-min incubations at 4ºC with substrate buffer. Then the staining enzymatic reaction was conducted by incubation of the samples with reaction buffer at 37ºC for four hours. Then, samples were decanted, slightly dried and mounted on glass slides with DPX mountant for histology (Sigma-Aldrich) and glass coverslips (Menzel-Gläser, Thermo Fisher Scientific). Photographs were taken under the zoom stereomicroscope and the bright-field microscope.

Equilibration buffer: 0.05 M NaOAc pH 4.5 (Panreac)
Substrate buffer: 0.25 mM Naphthol AS-BI β-D-glucuronide (Sigma-Aldrich) in 0.05 M NaOAc pH 4.5.
Reaction buffer: 0.25 mM Naphthol AS-BI β-D-glucuronide in 0.05 M NaOAc pH 5.2, with 1:1000 dilution of 2% hexazotized pararosaniline
2% hexazotized pararosaniline: prepared by mixing equal volumes of two components:
Pararosaniline hydrochloride (Sigma-Aldrich): 0.4 g in 10 ml of 2 M HCl.
Sodium nitrite (Panreac): 0.4 g in 10 ml of deionized water.
Add pararosaniline hydrochloride to sodium nitrite and filter if there is precipitate. Stable for 1 hour at RT.

2.3. ANTIBODY-BASED TECHNIQUES

2.3.1. Serum antibody analysis

2.3.1.1. ELISA

After the intravenous injection of the different AAV serotypes to mice as described before, we quantified the total IgG against the different AAV serotypes by ELISA. A home-made ELISA was set up based on methods previously reported (Boutin et al. (2010), Treleaven et al. (2012)), using F96 maxisorp microwell plates (Thermo Fisher Scientific). The wells were coated with 50 µl of virus diluted to 2 x 10^{10} pp/ml in carbonate buffer by an overnight incubation at 4ºC. A standard curve for absolute quantification was set by coating the appropriate wells with serial dilutions of mouse IgG (Sigma-Aldrich) in carbonate buffer starting from 1500 ng/ml. After overnight coating, plates were washed three times with wash buffer using an automated ELISA washer (ELX50 autostrip washer, Bio-Tek, Winooski, VT, USA). They were then incubated with blocking solution for 1 hour at 37ºC, and subsequently washed three times as above.

As the primary antibody source for the ELISA, 100 µl of serum dilutions in duplicate were added to appropriate wells. A range of 3- and 2-fold dilutions was tested to determine the optimum range for quantification with respect to the linear region of the standard curve (in most cases between 1:450 and 1:1350). The plate was then incubated for 1 hour at 37ºC. Note: serum dilution buffer was placed into the standard curve wells during blocking and primary incubation. Serum incubation was followed by three washes and the subsequent incubation with the secondary antibody, which was conjugated to horseradish peroxidase (HRP). The secondary antibody diluted to 1:80,000 in wash buffer was added to the wells (see Table 8) and incubated at 37ºC for 1 hour. Then wells were washed three times and were ready for detection.

For detection, 100 µl of freshly prepared 3,3',5,5' tetramethylbenzidine (TMB) substrate reagent (BD Biosciences, San Jose, CA, USA) were added to each well and the plate was incubated in the dark for 30 min. The reaction was quenched with 100 µl of 2M H_2SO_4 (Panreac) and the absorbance at λ = 450 nm was measured with a

microplate reader Power Wave HT and KC4 v3.3 software (Bio-Tek). The standard curve was obtained using a 4-parameter logistic nonlinear regression. Results were expressed as total IgG anti-AAV in µg/ml.

Wash buffer: D-PBS pH 7.4, 0.05% TWEEN® 20 (Sigma-Aldrich)
Blocking solution: D-PBS pH 7.2, 0.5% BSA (Sigma-Aldrich)
Serum dilution buffer: D-PBS pH 7.4, 0.05% TWEEN® 20, BSA 0.5%

2.3.1.2. Neutralizing assay

After intravenous injection of the different AAV serotypes to mice, we performed a relative quantification of the neutralizing antibodies present in the mouse sera. This was done by analyzing the relative neutralizing capacity of the different sera when the corresponding viral vector coding for a luciferase reporter gene was incubated with the serum before infection of HEK293 cells. The viral vectors used in the in vitro analysis were AAV9-Luciferase and AAVrh10-Luciferase (see table 7). Each serum from AAV-injected mice was analyzed in vitro against its corresponding AAV serotype. We analyzed the raw serum and three dilutions (1:50, 1:100 and 1:200; diluted in infection medium) to detect a decrease in the neutralizing capacity of the serum throughout the dilutions.

The vector was incubated at 37ºC for 30 min with the different dilutions of each serum. Then, serum-vector mixes were added in duplicate in a volume of 60 µl to HEK293 cells previously grown to 70% confluence in 96-well plates (Thermo Fisher Scientific). The incubation and addition of the serum-vector mix were performed so that the amount of viral vector added to each well was 10^9 vg/well, which had previously been established by titration to give 100% infection without any neutralizing agent. Approximately 5 hours post infection, 100 µl of growth medium were added to each well and the cells were incubated for 48 hours at 37ºC. After this period, the infection in each well was assessed by luciferase activity detection using Pierce Firefly Luciferase Flash Assay kit (Thermo Fisher Scientific), following manufacturer's instructions. Briefly, cells in each well were lysed in 100 µl of lysis buffer, and 20µl of each lysate were transferred to opaque white 96 well plates.

Luciferase activity was detected by adding luciferin substrate and reading the resulting luminescence using Wallac 1420 Victor3. In parallel, the total amount of protein in each sample was quantified following the procedure specified later on in this work without diluting the samples. Transduction efficiency was expressed as luminescence, normalized by the amount of protein per well, giving final values of luminescence per microgram of protein.

Infection medium: DMEM, 10% FBS + 1% Penicillin/Streptomycin
Growth medium: DMEM, 2% FBS + 1% Penicillin/Streptomycin
(All culture mediums and supplements from PAA, GE Healthcare, Waukesha, WI, USA.)

2.3.2. Immunofluorescence

The immunofluorescence technique consists in the labeling of antigens on fixed tissue by specific antibodies and fluorophores. In this work, we used primary antibodies specific for the antigens and secondary antibodies conjugated to fluorescent molecules.

2.3.2.1. Sample processing

Fixed tissues were kept in 4% PFA at 4ºC from dissection until processing. During the day, several 1-2 hour washes with PBS shaking were performed to remove the excess of PFA of the samples. Then, samples were cryoprotected in a solution of saccharose 30% (Panreac), in D-PBS. Each sample was placed into a Cryomold® and embedded in Tissue-Tek® O.C.T™ Compound (Sakura Finetechnical Co, Tokyo, Japan). Dry-ice frozen samples were kept at -20ºC until they were sectioned. 10-20 μm sections were obtained using a cryostate (Leica CM1900). Sections were placed on glass slides (Menzel-Gläser Super Frost Plus; Thermo Fisher Scientific) and kept at -20ºC until required for analysis.

2.3.2.2. Immunofluorescence staining

The immunofluorescence protocol started with hydration of the samples by a 5-10 min wash in 50 mM Tris-HCl pH 7.4 followed by two 5-10 min washes with wash buffer to permeabilize the cells. Then the samples were blocked, in order to avoid subsequent non-specific antibody binding, by incubation with blocking buffer 1 hour at RT. Then samples were incubated overnight at 4ºC with the primary antibody or antibodies in case of multiple immunofluorescence (see Table 8), which were diluted in blocking buffer. After washing, samples they were incubated in the dark for 1 hour at RT with secondary antibodies, which were conjugated with fluorophores. At this point, unless some counterstaining was required, samples were ready to mount, for which we used Fluoromount (Sigma-Aldrich) and glass coverslips.

Some samples from brain and spinal cord were counterstained with a fluorescent Nissl stain (see Table 8) in order to visualize the morphology of the neurons and allow identification of different brain areas. The staining procedure was performed following manufacturer's instructions. Briefly, after washing in D-PBS, a 20-min incubation with the fluorescent Nissl Stain was performed at RT. Then samples were washed in D-PBS with 0.1% Triton X-100 (Sigma-Aldrich), followed by some washes with D-PBS. Besides, some samples were counterstained with Hoechst stain solution (see Table 8) to visualize the cell nuclei. Hoechst staining was performed for 10 min at RT without subsequent wash.

Images of the immunofluorescence analysis were taken using the epifluorescence microscope and the confocal microscope previously described.

Wash buffer: 50 mM Tris-HCl pH 7.4, 0.01% TWEEN® 20
Blocking buffer: 50 mM Tris-HCl pH 7.4, 0.01% TWEEN® 20, 0.05% BSA
Antibodies and counterstaining reagents: see Table 8

2.3.3. Western blot

The analysis of protein samples by western blot allows the identification of specific proteins, and also a relative quantification by subsequent image analysis software. First, a denaturing polyacrylamide gel electrophoresis (SDS-PAGE) separates the proteins by their molecular weight. Then, proteins are transferred to a PVDF membrane, on which the immunodetection of the desired proteins is performed using specific antibodies and a chemiluminescent reagent. The images of the immunodetection can be quantified by specific image analysis software, allowing the comparison of the amount of protein between different samples. Before comparing between different samples, they are normalized by the total amount of protein by a loading control. The loading controls used in this work were tubulin and actin, two proteins of the cytoskeleton.

2.3.3.1. Sample preparation

Tissue samples previously homogenized and quantified were used for western blot analysis. For each sample, 20 μg of protein were diluted in deionized water to an adequate volume before the addition of the appropriate volume of 6X loading buffer. Samples were denatured for 10 min at 98ºC before loading to the electrophoresis gel. With this process, proteins are denatured and get a negative charge relative to their molecular weight that allows the separation by electrophoresis. To identify the molecular weight of the proteins, standards are required in each western blot (PageRuler Prestained Protein Ladder, Thermo Fisher Scientific)

6X Loading buffer: 0.35 M Tris-HCl pH 6.8, 3.3% glycerol (Sigma-Aldrich), 10% SDS (USB, Affymetrix), 0.015% bromophenol blue (Sigma-Aldrich), 0.6 M DL-dithiothreitol (Sigma-Aldrich).

2.3.3.2. Denaturing gel electrophoresis

Homemade discontinuous denaturing polyacrylamide gels were used for electrophoresis. The stacking part of gel allows the loading of the samples into wells and their concentration before entering the resolving gel, where they get separated depending on their molecular weight. Stacking gel contains 3.9% acrylamide while

the percentage of acrylamide of the resolving gel depends on the molecular weight of the proteins to be resolved (i.e. 12% for LAMP-1 and tubulin; 10% for GFAP and actin, in this work).

Electrophoresis was run using an electrophoresis chamber (Mini-Protean® Tetra Cell, Bio-Rad, Hercules, CA, USA) filled with electrophoresis buffer and connected to a voltage source (Bio-Rad). After loading the samples and the molecular weight marker into the wells of the gel, electrophoresis was run at low voltage (80-100 V) for 10-15 min until proteins reached the resolving gel. Then it was raised to 130-150 V until the end of the run, which was defined checking the prestained protein standards mobility.

Preparation of the polyacrilamide gels

Stacking gel: 3.9% Acryl/Bis 29:1 (Acryl/Bis 29:1 40% w/v solution (Amresco), 0.5 M Tris-HCl pH 6.8, 0.4% SDS.

Resolving gel: 10-12% Acryl/Bis 29:1, 1.5 M Tris-HCl pH 8.8, 0.4% SDS.

For polymerization, add 25-50 μl of ammonium persulfate (Amresco) and 5-10 μl of TEMED (N, N, N', N', tetrametil-etilen-diamine, Sigma-Aldrich).

Electrophoresis buffer: 25 mM Tris, 192 mM Glycine (Serva Electrophoresis GmbH, Heidelberg, Germany), 1% SDS

2.3.3.3. Transfer and blocking

After electrophoresis, proteins were transferred to a PVDF membrane (Amersham Hybond P 0.2 PVDF, GE Healthcare) using a semidry electrotransfer system (Trans-Blot® SD Semi-Dry Transfer Cell, Bio-Rad) connected to a voltage source (Bio-Rad). Before transfer, PVDF membrane required activation in methanol for 10 seconds and 10-min equilibration in transfer buffer. Polyacrylamide gel required 10-min equilibration in transfer buffer as well. The transfer sandwich was formed with the gel and the membrane stacked together between two extra-thick western blotting filter papers (Thermo Fisher Scientific) previously soaked in transfer buffer. Transfer was performed at 25 V during 45 min. Then it was checked by staining the membrane with Ponceau solution during 5 min shaking, followed by destaining with water.

Transfer buffer: 25 mM Tris, 192 mM Glycine, 20% methanol (Panreac)

Ponceau solution: 0.5% Ponceau S (Sigma-Aldrich), 1% acetic acid (Panreac)

2.3.3.4. Immunoblotting

For the detection of the desired proteins, specific primary and secondary antibodies are used. The antibodies used in this work are specified in Table 8, together with the dilution used for each one. Secondary antibodies are conjugated to horseradish peroxidase (HRP), which cleaves a chemiluminescent agent and the reaction produces luminescence in proportion to the amount of protein. This luminescence is detected and can be quantified.

In order to avoid non-specific binding of the antibodies to the membrane, it was blocked with the blocking solution for 1 hour shaking at RT prior to immunodetection. The membrane was incubated with the primary antibody diluted in blocking solution overnight shaking at 4ºC. After three 10-min washes with TBS-T, the membrane was incubated with the secondary antibody diluted in blocking solution for 1 hour at RT. Three 10-min washes with TBS-T were used to remove the excess of secondary antibodies prior to immunodetection.

TBS: 50 mM Tris, 136 mM NaCl, 40 mM KCl; pH 7.3
TBS-T: 0.1% TWEEN-20 in TBS
Blocking solution: 5% non-fat dry milk in TBS-T

2.3.3.5. Chemiluminescent detection and quantification

Immunodetection was performed by 5-min incubation at RT with a chemiluminescent substrate (EMD Millipore Immobilon™ Western Chemiluminescent HRP Substrate, Thermo Fisher Scientific) using ChemiDoc™ MP System (Bio-Rad) for luminescence detection. Luminescence data were acquired at different exposition times, and the best acquisition file was considered to be the one that displayed higher signal without image saturation. The best acquisition file was used for density quantification using Quantity One® software (Bio-Rad).

2.4. HISTOLOGICAL ANALYSIS

Histopathological features were analyzed on fixed tissue samples, which underwent paraffin inclusion and section, followed by general staining protocols.

2.4.1. Sample processing

Fixed tissue samples were enclosed into Tespa tissue-embedding cassettes (Casa Álvarez, Madrid, Spain) and were dehydrated with consecutive washes in increasing concentrations of ethanol (Panreac) and cleared with xylol (Panreac). Then samples were embedded in paraffin using an embedding station (Microm A280; Zeiss, Oberkochen, Germany) and paraffin (Casa Álvarez) melted at 59ºC, by overnight incubation and subsequent cooling. Then samples were sectioned with using a microtome (Leica RM 2125RT) obtaining 2-μm-thick sections that were placed on glass slides and kept at room temperature until required for staining and analysis.

2.4.2. Histological staining

Sections of different organs were stained for histopathological analysis using two different protocols: hematoxylin and eosin staining for liver, and toluidine blue staining for nervous system tissues. Before staining, samples were deparafinized with xylol, and rehydrated with decreasing concentrations of ethanol and water.

For hematoxilin and eosin staining, samples were placed in a solution of hematoxylin (Sigma-Aldrich) during 6 minutes, followed by a quick wash of 2 seconds in HCl 0.25% and a 5-min wash with running water. Then, eosin staining was performed with eosin solution (Sigma-Aldrich) during 30-60 seconds.

Toluidine blue staining was performed with a solution 0.5% toluidine blue O (Merck-Millipore) for 30 minutes, followed by washing with water.

After staining, samples were dehydrated and cleared. Then they were mounted using DPX mountant for histology and glass coverslips. Samples were analyzed by bright-field microscopy and pictures were taken with 1000X magnification.

2.5. VIRAL VECTOR DNA QUANTIFICATION

To detect and quantify the genomes of viral vector present in different organs and areas we performed Hirt DNA extraction followed by quantitative PCR (qPCR).

2.5.1. Hirt DNA extraction

This DNA extraction method (adapted from Hirt (1967)) is used to favor the extraction of low molecular weight DNA. Frozen tissue samples were kept at -80ºC in microcentrifuge tubes. Approximately 10 µl of Hirt digestion buffer per mg of tissue were dispensed on frozen tissue samples and were incubated at 50ºC overnight, shaking at approximately 120 rpm. After digestion, NaCl concentration was adjusted to 1 M using 5 M NaCl and samples were placed either on ice for three hours or overnight at 4ºC. Then, debris was removed by centrifugation (> 14,000 rcf, 4ºC, 30 min; Eppendorf 5415R) and supernatant was carefully taken and placed into a new tube. Then supernatant was diluted 2X with deionized water to reduce the salt concentration. One volume of phenol/$CHCl_3$/isoamyl alcohol (25:24:1) was added to each sample (Amresco), which was then centrifuged to separate the aqueous and organic phases (300 rcf, RT, 10 min; Eppendorf 5415R). The upper phase was removed and placed into a new tube, where two volumes of 100% ethanol were added, followed by centrifugation (> 14,000 rcf, RT, 10 min; Eppendorf 5415R) to achieve DNA precipitation. Supernatant was discarded and DNA pellet was dried for 5 min at RT. DNA was resuspended in 30-50 µl of deionized water containing 100 µg/ml of RNase A (Qiagen, Valencia, CA, USA), and kept at -20ºC until quantification or analysis. DNA quantification was performed using NanoDrop 1000 (Thermo Fisher Scientific).

Hirt digestion buffer: 20 mM Tris-HCl pH 8.0, 10 mM EDTA pH 8.0, 0.6% SDS, 0.2 mg/ml proteinase K (Roche Diagnostics, Basel, Switzerland).
Note: Proteinase K is freshly added to the buffer prior to use.

2.5.2. Quantitative PCR

To assess the vector genomes per cell in tissues, we performed quantitative PCR (qPCR) analysis using specific primers for a region of the CAG promoter present in the vector genome. In parallel, we performed qPCR analysis of cyclophilin B, a monocopy gene in the mouse genome (MGI:97750 in Mouse Genome Informatics; www.informatics.jax.org), to normalize the CAG copies per number of cells. For the absolute quantification of both sequences, a standard curve for each sequence was made with series of dilutions of known DNA concentration.

2.5.2.1. Standards for qPCR

A purified DNA preparation of the plasmid pAAV-CAG-GFP-WPRE, which had been quantified using NanoDrop 1000, was used to prepare a series of 1:10 dilutions that will be specified later on.

In the case of cyclophilin B, a 525 bp DNA sequence was amplified from mouse liver using specific primers. Subsequently, this PCR product was isolated by DNA electrophoresis, purified using GeneClean Kit (MPBio, Santa Ana, CA, USA) and quantified using Quant-iT™ PicoGreen® dsDNA Assay Kit (Life Technologies, Carlsbad, CA, USA) following manufacturer's instructions.

Cyclophilin B standard PCR
Template: 200 ng of mouse liver DNA.
Primers: Fwd = catgcctatggtcctagctt; Rv = ggtttctccacttcgatcttgc.
Polymerase and buffer: Dream Taq DNA polymerase (Thermo Fisher Scientific).
Reaction: 40 x (denaturing 15" at 95ºC; annealing 30" at 57ºC; extension 45" at 72ºC)
Thermocycler: Mastercycler gradient (Eppendorf AG).

2.5.2.2. qPCR procedure

Quantitative PCR was performed using 384-well plates and the thermocycler Bio-Rad CFX284. Each sample or standard was analyzed in triplicate, in a total volume of 10 µl, which included 0,84 µg of DNA, 5 µl of iTaq Universal SYBR Green Supermix (Bio-Rad) and 0.4 µl of each primer (**Table 9**).

qPCR program (Fluorescence measured in extension step of PCR and in melting process)
Hot start: 3' at 95ºC
Reaction: 40 x (10'' at 95ºC; 20'' at 58ºC; 20'' at 72ºC) + 10'' at 95ºC
Melting analysis: stepwise T increase from 65ºC to 95ºC, in 0.5ºC steps and 5'' periods

For each well, we obtained an amplification curve from the PCR procedure, from which a Cq value was extracted using Bio-Rad CFX Manager software and used for vector genome copies calculation. We also obtained a melting curve from the melting analysis, which was used for quality control of specific amplification.

The standard curves for CAG and cyclophilin B were prepared by 1:10 serial dilutions using the previously described standards. For each dilution, each specific DNA was mixed with stuffer DNA (DNA sodium salt from salmon testes, Sigma-Aldrich) up to a concentration of 1 μg/ml. After qPCR, the dilutions whose Cq values presented a linear correlation ranged from 10,000 to 10 fg for CAG standards, and from 1,000 to 0.1 fg for cyclophilin standards.

Table 9: Primers for vector DNA quantification

primer name	primer sequence	product length
CAG Fwd	tggctgaccgcccaacgac	155 bp
CAG Rv	tacttggcatatgatacact	
cyclophilin B Fwd	tcaacctctcctctcctgcc	133 bp
cyclophilin B Rv	ggtttctcdcacttcgatcttgc	

2.5.2.3. qPCR data analysis

Data obtained with the qPCR were a Cq value for each reaction, for both mouse DNA samples and standards. Replicates were checked for homogeneity and reliability with Bio-Rad CFX Manager software. Then, standard curves for each sequence were used to extrapolate the amount of DNA present in the tissue DNA samples, using the Cq values obtained for these samples. The quantity of sequence-specific DNA in each sample was converted to dsDNA copies using a general assumption of the molecular weight of dsDNA [MW (g/mol) dsDNA = (#nucleotides · 607.4) + 157.9] and the Avogadro number [6.023 x 10^{23} DNA molecules DNA/mol]. Finally, a ratio between CAG and cyclophilin B copy numbers was calculated for each sample.

2.6. STATISTICAL ANALYSIS

All the statistics presented in this work were performed using IBM SPSS Statistics Version 21 software (IBM, Armonk, NY, USA). We used some general statistical tests and also other specific tests for some groups of data.

In general we used two-tailed *t*-tests to analyze a dependent variable between two independent variables (groups). We used one-way ANOVA to analyze one dependent variable among three or more independent variables (groups). In these cases, we used Tukey *post hoc* tests for pairwise comparisons between groups. Finally, we performed two-way ANOVA to compare the data of a dependent variable and check for the effects and interaction of two independent variables (e.g. "liver weight" as the dependent variable and "age" and "group" the independent variables). In most of the data analyzed, we did not compare the data between the two different ages due to experimental limitations in the sample processing and/or analyzing procedures.

Several specific statistical analyses were performed for some sets of data. Non-parametric tests were used for β-gluc and β-hex activities because the variances of the data presented high differences among groups, which prevented the use of ANOVA. The difference of the variances among groups was checked by Levene test, and the non-parametric statistical analysis was performed by Kruskal-Wallis test and was followed by successive Mann-Withney U tests to do the pairwise comparisons. Another specific test, the Repeated Measures ANOVA, was performed to analyze the 2-day water maze test in order to check for differences in the learning patterns. Finally, Kaplan-Meier analysis was used for the survival data.

Data are represented as **mean ± SEM**, except for scatter plots, where — denotes the mean and SEM is not depicted. The statistical signification depicted on the graphs and tables corresponds to * $\boldsymbol{p < 0.05}$, ** $\boldsymbol{p < 0.01}$ and *** $\boldsymbol{p < 0.001}$. The different pairwise comparisons are depicted using different symbols, which are specified in each graph or table.

REFERENCES

REFERENCES

1. BIBLIOGRAPHIC REFERENCES

Acland G, Aguirre G, Bennett J, Aleman T, Cideciyan A, Bennicelli J, Dejneka N, Pearcekelling S, Maguire A, Palczewski K (2005) Long-Term Restoration of Rod and Cone Vision by Single Dose rAAV-Mediated Gene Transfer to the Retina in a Canine Model of Childhood Blindness. Molecular Therapy 12:1072-1082.

Aits S, Jäättelä M (2013) Lysosomal cell death at a glance. Journal of cell science 126:1905-1912.

Andrejewski N, Punnonen EL, Guhde G, Tanaka Y, Lullmann-Rauch R, Hartmann D, von Figura K, Saftig P (1999) Normal Lysosomal Morphology and Function in LAMP-1-deficient Mice. Journal of Biological Chemistry 274:12692-12701.

Ariza L, Giménez-Llort L, Cubizolle A, Pagès G, García-Lareu B, Serratrice N, Cots D, Thwaite R, Chillón M, Kremer EJ, Bosch A (2014) Central Nervous System Delivery of Helper-Dependent Canine Adenovirus Corrects Neuropathology and Behavior in Mucopolysaccharidosis Type VII Mice. Human gene therapy 25:199-211.

Asokan A, Schaffer DV, Jude Samulski R (2012) The AAV Vector Toolkit: Poised at the Clinical Crossroads. Molecular Therapy 20:699-708.

Baldo G, Mayer FQ, Martinelli B, Dilda A, Meyer F, Ponder KP, Giugliani R, Matte U (2012) Evidence of a progressive motor dysfunction in Mucopolysaccharidosis type I mice. Behavioural brain research 233:169-175.

Ballabio A, Gieselmann V (2009) Lysosomal disorders: From storage to cellular damage. Biochimica et biophysica acta 1793:684-696.

Bartel M, Schaffer D, Büning H (2011) Enhancing the Clinical Potential of AAV Vectors by Capsid Engineering to Evade Pre-Existing Immunity. Frontiers in microbiology 2:204.

Bartlett JS, Samulski RJ, McCown TJ (1998) Selective and rapid uptake of adeno-associated virus type 2 in brain. Human gene therapy 9:1181-1186.

Basner-Tschakarjan E, Mingozzi F (2014) Cell-Mediated Immunity to AAV Vectors, Evolving Concepts and Potential Solutions. Frontiers in immunology 5:350.

Bastedo L, Sands MS, Lambert DT, Pisa MA, Birkenmeier E, Chang PL (1994) Behavioral consequences of bone marrow transplantation in the treatment of murine mucopolysaccharidosis type VII. The Journal of clinical investigation 94:1180-1186.

Bell CL, Vandenberghe LH, Bell P, Limberis MP, Gao G-P, Van Vliet K, Agbandje-McKenna M, Wilson JM (2011) The AAV9 receptor and its modification to improve in vivo lung gene transfer in mice. The Journal of clinical investigation 121:2427-2435.

Berges B, Yellayi S, Karolewski B, Miselis R, Wolfe J, Fraser N (2006) Widespread Correction of Lysosomal Storage in the Mucopolysaccharidosis Type VII Mouse Brain with a Herpes Simplex Virus Type 1 Vector Expressing β-Glucuronidase. Molecular Therapy 13:859-869.

Bergwerk KE, Falk RE, Glasgow BJ, Rabinowitz YS (2000) Corneal transplantation in a patient with mucopolysaccharidosis type VII (Sly disease). Ophthalmic genetics 21:17-20.

Bernsen PL, Wevers RA, Gabreëls FJ, Lamers KJ, Sonnen AE, Stekhoven JH (1987) Phenotypic expression in mucopolysaccharidosis VII. Journal of neurology, neurosurgery, and psychiatry 50:699-703.

Beutler E (2006) Lysosomal storage diseases: Natural history and ethical and economic aspects. Molecular Genetics and Metabolism 88:208-215.

Bevan AK, Duque S, Foust KD, Morales PR, Braun L, Schmelzer L, Chan CM, McCrate M, Chicoine LG, Coley BD, Porensky PN, Kolb SJ, Mendell JR, Burghes AHM, Kaspar BK (2011) Systemic gene delivery in large species for targeting spinal cord, brain, and peripheral tissues for pediatric disorders. Molecular Therapy 19:1971-1980.

Bielicki J, Mcintyre C, Anson DS (2010) Comparison of ventricular and intravenous lentiviral-mediated gene therapy for murine MPS VII. Molecular Genetics and Metabolism 101:370-382.

Biffi A, Montini E, Lorioli L, Cesani M, Fumagalli F, Plati T, Baldoli C, Martino S, Calabria A, Canale S, Benedicenti F, Vallanti G, Biasco L, Leo S, Kabbara N, Zanetti G, Rizzo WB, Mehta NAL, Cicalese MP, Casiraghi M, Boelens JJ, Del Carro U, Dow DJ, Schmidt M, Assanelli A, Neduva V, Di Serio C, Stupka E, Gardner J, von Kalle C, Bordignon C, Ciceri F, Rovelli A, Roncarolo MG, Aiuti A, Sessa M, Naldini L (2013) Lentiviral hematopoietic stem cell gene therapy benefits metachromatic leukodystrophy. Science 341:1233158.

Bigg PW, Sleeper MM, O'donnell PA, Liu Y, Wu S, Casal ML, Haskins ME, Ponder KP (2013) The effect of neonatal gene therapy with a gamma retroviral vector on cardiac valve disease in mucopolysaccharidosis VII dogs after a decade. Molecular Genetics and Metabolism 110:311-318.

Birkenmeier EH, Barker JE, Vogler CA, Kyle JW, Sly WS, Gwynn B, Levy B, Pegors C (1991) Increased life span and correction of metabolic defects in murine mucopolysaccharidosis type VII after syngeneic bone marrow transplantation. Blood 78:3081-3092.

Birkenmeier EH, Davisson MT, Beamer WG, Ganschow RE, Vogler CA, Gwynn B, Lyford KA, Maltais LM, Wawrzyniak CJ (1989) Murine mucopolysaccharidosis type VII. Characterization of a mouse with beta-glucuronidase deficiency. The Journal of clinical investigation 83:1258-1266.

Bosch A, Heard JM (2003) Gene therapy for mucopolysaccharidosis. International review of neurobiology 55:271-296.

Bosch A, Perret E, Desmaris N, Heard JM (2000a) Long-term and significant correction of brain lesions in adult mucopolysaccharidosis type VII mice using recombinant AAV vectors. Molecular therapy 1:63-70.

Bosch A, Perret E, Desmaris N, Trono D, Heard JM (2000b) Reversal of pathology in the entire brain of mucopolysaccharidosis type VII mice after lentivirus-mediated gene transfer. Human gene therapy 11:1139-1150.

Bourdenx M, Dutheil N, Bezard E, Dehay B (2014) Systemic gene delivery to the central nervous system using Adeno-associated virus. Frontiers in Molecular Neuroscience 7:1-8.

Boutin S, Monteilhet V, Veron P, Leborgne C, Benveniste O, Montus MF, Masurier C (2010) Prevalence of serum IgG and neutralizing factors against adeno-associated virus (AAV) types 1, 2, 5, 6, 8, and 9 in the healthy population: implications for gene therapy using AAV vectors. Human gene therapy 21:704-712.

Braulke T, Bonifacino JS (2009) Sorting of lysosomal proteins. BBA - Molecular Cell Research 1793:605-614.

Calcedo R, Vandenberghe LH, Gao G, Lin J, Wilson JM (2009) Worldwide epidemiology of neutralizing antibodies to adeno-associated viruses. The Journal of infectious diseases 199:381-390.

Calcedo R, Wilson JM (2013) Humoral Immune Response to AAV. Frontiers in immunology 4:341.

Carlsson SR, Roth J, Piller F, Fukuda M (1988) Isolation and characterization of human lysosomal membrane glycoproteins, h-lamp-1 and h-lamp-2. Major sialoglycoproteins carrying polylactosaminoglycan. The Journal of biological chemistry 263:18911-18919.

Cartier N, Aubourg P (2010) Hematopoietic Stem Cell Transplantation and Hematopoietic Stem Cell Gene Therapy in X-Linked Adrenoleukodystrophy. Brain Pathology 20:857-862.

Cartier N, Hacein-Bey-Abina S, Bartholomae CC, Bougnères P, Schmidt M, von Kalle C, Fischer A, Cavazzana-Calvo M, Aubourg P (2012) Lentiviral Hematopoietic Cell Gene Therapy for X-Linked Adrenoleukodystrophy: Elsevier Inc.

Cartier N, Hacein-Bey-Abina S, Bartholomae CC, Veres G, Schmidt M, Kutschera I, Vidaud M, Abel U, Dal-Cortivo L, Caccavelli L, Mahlaoui N, Kiermer V, Mittelstaedt D, Bellesme C, Lahlou N, Lefrère F, Blanche S, Audit M, Payen E, Leboulch P, l'Homme B, Bougnères P, von Kalle C, Fischer A, Cavazzana-Calvo M, Aubourg P (2009) Hematopoietic stem cell gene therapy with a lentiviral vector in X-linked adrenoleukodystrophy. Science 326:818-823.

Carty N, Nash KR, Brownlow M, Cruite D, Wilcock D, Selenica M-LB, Lee DC, Gordon MN, Morgan D (2013) Intracranial Injection of AAV Expressing NEP but Not IDE Reduces Amyloid Pathology in APP+PS1 Transgenic Mice. PLoS ONE 8:e59626.

Castle MJ, Gershenson ZT, Giles AR, Holzbaur ELF, Wolfe JH (2014) Adeno-Associated Virus Serotypes 1, 8, and 9 Share Conserved Mechanisms for Anterograde and Retrograde Axonal Transport. Human gene therapy 25:705-720.

Cearley CN, Vandenberghe LH, Parente MK, Carnish ER, Wilson JM, Wolfe JH (2008) Expanded Repertoire of AAV Vector Serotypes Mediate Unique Patterns of Transduction in Mouse Brain. Molecular Therapy 16:1710-1718.

Cearley CN, Wolfe JH (2006) Transduction characteristics of adeno-associated virus vectors expressing cap serotypes 7, 8, 9, and Rh10 in the mouse brain. Molecular therapy : the journal of the American Society of Gene Therapy 13:528-537.

Cearley CN, Wolfe JH (2007) A Single Injection of an Adeno-Associated Virus Vector into Nuclei with Divergent Connections Results in Widespread Vector Distribution in the Brain and Global Correction of a Neurogenetic Disease. Journal of Neuroscience 27:9928-9940.

Chakrabarty P, Rosario A, Cruz P, Siemienski Z, Ceballos-Diaz C, Crosby K, Jansen K, Borchelt DR, Kim J-Y, Jankowsky JL, Golde TE, Levites Y (2013) Capsid Serotype and Timing of Injection Determines AAV Transduction in the Neonatal Mice Brain. PLoS ONE 8:e67680.

Chen YH, Chang M, Davidson BL (2009) Molecular signatures of disease brain endothelia provide new sites for CNS-directed enzyme therapy. Nature medicine 15:1215-1218.

Chen YH, Claflin K, Geoghegan JC, Davidson BL (2012) Sialic acid deposition impairs the utility of AAV9, but not peptide-modified AAVs for brain gene therapy in a mouse model of lysosomal storage disease. Molecular Therapy 20:1393-1399.

Ciesielska A, Hadaczek P, Mittermeyer G, Zhou S, Wright JF, Bankiewicz KS, Forsayeth J (2013) Cerebral infusion of AAV9 vector-encoding non-self proteins can elicit cell-mediated immune responses. Molecular Therapy 21:158-166.

Ciron C, Desmaris N, Colle M-A, Raoul S, Joussemet B, Vérot L, Ausseil J, Froissart R, Roux F, Chérel Y, Ferry N, Lajat Y, Schwartz B, Vanier M-T, Maire I, Tardieu M, Moullier P,

Heard J-M (2006) Gene therapy of the brain in the dog model of Hurler's syndrome. Annals of neurology 60:204-213.

Crystal RG, Sondhi D, Hackett NR, Kaminsky SM, Worgall S, Stieg P, Souweidane M, Hosain S, Heier L, Ballon D, Dinner M, Wisniewski K, Kaplitt M, Greenwald BM, Howell JD, Strybing K, Dyke J, Voss H (2004) Clinical protocol. Administration of a replication-deficient adeno-associated virus gene transfer vector expressing the human CLN2 cDNA to the brain of children with late infantile neuronal ceroid lipofuscinosis. Human gene therapy 15:1131-1154.

Cubizolle A, Serratrice N, Skander N, Colle M-A, Ibanes S, Gennetier A, Bayo-Puxan N, Mazouni K, Mennechet F, Joussemet B, Chérel Y, Lajat Y, Vite C, Bernex F, Kalatzis V, Haskins ME, Kremer EJ (2014) Corrective GUSB Transfer to the Canine Mucopolysaccharidosis VII Brain. Molecular Therapy 22:762-773.

Daly TM, Ohlemiller KK, Roberts MS, Vogler CA, Sands MS (2001) Prevention of systemic clinical disease in MPS VII mice following AAV-mediated neonatal gene transfer. Gene therapy 8:1291-1298.

Daly TM, Okuyama T, Vogler C, Haskins ME, Muzyczka N, Sands MS (1999a) Neonatal intramuscular injection with recombinant adeno-associated virus results in prolonged beta-glucuronidase expression in situ and correction of liver pathology in mucopolysaccharidosis type VII mice. Human gene therapy 10:85-94.

Daly TM, Vogler C, Levy B, Haskins ME, Sands MS (1999b) Neonatal gene transfer leads to widespread correction of pathology in a murine model of lysosomal storage disease. Proceedings of the National Academy of Sciences of the United States of America 96:2296-2300.

Davidoff AM, Ng CYC, Zhou J, Spence Y, Nathwani AC (2003) Sex significantly influences transduction of murine liver by recombinant adeno-associated viral vectors through an androgen-dependent pathway. Blood 102:480-488.

Davidson BL, Stein CS, Heth JA, Martins I, Kotin RM, Derksen TA, Zabner J, Ghodsi A, Chiorini JA (2000) Recombinant adeno-associated virus type 2, 4, and 5 vectors: transduction of variant cell types and regions in the mammalian central nervous system. Proceedings of the National Academy of Sciences of the United States of America 97:3428-3432.

de Ruijter J, Valstar MJ, Narajczyk M, Wegrzyn G, Kulik W, IJlst L, Wagemans T, van der Wal WM, Wijburg FA (2012) Genistein in Sanfilippo disease: A randomized controlled crossover trial. Annals of neurology 71:110-120.

Delgadillo V, O'Callaghan MDM, Artuch R, Montero R, Pineda M (2011) Genistein supplementation in patients affected by Sanfilippo disease. Journal of inherited metabolic disease 34:1039-1044.

Derrick-Roberts ALK, Pyragius CE, Kaidonis XM, Jackson MR, Anson DS, Byers S (2014) Lentiviral-Mediated Gene Therapy Results in Sustained Expression of β-Glucuronidase for up to 12 Months in the Gus mps/mpsand up to 18 Months in the Gus tm(L175F)Sly Mouse Models of Mucopolysaccharidosis Type VII. Human gene therapy 25(29):798-810.

Donsante A, Miller DG, Li Y, Vogler C, Brunt EM, Russell DW, Sands MS (2007) AAV Vector Integration Sites in Mouse Hepatocellular Carcinoma. Science 317:477-477.

Donsante A, Vogler C, Muzyczka N, Crawford JM, Barker J, Flotte T, Campbell-Thompson M, Daly T, Sands MS (2001) Observed incidence of tumorigenesis in long-term rodent studies of rAAV vectors. Gene therapy 8:1343-1346.

Dufour BD, Smith CA, Clark RL, Walker TR, McBride JL (2014) Intrajugular Vein Delivery of AAV9-RNAi Prevents Neuropathological Changes and Weight Loss in Huntington's Disease Mice. Molecular therapy 22:797-810.

Elliger SS, Elliger CA, Aguilar CP, Raju NR, Watson GL (1999) Elimination of lysosomal storage in brains of MPS VII mice treated by intrathecal administration of an adeno-associated virus vector. Gene therapy 6:1175-1178.

Elliger SS, Elliger CA, Lang C, Watson GL (2002) Enhanced secretion and uptake of beta-glucuronidase improves adeno-associated viral-mediated gene therapy of mucopolysaccharidosis type VII mice. Molecular therapy 5:617-626.

Ellinwood NM, Ausseil J, Desmaris N, Bigou S, Liu S, Jens JK, Snella EM, Mohammed EE, Thomson CB, Raoul S, Joussemet B, Roux F, Chérel Y, Lajat Y, Piraud M, Benchaouir R, Hermening S, Petry H, Froissart R, Tardieu M, Ciron C, Moullier P, Parkes J, Kline KL, Maire I, Vanier M-T, Heard J-M, Colle M-A (2010) Safe, Efficient, and Reproducible Gene Therapy of the Brain in the Dog Models of Sanfilippo and Hurler Syndromes. Molecular Therapy 19:251-259.

Federici T, Taub JS, Baum GR, Gray SJ, Grieger JC, Matthews KA, Handy CR, Passini MA, Samulski RJ, Boulis NM (2012) Robust spinal motor neuron transduction following intrathecal delivery of AAV9 in pigs. Gene therapy 19:852-859.

Ferla R, Claudiani P, Cotugno G, Saccone P, De Leonibus E, Auricchio A (2014) Similar Therapeutic Efficacy Between a Single Administration of Gene Therapy and Multiple Administrations of Recombinant Enzyme in a Mouse Model of Lysosomal Storage Disease. Human gene therapy 25:609-618.

Foust KD, Nurre E, Montgomery CL, Hernandez A, Chan CM, Kaspar BK (2009) Intravascular AAV9 preferentially targets neonatal neurons and adult astrocytes. Nature Biotechnology 27:59-65.

Fox JE, Volpe L, Bullaro J, Kakkis ED, Sly WS (2015) First human treatment with investigational rhGUS enzyme replacement therapy in an advanced stage MPS VII patient. Molecular Genetics and Metabolism 114:203-208.

Frisella WA, O'Connor LH, Vogler CA, Roberts M, Walkley S, Levy B, Daly TM, Sands MS (2001) Intracranial injection of recombinant adeno-associated virus improves cognitive function in a murine model of mucopolysaccharidosis type VII. Molecular therapy 3:351-358.

Fu H, DiRosario J, Killedar S, Zaraspe K, McCarty DM (2009) Correction of Neurological Disease of Mucopolysaccharidosis IIIB in Adult Mice by rAAV9 Trans-Blood–Brain Barrier Gene Delivery. Molecular Therapy 19:1025-1033.

Fukuhara Y, Li X, Kitazawa Y, Inagaki M, Matsuoka K, Kosuga M, Kosaki R, Shimazaki T, Endo H, Umezawa A (2006) Histopathological and Behavioral Improvement of Murine Mucopolysaccharidosis Type VII by Intracerebral Transplantation of Neural Stem Cells. Molecular Therapy 13:548-555.

Fyfe JC, Kurzhals RL, Lassaline ME, Henthorn PS, Alur PR, Wang P, Wolfe JH, Giger U, Haskins ME, Patterson DF, Sun H, Jain S, Yuhki N (1999) Molecular basis of feline beta-glucuronidase deficiency: an animal model of mucopolysaccharidosis VII. Genomics 58:121-128.

Gao G, Vandenberghe LH, Alvira MR, Lu Y, Calcedo R, Zhou X, Wilson JM (2004) Clades of Adeno-Associated Viruses Are Widely Disseminated in Human Tissues. Journal of Virology 78:6381-6388.

Gao G-P, Alvira MR, Wang L, Calcedo R, Johnston J, Wilson JM (2002) Novel adeno-associated viruses from rhesus monkeys as vectors for human gene therapy. Proceedings of the National Academy of Sciences of the United States of America 99:11854-11859.

Ghodsi A, Stein C, Derksen T, Yang G, Anderson RD, Davidson BL (1998) Extensive beta-glucuronidase activity in murine central nervous system after adenovirus-mediated gene transfer to brain. Human gene therapy 9:2331-2340.

Giménez-Llort L, Fernández-Teruel A, Escorihuela RM, Fredholm BB, Tobeña A, Pekny M, Johansson B (2002) Mice lacking the adenosine A1 receptor are anxious and aggressive, but are normal learners with reduced muscle strength and survival rate. European Journal of Neuroscience 16:547-550.

Ginn SL, Alexander IE, Edelstein ML, Abedi MR, Wixon J (2013) Gene therapy clinical trials worldwide to 2012 - an update. The Journal of Gene Medicine 15:65-77.

Gitzelmann R, Bosshard NU, Superti-Furga A, Spycher MA, Briner J, Wiesmann U, Lutz H, Litschi B (1994) Feline mucopolysaccharidosis VII due to beta-glucuronidase deficiency. Veterinary pathology 31:435-443.

Gray SJ, Kalburgi SN, McCown TJ, Samulski RJ (2013) Global CNS gene delivery and evasion of anti-AAV-neutralizing antibodies by intrathecal AAV administration in non-human primates. Gene therapy 20:450-459.

Gray SJ, Matagne V, Bachaboina L, Yadav S, Ojeda SR, Samulski RJ (2011) Preclinical Differences of Intravascular AAV9 Delivery to Neurons and Glia: A Comparative Study of Adult Mice and Nonhuman Primates. Molecular Therapy 19:1058-1069.

Grieger JC, Samulski RJ (2012) Adeno-Associated Virus Vectorology, Manufacturing, and Clinical Applications: Elsevier Inc.

Grubb JH, Vogler C, Levy B, Galvin N, Tan Y, Sly WS (2008) Chemically modified beta-glucuronidase crosses blood-brain barrier and clears neuronal storage in murine mucopolysaccharidosis VII. Proceedings of the National Academy of Sciences of the United States of America 105:2616-2621.

Guffon N, Bin-Dorel S, Decullier E, Paillet C, PharmD JG, Fouilhoux A (2011) Evaluation of Miglustat Treatment in Patients with Type III Mucopolysaccharidosis: A Randomized, Double-Blind, Placebo-Controlled Study. The Journal of pediatrics 159:838-844.e831.

Gulinello M, Gertner M, Mendoza G, Schoenfeld BP, Oddo S, LaFerla F, Choi CH, McBride SMJ, Faber DS (2009) Validation of a 2-day water maze protocol in mice. Behavioural brain research 196:220-227.

Gwynn B, Lueders K, Sands MS, Birkenmeier EH (1998) Intracisternal A-particle element transposition into the murine beta-glucuronidase gene correlates with loss of enzyme activity: a new model for beta-glucuronidase deficiency in the C3H mouse. Molecular and cellular biology 18:6474-6481.

Hadaczek P, Forsayeth J, Mirek H, Munson K, Bringas J, Pivirotto P, McBride JL, Davidson BL, Bankiewicz KS (2009) Transduction of nonhuman primate brain with adeno-associated virus serotype 1: vector trafficking and immune response. Human gene therapy 20:225-237.

Haskins ME, Aguirre GD, Jezyk PF, Schuchman EH, Desnick RJ, Patterson DF (1991) Mucopolysaccharidosis type VII (Sly syndrome). Beta-glucuronidase-deficient mucopolysaccharidosis in the dog. The American journal of pathology 138:1553-1555.

Haskins ME, Desnick RJ, DiFerrante N, Jezyk PF, Patterson DF (1984) Beta-glucuronidase deficiency in a dog: a model of human mucopolysaccharidosis VII. Pediatric Research 18:980-984.

Hassan MI, Waheed A, Grubb JH, Klei HE, Korolev S, Sly WS (2013) High Resolution Crystal Structure of Human β-Glucuronidase Reveals Structural Basis of Lysosome Targeting. PLoS ONE 8:e79687.

Haurigot V, Marco S, Ribera A, Garcia M, Ruzo A, Villacampa P, Ayuso E, Añor S, Andaluz A, Pineda M, García-Fructuoso G, Molas M, Maggioni L, Muñoz S, Motas S, Ruberte J,

Mingozzi F, Pumarola M, Bosch F (2013) Whole body correction of mucopolysaccharidosis IIIA by intracerebrospinal fluid gene therapy. The Journal of clinical investigation 123:3254-3271.

Hauswirth WW, Aleman TS, Kaushal S, Cideciyan AV, Schwartz SB, Wang L, Conlon TJ, Boye SL, Flotte TR, Byrne BJ, Jacobson SG (2008) Treatment of leber congenital amaurosis due to RPE65 mutations by ocular subretinal injection of adeno-associated virus gene vector: short-term results of a phase I trial. Human gene therapy 19:979-990.

Hennig AK, Ogilvie JM, Ohlemiller KK, Timmers AM, Hauswirth WW, Sands MS (2004) AAV-mediated intravitreal gene therapy reduces lysosomal storage in the retinal pigmented epithelium and improves retinal function in adult MPS VII mice. Molecular therapy : the journal of the American Society of Gene Therapy 10:106-116.

Herati RS, Knox VW, O'donnell P, D'angelo M, Haskins ME, Ponder KP (2008) Radiographic evaluation of bones and joints in mucopolysaccharidosis I and VII dogs after neonatal gene therapy. Molecular Genetics and Metabolism 95:142-151.

Heuer GG, Passini MA, Jiang K, Parente MK, Lee VM-Y, Trojanowski JQ, Wolfe JH (2002) Selective neurodegeneration in murine mucopolysaccharidosis VII is progressive and reversible. Annals of neurology 52:762-770.

Hinderer C, Bell P, Gurda BL, Wang Q, Louboutin J-P, Zhu Y, Bagel J, O'donnell P, Sikora T, Ruane T, Wang P, Haskins ME, Wilson JM (2014) Intrathecal gene therapy corrects CNS pathology in a feline model of mucopolysaccharidosis I. Molecular Therapy 22:2018-2027.

Hirai T, Enomoto M, Kaburagi H, Sotome S, Yoshida-Tanaka K, Ukegawa M, Kuwahara H, Yamamoto M, Tajiri M, Miyata H, Hirai Y, Tominaga M, Shinomiya K, Mizusawa H, Okawa A, Yokota T (2014) Intrathecal AAV Serotype 9-mediated Delivery of shRNA Against TRPV1 Attenuates Thermal Hyperalgesia in a Mouse Model of Peripheral Nerve Injury. Molecular therapy : the journal of the American Society of Gene Therapy 22:409-419.

Hirt B (1967) Selective extraction of polyoma DNA from infected mouse cell cultures. Journal of molecular biology 26:365-369.

Homs J, Pagès G, Ariza L, Casas C, Chillón M, Navarro X, Bosch A (2014) Intrathecal administration of IGF-I by AAVrh10 improves sensory and motor deficits in a mouse model of diabetic neuropathy. Molecular Therapy — Methods & Clinical Development 1:7.

Hordeaux J, Dubreil L, Deniaud J, Iacobelli F, Moreau S, Ledevin M, Le Guiner C, Blouin V, Le Duff J, Mendes-Madeira A, Rolling F, Cherel Y, Moullier P, Colle M-A (2015) Efficient central nervous system AAVrh10-mediated intrathecal gene transfer in adult and neonate rats. 22:316-324.

Hu C, Busuttil RW, Lipshutz GS (2010) RH10 provides superior transgene expression in mice when compared with natural AAV serotypes for neonatal gene therapy. The Journal of Gene Medicine 12:766-778.

Huang L-Y, Halder S, Agbandje-McKenna M (2014) Parvovirus glycan interactions. Current Opinion in Virology 7:108-118.

Huynh HT, Grubb JH, Vogler C, Sly WS (2012) Biochemical evidence for superior correction of neuronal storage by chemically modified enzyme in murine mucopolysaccharidosis VII. Proceedings of the National Academy of Sciences of the United States of America 109:17022-17027.

Iliff JJ, Lee H, Yu M, Feng T, Logan J, Nedergaard M, Benveniste H (2013) Brain-wide pathway for waste clearance captured by contrast-enhanced MRI. The Journal of clinical investigation 123:1299-1309.

Iliff JJ, Wang M, Liao Y, Plogg BA, Peng W, Gundersen GA, Benveniste H, Vates GE, Deane R, Goldman SA, Nagelhus EA, Nedergaard M (2012) A Paravascular Pathway Facilitates CSF Flow Through the Brain Parenchyma and the Clearance of Interstitial Solutes, Including Amyloid Science Translational Medicine 4:147ra111-147ra111.

Imundo L, Leduc CA, Guha S, Brown M, Perino G, Gushulak L, Triggs-Raine B, Chung WK (2011) A complete deficiency of Hyaluronoglucosaminidase 1 (HYAL1) presenting as familial juvenile idiopathic arthritis. Journal of inherited metabolic disease 34:1013-1022.

Inagaki K, Fuess S, Storm TA, Gibson GA, Mctiernan CF, Kay MA, Nakai H (2006) Robust systemic transduction with AAV9 vectors in mice: efficient global cardiac gene transfer superior to that of AAV8. Molecular therapy 14:45-53.

Irani DN (2009) Cerebrospinal fluid in clinical practice. Philadelphia: Saunders/Elsevier.

Jain S, Drendel WB, Chen ZW, Mathews FS, Sly WS, Grubb JH (1996) Structure of human beta-glucuronidase reveals candidate lysosomal targeting and active-site motifs. Nature structural biology 3:375-381.

Jaski BE, Jessup ML, Mancini DM, Cappola TP, Pauly DF, Greenberg B, Borow K, Dittrich H, Zsebo KM, Hajjar RJ (2009) Calcium upregulation by percutaneous administration of gene therapy in cardiac disease (CUPID Trial), a first-in-human phase 1/2 clinical trial. Journal of cardiac failure 15:171-181.

Kamata Y, Tanabe A, Kanaji A, Kosuga M, Fukuhara Y, Li X-K, Suzuki S, Yamada M, Azuma N, Okuyama T (2003) Long-term normalization in the central nervous system, ocular manifestations, and skeletal deformities by a single systemic adenovirus injection into neonatal mice with mucopolysaccharidosis VII. Gene therapy 10:406-414.

Kanaji A, Kosuga M, Li XK, Fukuhara Y, Tanabe A, Kamata Y, Azuma N, Yamada M, Sakamaki T, Toyama Y, Okuyama T (2003) Improvement of skeletal lesions in mice with

mucopolysaccharidosis type VII by neonatal adenoviral gene transfer. Molecular therapy : the journal of the American Society of Gene Therapy 8:718-725.

Karda R, Buckley SMK, Mattar CN, Ng J, Massaro G, Hughes MP, Kurian MA, Baruteau J, Gissen P, Chan JKY, Bacchelli C, Waddington SN, Rahim AA (2014) Perinatal systemic gene delivery using adeno-associated viral vectors. Frontiers in Molecular Neuroscience 7:89.

Karolewski B, Wolfe J (2006) Genetic correction of the fetal brain increases the lifespan of mice with the severe multisystemic disease mucopolysaccharidosis type VII. Molecular Therapy 14:14-24.

Kaushik S, Cuervo AM (2012) Chaperone-mediated autophagy: a unique way to enter the lysosome world. Trends in Cell Biology 22:407-417.

Kim KH, Dodsworth C, Paras A, Burton BK (2013) High dose genistein aglycone therapy is safe in patients with mucopolysaccharidoses involving the central nervous system. Molecular Genetics and Metabolism 109:382-385.

Klein R, Dayton R, Leidenheimer N, Jansen K, Golde T, Zweig R (2006) Efficient Neuronal Gene Transfer with AAV8 Leads to Neurotoxic Levels of Tau or Green Fluorescent Proteins. Molecular Therapy 13:517-527.

Klein RL, Dayton RD, Tatom JB, Henderson KM, Henning PP (2007) AAV8, 9, Rh10, Rh43 Vector Gene Transfer in the Rat Brain: Effects of Serotype, Promoter and Purification Method. Molecular Therapy 16:89-96.

Kosuga M, Takahashi S, Sasaki K, Li X-K, Fujino M, Hamada H, Suzuki S, Yamada M, Matsuo N, Okuyama T (2000) Adenovirus-mediated gene therapy for mucopolysaccharidosis VII: involvement of cross-correction in wide-spread distribution of the gene products and long-term effects of CTLA-4Ig coexpression. Molecular therapy 1:406-413.

Kotterman MA, Schaffer DV (2014) Engineering adeno-associated viruses for clinical gene therapy. Nature Reviews Genetics 15:445-451.

Kumar M, Nasrallah IM, Kim S, Ittyerah R, Pickup S, Li J, Parente MK, Wolfe JH, Poptani H (2014) High-Resolution Magnetic Resonance Microscopy and Diffusion Tensor Imaging to Assess Brain Structural Abnormalities in the Murine Mucopolysaccharidosis VII Model. Journal of Neuropathology & Experimental Neurology 73:39-49.

Kyle JW, Birkenmeier EH, Gwynn B, Vogler C, Hoppe PC, Hoffmann JW, Sly WS (1990) Correction of murine mucopolysaccharidosis VII by a human beta-glucuronidase transgene. Proceedings of the National Academy of Sciences of the United States of America 87:3914-3918.

Lawlor PA, Bland RJ, Mouravlev A, Young D, During MJ (2009) Efficient Gene Delivery and Selective Transduction of Glial Cells in the Mammalian Brain by AAV Serotypes Isolated From Nonhuman Primates. Molecular Therapy 17:1692-1702.

LeBowitz JH, Grubb JH, Maga JA, Schmiel DH, Vogler C, Sly WS (2004) Glycosylation-independent targeting enhances enzyme delivery to lysosomes and decreases storage in mucopolysaccharidosis type VII mice. Proceedings of the National Academy of Sciences of the United States of America 101:3083-3088.

Lehman TJA, Miller N, Norquist B, Underhill L, Keutzer J (2011) Diagnosis of the mucopolysaccharidoses. Rheumatology 50 Suppl 5:v41-48.

Lieberman AP, Puertollano R, Raben N, Slaugenhaupt S, Walkley SU, Ballabio A (2012) Autophagy in lysosomal storage disorders. Autophagy 8:719-730.

Liu G, Chen YH, He X, Martins I, Heth JA, Chiorini JA, Davidson BL (2007) Adeno-associated Virus Type 5 Reduces Learning Deficits and Restores Glutamate Receptor Subunit Levels in MPS VII Mice CNS. Molecular Therapy 15:242-247.

Liu G, Martins I, Wemmie JA, Chiorini JA, Davidson BL (2005) Functional correction of CNS phenotypes in a lysosomal storage disease model using adeno-associated virus type 4 vectors. Journal of Neuroscience 25:9321-9327.

Loeb JE, Cordier WS, Harris ME, Weitzman MD, Hope TJ (1999) Enhanced expression of transgenes from adeno-associated virus vectors with the woodchuck hepatitis virus posttranscriptional regulatory element: implications for gene therapy. Human gene therapy 10:2295-2305.

Louis Jeune V, Joergensen JA, Hajjar RJ, Weber T (2013) Pre-existing Anti–Adeno-Associated Virus Antibodies as a Challenge in AAV Gene Therapy. Human Gene Therapy Methods 24:59-67.

Macsai CE, Derrick-Roberts ALK, Ding X, Zarrinkalam KH, Mcintyre C, Anderson PH, Anson DS, Byers S (2012) Skeletal response to lentiviral mediated gene therapy in a mouse model of MPS VII. Molecular Genetics and Metabolism 106:202-213.

Malinová V, Wegrzyn G, Narajczyk M (2012) The use of elevated doses of genistein-rich soy extract in the gene expression-targeted isoflavone therapy for Sanfilippo disease patients. JIMD reports 5:21-25.

Malinowska M, Wilkinson FL, Langford-Smith KJ, Langford-Smith A, Brown JR, Crawford BE, Vanier MT, Grynkiewicz G, Wynn RF, Wraith JE, Wegrzyn G, Bigger BW (2010) Genistein Improves Neuropathology and Corrects Behaviour in a Mouse Model of Neurodegenerative Metabolic Disease. PLoS ONE 5:e14192.

Mango RL, Xu L, Sands MS, Vogler C, Seiler G, Schwarz T, Haskins ME, Ponder KP (2004) Neonatal retroviral vector-mediated hepatic gene therapy reduces bone, joint, and

cartilage disease in mucopolysaccharidosis VII mice and dogs. Molecular Genetics and Metabolism 82:4-19.

Manno CS, Pierce GF, Arruda VR, Glader B, Ragni M, Rasko JJE, Ozelo MC, Hoots K, Blatt P, Konkle B, Dake M, Kaye R, Razavi M, Zajko A, Zehnder J, Rustagi PK, Nakai H, Chew A, Leonard D, Wright JF, Lessard RR, Sommer JM, Tigges M, Sabatino D, Luk A, Jiang H, Mingozzi F, Couto L, Ertl HC, High KA, Kay MA (2006) Successful transduction of liver in hemophilia by AAV-Factor IX and limitations imposed by the host immune response. Nature medicine 12:342-347.

Maréchal V, Naffakh N, Danos O, Heard JM (1993) Disappearance of lysosomal storage in spleen and liver of mucopolysaccharidosis VII mice after transplantation of genetically modified bone marrow cells. Blood 82:1358-1365.

Masamizu Y, Okada T, Kawasaki K, Ishibashi H, Yuasa S, Takeda S, Hasegawa I, Nakahara K (2011) Local and retrograde gene transfer into primate neuronal pathways via adeno-associated virus serotype 8 and 9. Neuroscience 193:249-258.

Masat E, Pavani G, Mingozzi F (2013) Humoral Immunity to AAV Vectors in Gene Therapy: Challenges and Potential Solutions. Discovery Medicine.

Mattar CN, Waddington SN, Biswas A, Johana N, Ng XW, Fisk AS, Fisk NM, Tan LG, Rahim AA, Buckley SMK, Tan MH, Lu J, Choolani M, Chan JKY (2012) Systemic delivery of scAAV9 in fetal macaques facilitates neuronal transduction of the central and peripheral nervous systems. Gene therapy 20:69-83.

McCarty DM, Young SM, Jr., Samulski RJ (2004) Integration of adeno-associated virus (AAV) and recombinant AAV vectors. Annual review of genetics 38:819-845.

McCurdy VJ, Rockwell HE, Arthur JR, Bradbury AM, Johnson AK, Randle AN, Brunson BL, Hwang M, Gray-Edwards HL, Morrison NE, Johnson JA, Baker HJ, Cox NR, Seyfried TN, Sena-Esteves M, Martin DR (2015) Widespread correction of central nervous system disease after intracranial gene therapy in a feline model of Sandhoff disease. Gene Therapy 22:181-189.

McNeil PL, Kirchhausen T (2005) An emergency response team for membrane repair. Nature reviews Molecular cell biology 6:499-505.

Mehta AB, Winchester B (2012) Lysosomal storage disorders : a practical guide. Oxford: Wiley-Blackwell.

Meyer K, Ferraiuolo L, Schmelzer L, Braun L, McGovern V, Likhite S, Michels O, Govoni A, Fitzgerald J, Morales P, Foust KD, Mendell JR, Burghes AHM, Kaspar BK (2015) Improving Single Injection CSF Delivery of AAV9-mediated Gene Therapy for SMA: A Dose–response Study in Mice and Nonhuman Primates. Molecular Therapy 23:477-487.

Mingozzi F, High KA (2013) Immune responses to AAV vectors: overcoming barriers to successful gene therapy. Blood 122:23-36.

Miyazaki J, Takaki S, Araki K, Tashiro F, Tominaga A, Takatsu K, Yamamura K (1989) Expression vector system based on the chicken beta-actin promoter directs efficient production of interleukin-5. Gene 79:269-277.

Montaño AM, Oikawa H, Tomatsu S, Nishioka T, Vogler C, Gutierrez MA, Oguma T, Tan Y, Grubb JH, Dung VC, Ohashi A, Miyamoto K-I, Orii T, Yoneda Y, Sly WS (2008) Acidic amino acid tag enhances response to enzyme replacement in mucopolysaccharidosis type VII mice. Molecular Genetics and Metabolism 94:178-189.

Moullier P, Bohl D, Heard JM, Danos O (1993) Correction of lysosomal storage in the liver and spleen of MPS VII mice by implantation of genetically modified skin fibroblasts. Nature genetics 4:154-159.

Muenzer J (2014) Early initiation of enzyme replacement therapy for the mucopolysaccharidoses. Molecular Genetics and Metabolism 111:63-72.

Mullen RJ, Buck CR, Smith AM (1992) NeuN, a neuronal specific nuclear protein in vertebrates. Development 116:201-211.

Murlidharan G, Samulski RJ, Asokan A (2014) Biology of adeno-associated viral vectors in the central nervous system. Frontiers in Molecular Neuroscience 7:76.

Murrey DA, Naughton BJ, Duncan FJ, Meadows AS, Ware TA, Campbell KJ, Bremer WG, Walker CM, Goodchild L, Bolon B, La Perle K, Flanigan KM, McBride KL, McCarty DM, Fu H (2014) Feasibility and Safety of Systemic rAAV9-h NAGLUDelivery for Treating Mucopolysaccharidosis IIIB: Toxicology, Biodistribution, and Immunological Assessments in Primates. Human Gene Therapy Clinical Development 25:72-84.

Nathwani AC, Rosales C, McIntosh J, Rastegarlari G, Nathwani D, Raj D, Nawathe S, Waddington SN, Bronson R, Jackson S, Donahue RE, High KA, Mingozzi F, Ng CY, Zhou J, Spence Y, McCarville MB, Valentine M, Allay J, Coleman J, Sleep S, Gray JT, Nienhuis AW, Davidoff AM (2011a) Long-term Safety and Efficacy Following Systemic Administration of a Self-complementary AAV Vector Encoding Human FIX Pseudotyped With Serotype 5 and 8 Capsid Proteins. Molecular Therapy 19:876-885.

Nathwani AC, Tuddenham EGD, Rangarajan S, Rosales C, McIntosh J, Linch DC, Chowdary P, Riddell A, Pie AJ, Harrington C, O'Beirne J, Smith K, Pasi J, Glader B, Rustagi P, Ng CYC, Kay MA, Zhou J, Spence Y, Morton CL, Allay J, Coleman J, Sleep S, Cunningham JM, Srivastava D, Basner-Tschakarjan E, Mingozzi F, High KA, Gray JT, Reiss UM, Nienhuis AW, Davidoff AM (2011b) Adenovirus-associated virus vector-mediated gene transfer in hemophilia B. The New England journal of medicine 365:2357-2365.

National Library of Medicine (U.S.) (1998) MedlinePlus. Bethesda, Md.: U.S. National Library of Medicine,.

Natowicz MR, Short MP, Wang Y, Dickersin GR, Gebhardt MC, Rosenthal DI, Sims KB, Rosenberg AE (1996) Clinical and biochemical manifestations of hyaluronidase deficiency. The New England journal of medicine 335:1029-1033.

Noh H, Lee JI (2014) Current and potential therapeutic strategies for mucopolysaccharidoses. Journal of Clinical Pharmacy and Therapeutics 39:215-224.

O'Connor LH, Erway LC, Vogler CA, Sly WS, Nicholes A, Grubb J, Holmberg SW, Levy B, Sands MS (1998) Enzyme replacement therapy for murine mucopolysaccharidosis type VII leads to improvements in behavior and auditory function. The Journal of clinical investigation 101:1394-1400.

Ohashi T, Watabe K, Uehara K, Sly WS, Vogler C, Eto Y (1997) Adenovirus-mediated gene transfer and expression of human beta-glucuronidase gene in the liver, spleen, and central nervous system in mucopolysaccharidosis type VII mice. Proceedings of the National Academy of Sciences of the United States of America 94:1287-1292.

Ojala DS, Amara DP, Schaffer DV (2015) Adeno-Associated Virus Vectors and Neurological Gene Therapy. The Neuroscientist 21:84-98.

Oshima A, Kyle JW, Miller RD, Hoffmann JW, Powell PP, Grubb JH, Sly WS, Tropak M, Guise KS, Gravel RA (1987) Cloning, sequencing, and expression of cDNA for human beta-glucuronidase. Proceedings of the National Academy of Sciences of the United States of America 84:685-689.

Palmucci S, Attinà G, Lanza ML, Belfiore G, Cappello G, Foti PV, Milone P, Di Bella D, Barone R, Fiumara A, Sorge G, Ettorre GC (2013) Imaging findings of mucopolysaccharidoses: a pictorial review. Insights into imaging 4:443-459.

Pañeda A, Vanrell L, Mauleon I, Crettaz JS, Berraondo P, Timmermans EJ, Beattie SG, Twisk J, van Deventer S, Prieto J, Fontanellas A, Rodriguez-Pena MS, Gonzalez-Aseguinolaza G (2009) Effect of adeno-associated virus serotype and genomic structure on liver transduction and biodistribution in mice of both genders. Human gene therapy 20:908-917.

Parente MK, Rozen R, Cearley CN, Wolfe JH (2012) Dysregulation of Gene Expression in a Lysosomal Storage Disease Varies between Brain Regions Implicating Unexpected Mechanisms of Neuropathology. PLoS ONE 7:e32419.

Passini MA, Bu J, Richards AM, Treleaven CM, Sullivan JA, O'Riordan CR, Scaria A, Kells AP, Samaranch L, San Sebastian W, Federici T, Fiandaca MS, Boulis NM, Bankiewicz KS, Shihabuddin LS, Cheng SH (2014) Translational Fidelity of Intrathecal Delivery of Self-Complementary AAV9–Survival Motor Neuron 1 for Spinal Muscular Atrophy. Human gene therapy 25:619-630.

Passini MA, Lee EB, Heuer GG, Wolfe JH (2002) Distribution of a lysosomal enzyme in the adult brain by axonal transport and by cells of the rostral migratory stream. Journal of Neuroscience 22:6437-6446.

Passini MA, Watson DJ, Vite CH, Landsburg DJ, Feigenbaum AL, Wolfe JH (2003) Intraventricular brain injection of adeno-associated virus type 1 (AAV1) in neonatal mice results in complementary patterns of neuronal transduction to AAV2 and total long-term correction of storage lesions in the brains of beta-glucuronidase-deficient mice. Journal of Virology 77:7034-7040.

Passini MA, Wolfe JH (2001) Widespread Gene Delivery and Structure-Specific Patterns of Expression in the Brain after Intraventricular Injections of Neonatal Mice with an Adeno-Associated Virus Vector. Journal of Virology 75:12382-12392.

Peden CS, Burger C, Muzyczka N, Mandel RJ (2004) Circulating anti-wild-type adeno-associated virus type 2 (AAV2) antibodies inhibit recombinant AAV2 (rAAV2)-mediated, but not rAAV5-mediated, gene transfer in the brain. Journal of Virology 78:6344-6359.

Piedra J, Ontiveros M, Miravet S, Penalva C, Monfar M, Chillón M (2015) Development of a Rapid, Robust, and Universal PicoGreen-Based Method to Titer Adeno-Associated Vectors. Human Gene Therapy Methods 26:35-42.

Piotrowska E, Jakobkiewicz-Banecka J, Maryniak A, Tylki-Szymanska A, Puk E, Liberek A, Wegrzyn A, Czartoryska B, Slominska-Wojewodzka M, Wegrzyn G (2011) Two-year follow-up of Sanfilippo Disease patients treated with a genistein-rich isoflavone extract: assessment of effects on cognitive functions and general status of patients. Medical science monitor : international medical journal of experimental and clinical research 17:CR196-202.

Platt FM, Boland B, van der Spoel AC (2012) The cell biology of disease: lysosomal storage disorders: the cellular impact of lysosomal dysfunction. The Journal of cell biology 199:723-734.

Ponder KP, Melniczek JR, Xu L, Weil MA, O'malley TM, O'donnell PA, Knox VW, Aguirre GD, Mazrier H, Ellinwood NM, Sleeper M, Maguire AM, Volk SW, Mango RL, Zweigle J, Wolfe JH, Haskins ME (2002) Therapeutic neonatal hepatic gene therapy in mucopolysaccharidosis VII dogs. Proceedings of the National Academy of Sciences of the United States of America 99:13102-13107.

Prasad VK, Kurtzberg J (2010) Transplant Outcomes in Mucopolysaccharidoses. Seminars in Hematology 47:59-69.

Quiney FRE, Amirfeyz R, Smithson S, Gargan M, Monsell F (2012) The mucopolysaccaridoses. Orthopaedics and Trauma 26:60-63.

Rahim AA, Wong AMS, Hoefer K, Buckley SMK, Mattar CN, Cheng SH, Chan JKY, Cooper JD, Waddington SN (2011) Intravenous administration of AAV2/9 to the fetal and neonatal mouse leads to differential targeting of CNS cell types and extensive transduction of the nervous system. The FASEB Journal 25:3505-3518.

Ribera A, Haurigot V, Garcia M, Marco S, Motas S, Villacampa P, Maggioni L, Leon X, Molas M, Sanchez V, Munoz S, Leborgne C, Moll X, Pumarola M, Mingozzi F, Ruberte J, Anor S, Bosch F (2015) Biochemical, histological and functional correction of mucopolysaccharidosis Type IIIB by intra-cerebrospinal fluid gene therapy. Human Molecular Genetics 24:2078-2095.

Richard M, Arfi A, Seguin J, Gandolphe C, Scherman D (2009) Widespread biochemical correction of murine mucopolysaccharidosis type VII pathology by liver hydrodynamic plasmid delivery. 16:746-756.

Roberts S, Evans H, Trivedi J, Menage J (2006) Histology and pathology of the human intervertebral disc. The Journal of bone and joint surgery American volume 88 Suppl 2:10-14.

Rogers DC, Fisher EM, Brown SD, Peters J, Hunter AJ, Martin JE (1997) Behavioral and functional analysis of mouse phenotype: SHIRPA, a proposed protocol for comprehensive phenotype assessment. Mammalian genome : official journal of the International Mammalian Genome Society 8:711-713.

Rosenberg JB, Sondhi D, Rubin DG, Monette S, Chen A, Cram S, De BP, Kaminsky SM, Sevin C, Aubourg P, Crystal RG (2014) Comparative Efficacy and Safety of Multiple Routes of Direct CNS Administration of Adeno-Associated Virus Gene Transfer Vector Serotype rh.10 Expressing the Human Arylsulfatase A cDNA to Nonhuman Primates. Human Gene Therapy Clinical Development 25:164-177.

Ross CJD, Twisk J, Bakker AC, Miao F, Verbart D, Rip J, Godbey T, Dijkhuizen P, Hermens WTJMC, Kastelein JJP, Kuivenhoven JA, Meulenberg JM, Hayden MR (2006) Correction of feline lipoprotein lipase deficiency with adeno-associated virus serotype 1-mediated gene transfer of the lipoprotein lipase S447X beneficial mutation. Human gene therapy 17:487-499.

Rowan DJ, Tomatsu S, Grubb JH, Haupt B, Montaño AM, Oikawa H, Sosa AC, Chen A, Sly WS (2012a) Long circulating enzyme replacement therapy rescues bone pathology in mucopolysaccharidosis VII murine model. Molecular Genetics and Metabolism 107:161-172.

Rowan DJ, Tomatsu S, Grubb JH, Montaño AM, Sly WS (2012b) Assessment of bone dysplasia by micro-CT and glycosaminoglycan levels in mouse models for mucopolysaccharidosis type I, IIIA, IVA, and VII. Journal of inherited metabolic disease 36:235-246.

Rubin LL, Staddon JM (1999) The cell biology of the blood-brain barrier. Annual review of neuroscience 22:11-28.

Rudick RA, Zirretta DK, Herndon RM (1982) Clearance of albumin from mouse subarachnoid space: a measure of CSF bulk flow. Journal of neuroscience methods 6:253-259.

Ruzo A, García M, Ribera A, Villacampa P, Haurigot V, Marco S, Ayuso E, Anguela XM, Roca C, Agudo J, Ramos D, Ruberte J, Bosch F (2009) Liver Production of Sulfamidase Reverses Peripheral and Ameliorates CNS Pathology in Mucopolysaccharidosis IIIA Mice. Molecular therapy 20:254-266.

Ruzo A, Marco S, García M, Villacampa P, Ribera A, Ayuso E, Maggioni L, Mingozzi F, Haurigot V, Bosch F (2012) Correction of pathological accumulation of glycosaminoglycans in central nervous system and peripheral tissues of MPSIIIA mice through systemic AAV9 gene transfer. Human gene therapy 23:1237-1246.

Saftig P, Klumperman J (2009) Lysosome biogenesis and lysosomal membrane proteins: trafficking meets function. Nature reviews Molecular cell biology 10:623-635.

Sakurai K, Iizuka S, Shen J-S, Meng X-L, Mori T, Umezawa A, Ohashi T, Eto Y (2004) Brain transplantation of genetically modified bone marrow stromal cells corrects CNS pathology and cognitive function in MPS VII mice. Gene therapy 11:1475-1481.

Samaranch L, Salegio EA, San Sebastian W, Kells AP, Bringas JR, Forsayeth J, Bankiewicz KS (2013a) Strong Cortical and Spinal Cord Transduction After AAV7 and AAV9 Delivery into the Cerebrospinal Fluid of Nonhuman Primates. Human gene therapy 24:526-532.

Samaranch L, Salegio EA, San Sebastian W, Kells AP, Foust KD, Bringas JR, Lamarre C, Forsayeth J, Kaspar BK, Bankiewicz KS (2012) Adeno-Associated Virus Serotype 9 Transduction in the Central Nervous System of Nonhuman Primates. Human gene therapy 23:382-389.

Samaranch L, Sebastian WS, Kells AP, Salegio EA, Heller G, Bringas JR, Pivirotto P, DeArmond S, Forsayeth J, Bankiewicz KS (2013b) AAV9-mediated Expression of a Non-self Protein in Nonhuman Primate Central Nervous System Triggers Widespread Neuroinflammation Driven by Antigen-presenting Cell Transduction. Molecular Therapy 22:329-337.

Sammarco C, Weil M, Just C, Weimelt S, Hasson C, O'Malley T, Evans SM, Wang P, Casal ML, Wolfe J, Haskins M (2000) Effects of bone marrow transplantation on the cardiovascular abnormalities in canine mucopolysaccharidosis VII. Bone marrow transplantation 25:1289-1297.

Sands MS, Barker JE, Vogler C, Levy B, Gwynn B, Galvin N, Sly WS, Birkenmeier E (1993) Treatment of murine mucopolysaccharidosis type VII by syngeneic bone marrow transplantation in neonates. Lab Invest 68:676-686.

Sands MS, Vogler C, Kyle JW, Grubb JH, Levy B, Galvin N, Sly WS, Birkenmeier EH (1994) Enzyme replacement therapy for murine mucopolysaccharidosis type VII. The Journal of clinical investigation 93:2324-2331.

Sanftner LM, Suzuki BM, Doroudchi MM, Feng L, McClelland A, Forsayeth JR, Cunningham J (2004) Striatal delivery of rAAV-hAADC to rats with preexisting immunity to AAV. Molecular therapy 9:403-409.

Sasisekharan R, Raman R, Prabhakar V (2006) Glycomics approach to structure-function relationships of glycosaminoglycans. Annual Review of Biomedical Engineering 8:181-231.

Schuster DJ, Dykstra JA, Riedl MS, Kitto KF, Belur LR, McIvor RS, Elde RP, Fairbanks CA, Vulchanova L (2014) Biodistribution of adeno-associated virus serotype 9 (AAV9) vector after intrathecal and intravenous delivery in mouse. Frontiers in neuroanatomy 8:42.

Schwartz C, Stanislovitis P, Phelan M, Klinger K, Taylor H, Stevenson R (1991) Deletion mapping of plasminogen activator inhibitor, type I (PLANH1) and beta-glucuronidase (GUSB) in 7q21----q22. Cytogenet Cell Genet 56:152-153.

Scriver CR, Childs B, Kinzler KW, Vogelstein B (2001) The metabolic & molecular bases of inherited disease. New York, N.Y. ; London: McGraw-Hill.

Serratrice N, Cubizolle A, Ibanes S, Mestre-Francés N, Bayo-Puxan N, Creyssels S, Gennetier A, Bernex F, Verdier J-M, Haskins ME, Couderc G, Malecaze F, Kalatzis V, Kremer EJ (2014) Corrective GUSB transfer to the canine mucopolysaccharidosis VII cornea using a helper-dependent canine adenovirus vector. Journal of Controlled Release 181:22-31.

Shen S, Bryant KD, Brown SM, Randell SH, Asokan A (2011) Terminal N-Linked Galactose Is the Primary Receptor for Adeno-associated Virus 9. Journal of Biological Chemistry 286:13532-13540.

Shipley JM, Grubb JH, Sly WS (1993) The role of glycosylation and phosphorylation in the expression of active human beta-glucuronidase. The Journal of biological chemistry 268:12193-12198.

Silverstein Dombrowski DC, Carmichael KP, Wang P, O'Malley TM, Haskins ME, Giger U (2004) Mucopolysaccharidosis type VII in a German Shepherd Dog. Journal of the American Veterinary Medical Association 224:553-557- 532-553.

Sleeper MM, Fornasari B, Ellinwood NM, Weil MA, Melniczek J, O'Malley TM, Sammarco CD, XU L, Ponder KP, Haskins ME (2004) Gene therapy ameliorates cardiovascular disease in dogs with mucopolysaccharidosis VII. Circulation 110:815-820.

Sly WS, Quinton BA, McAlister WH, Rimoin DL (1973) Beta glucuronidase deficiency: report of clinical, radiologic, and biochemical features of a new mucopolysaccharidosis. The Journal of pediatrics 82:249-257.

Sly WS, Vogler C, Grubb JH, Zhou M, Jiang J, Zhou XY, Tomatsu S, Bi Y, Snella EM (2001) Active site mutant transgene confers tolerance to human beta-glucuronidase without affecting the phenotype of MPS VII mice. Proceedings of the National Academy of Sciences of the United States of America 98:2205-2210.

Smith LJ, Baldo G, Wu S, Liu Y, Whyte MP, Giugliani R, Elliott DM, Haskins ME, Ponder KP (2012a) Pathogenesis of lumbar spine disease in mucopolysaccharidosis VII. Molecular Genetics and Metabolism 107:153-160.

Smith LJ, Martin JT, O'Donnell P, Wang P, Elliott DM, Haskins ME, Ponder KP (2012b) Effect of neonatal gene therapy on lumbar spine disease in mucopolysaccharidosis VII dogs. Molecular Genetics and Metabolism 107:145-152.

Smith LJ, Martin JT, Szczesny SE, Ponder KP, Haskins ME, Elliott DM (2010) Altered lumbar spine structure, biochemistry, and biomechanical properties in a canine model of mucopolysaccharidosis type VII. Journal of Orthopaedic Research 28:616-622.

Snyder BR, Gray SJ, Quach ET, Huang JW, Leung CH, Samulski RJ, Boulis NM, Federici T (2011) Comparison of adeno-associated viral vector serotypes for spinal cord and motor neuron gene delivery. Human gene therapy 22:1129-1135.

Snyder EY, Taylor RM, Wolfe JH (1995) Neural progenitor cell engraftment corrects lysosomal storage throughout the MPS VII mouse brain. Nature 374:367-370.

Sofroniew MV, Vinters HV (2009) Astrocytes: biology and pathology. Acta Neuropathologica 119:7-35.

Sondhi D, Johnson L, Purpura K, Monette S, Souweidane MM, Kaplitt MG, Kosofsky B, Yohay K, Ballon D, Dyke J, Kaminksy SM, Hackett NR, Crystal RG (2012) Long-Term Expression and Safety of Administration of AAVrh.10hCLN2 to the Brain of Rats and Nonhuman Primates for the Treatment of Late Infantile Neuronal Ceroid Lipofuscinosis. Human Gene Therapy Methods 23:324-335.

Sonntag F, Schmidt K, Kleinschmidt JA (2010) A viral assembly factor promotes AAV2 capsid formation in the nucleolus. Proceedings of the National Academy of Sciences of the United States of America 107:10220-10225.

Soper BW, Lessard MD, Vogler CA, Levy B, Beamer WG, Sly WS, Barker JE (2001) Nonablative neonatal marrow transplantation attenuates functional and physical defects of beta-glucuronidase deficiency. Blood 97:1498-1504.

Soper BW, Pung AW, Vogler CA, Grubb JH, Sly WS, Barker JE (1999) Enzyme Replacement Therapy Improves Reproductive Performance in Mucopolysaccharidosis Type VII Mice But Does Not Prevent Postnatal Losses. Pediatric Research 45:180-186.

Speleman F, Vervoort R, van Roy N, Liebaers I, Sly W, Lissens W (1996) Localization by fluorescence in situ hybridization of the human functional beta-glucuronidase gene (GUSB) to 7q11.21 --> q11.22 and two pseudogenes to 5p13 and 5q13. Cytogenet Cell Genet 72:53-55.

Stein CS, Ghodsi A, Derksen T, Davidson BL (1999) Systemic and central nervous system correction of lysosomal storage in mucopolysaccharidosis type VII mice. Journal of Virology 73:3424-3429.

Stewart PA, Hayakawa EM (1987) Interendothelial junctional changes underlie the developmental tightening of the blood-brain barrier. Brain Research 429:271-281.

Storek B, Reinhardt M, Wang C, Janssen WGM, Harder NM, Banck MS, Morrison JH, Beutler AS (2008) Sensory neuron targeting by self-complementary AAV8 via lumbar puncture for chronic pain. Proceedings of the National Academy of Sciences of the United States of America 105:1055-1060.

Stroes ES, Nierman MC, Meulenberg JJ, Franssen R, Twisk J, Henny CP, Maas MM, Zwinderman AH, Ross C, Aronica E, High KA, Levi MM, Hayden MR, Kastelein JJ, Kuivenhoven JA (2008) Intramuscular administration of AAV1-lipoprotein lipase S447X lowers triglycerides in lipoprotein lipase-deficient patients. Arteriosclerosis, thrombosis, and vascular biology 28:2303-2304.

Sun-Wada G-H, Wada Y, Futai M (2003) Lysosome and lysosome-related organelles responsible for specialized functions in higher organisms, with special emphasis on vacuolar-type proton ATPase. Cell structure and function 28:455-463.

Swain GP, Prociuk M, Bagel JH, O'Donnell P, Berger K, Drobatz K, Gurda BL, Haskins ME, Sands MS, Vite CH (2014) Adeno-associated virus serotypes 9 and rh10 mediate strong neuronal transduction of the dog brain. Gene therapy 21:28-36.

Tardieu M, Zérah M, Husson B, de Bournonville S, Deiva K, Adamsbaum C, Vincent F, Hocquemiller M, Broissand C, Furlan V, Ballabio A, Fraldi A, Crystal RG, Baugnon T, Roujeau T, Heard J-M, Danos O (2014) Intracerebral Administration of Adeno-Associated Viral Vector Serotype rh.10 Carrying Human SGSHand SUMF1cDNAs in Children with Mucopolysaccharidosis Type IIIA Disease: Results of a Phase I/II Trial. Human gene therapy 25:506-516.

Taylor RM, Wolfe JH (1997) Decreased lysosomal storage in the adult MPS VII mouse brain in the vicinity of grafts of retroviral vector-corrected fibroblasts secreting high levels of beta-glucuronidase. Nature medicine 3:771-774.

Thwaite R, Pages G, Chillon M, Bosch A (2015) AAVrh.10 immunogenicity in mice and humans. Relevance of antibody cross-reactivity in human gene therapy. Gene Ther 22:196-201.

Tomatsu S, Monta O AM, Dung VC, Grubb JH, Sly WS (2009) Mutations and polymorphisms in GUSB gene in mucopolysaccharidosis VII (Sly Syndrome). Human Mutation 30:511-519.

Tomatsu S, Orii KO, Vogler C, Jeffrey H Grubb EMS, Gutierrez M, Sly TDCHKSOKS (2003) Production of MPS VII mouse (Gustm(hE540AmE536A)Sly) doubly tolerant to human and mouse b-glucuronidase. Human Molecular Genetics 12:961-973.

Towne C, Pertin M, Beggah AT, Aebischer P, Decosterd I (2009) Recombinant adeno-associated virus serotype 6 (rAAV2/6)-mediated gene transfer to nociceptive neurons through different routes of delivery. Molecular Pain 5:52.

Treleaven CM, Tamsett TJ, Bu J, Fidler JA, Sardi SP, Hurlbut GD, Woodworth LA, Cheng SH, Passini MA, Shihabuddin LS, Dodge JC (2012) Gene Transfer to the CNS Is Efficacious in Immune-primed Mice Harboring Physiologically Relevant Titers of Anti-AAV Antibodies. Molecular Therapy 20:1713-1723.

Triggs-Raine B, Salo TJ, Zhang H, Wicklow BA, Natowicz MR (1999) Mutations in HYAL1, a member of a tandemly distributed multigene family encoding disparate hyaluronidase activities, cause a newly described lysosomal disorder, mucopolysaccharidosis IX. Proceedings of the National Academy of Sciences of the United States of America 96:6296-6300.

Valayannopoulos V, Wijburg FA (2011) Therapy for the mucopolysaccharidoses. Rheumatology 50:v49-v59.

Van Dorpe J, Moerman P, Pecceu A, Van den Steen P, Fryns JP (1996) Non-immune hydrops fetalis caused by beta-glucuronidase deficiency (mucopolysaccharidosis VII). Study of a family with 3 affected siblings. Genetic counseling 7:105-112.

Varki A (2009) Essentials of glycobiology. Cold Spring Harbor, N.Y.: Cold Spring Harbor Laboratory Press.

Vitry S, Bruyère J, Hocquemiller M, Bigou S, Ausseil J, Colle M-A, Prévost M-C, Heard J-M (2010) Storage Vesicles in Neurons Are Related to Golgi Complex Alterations in Mucopolysaccharidosis IIIB. The American journal of pathology 177:2984-2999.

Vogler C, Birkenmeier EH, Sly WS, Levy B, Pegors C, Kyle JW, Beamer WG (1990) A murine model of mucopolysaccharidosis VII. Gross and microscopic findings in beta-glucuronidase-deficient mice. The American journal of pathology 136:207-217.

Vogler C, Levy B, Galvin N, Lessard M, Soper B, Barker J (2005a) Early Onset of Lysosomal Storage Disease in a Murine Model of Mucopolysaccharidosis Type VII: Undegraded Substrate Accumulates in Many Tissues in the Fetus and Very Young MPS VII Mouse. Pediatric and Developmental Pathology 8:453-462.

Vogler C, Levy B, Galvin N, Sands MS, Birkenmeier EH, Sly WS, Barker J (2001) A novel model of murine mucopolysaccharidosis type VII due to an intracisternal a particle element

transposition into the beta-glucuronidase gene: clinical and pathologic findings. Pediatric Research 49:342-348.

Vogler C, Levy B, Galvin NJ, Thorpe C, Sands MS, Barker JE, Baty J, Birkenmeier EH, Sly WS (1999) Enzyme Replacement in Murine Mucopolysaccharidosis Type VII: Neuronal and Glial Response to β-Glucuronidase Requires Early Initiation of Enzyme Replacement Therapy. Pediatric Research 45:838-844.

Vogler C, Levy B, Grubb JH, Galvin N, Tan Y, Kakkis E, Pavloff N, Sly WS (2005b) Overcoming the blood-brain barrier with high-dose enzyme replacement therapy in murine mucopolysaccharidosis VII. Proceedings of the National Academy of Sciences of the United States of America 102:14777-14782.

Vogler C, Sands MS, Levy B, Galvin N, Birkenmeier EH, Sly WS (1996) Enzyme Replacement with Recombinant β-Glucuronidase in Murine Mucopolysaccharidosis Type VII: Impact of Therapy during the First Six Weeks of Life on Subsequent Lysosomal Storage, Growth, and Survival. Pediatric Research 39:1050-1054.

Vulchanova L, Schuster DJ, Belur LR, Riedl MS, Podetz-Pedersen KM, Kitto KF, Wilcox GL, McIvor RS, Fairbanks CA (2010) Differential adeno-associated virus mediated gene transfer to sensory neurons following intrathecal delivery by direct lumbar puncture. Molecular Pain 6:31.

Wang B, O'malley TM, Xu L, Vite C, Wang P, O'donnell PA, Ellinwood NM, Haskins ME, Ponder KP (2006) Expression in blood cells may contribute to biochemical and pathological improvements after neonatal intravenous gene therapy for mucopolysaccharidosis VII in dogs. Molecular Genetics and Metabolism 87:8-21.

Wang H, Yang B, Qiu L, Yang C, Kramer J, Su Q, Guo Y, Brown RH, Gao G, Xu Z (2014) Widespread spinal cord transduction by intrathecal injection of rAAV delivers efficacious RNAi therapy for amyotrophic lateral sclerosis. Human Molecular Genetics 23:668-681.

Wang WC, Lee N, Aoki D, Fukuda MN, Fukuda M (1991) The poly-N-acetyllactosamines attached to lysosomal membrane glycoproteins are increased by the prolonged association with the Golgi complex. The Journal of biological chemistry 266:23185-23190.

Watson GL, Sayles JN, Chen C, Elliger SS, Elliger CA, Raju NR, Kurtzman GJ, Podsakoff GM (1998) Treatment of lysosomal storage disease in MPS VII mice using a recombinant adeno-associated virus. Gene therapy 5:1642-1649.

Watts C (2012) The endosome-lysosome pathway and information generation in the immune system. Biochimica et biophysica acta 1824:14-21.

Wilkinson FL, Holley RJ, Langford-Smith KJ, Badrinath S, Liao A, Langford-Smith A, Cooper JD, Jones SA, Wraith JE, Wynn RF, Merry CLR, Bigger BW (2012) Neuropathology in Mouse Models of Mucopolysaccharidosis Type I, IIIA and IIIB. PLoS ONE 7:e35787.

Wolf DA, Lenander AW, Nan Z, Belur LR, Whitley CB, Gupta P, Low WC, McIvor RS (2011) Direct gene transfer to the CNS prevents emergence of neurologic disease in a murine model of mucopolysaccharidosis type I. Neurobiology of Disease 43:123-133.

Wolfe JH, Sands MS, Barker JE, Gwynn B, Rowe LB, Vogler CA, Birkenmeier EH (1992) Reversal of pathology in murine mucopolysaccharidosis type VII by somatic cell gene transfer. Nature 360:749-753.

Xiao X, Li J, McCown TJ, Samulski RJ (1997) Gene transfer by adeno-associated virus vectors into the central nervous system. Experimental Neurology 144:113-124.

Xing EM, Knox VW, O'donnell PA, Sikura T, Liu Y, Wu S, Casal ML, Haskins ME, Ponder KP (2013) The Effect of Neonatal Gene Therapy on Skeletal Manifestations in Mucopolysaccharidosis VII Dogs after a Decade. Molecular Genetics and Metabolism 109:183-193.

Xu L, Haskins ME, Melniczek JR, Gao C, Weil MA, O'malley TM, O'donnell PA, Mazrier H, Ellinwood NM, Zweigle J, Wolfe JH, Ponder KP (2002a) Transduction of hepatocytes after neonatal delivery of a Moloney murine leukemia virus based retroviral vector results in long-term expression of beta-glucuronidase in mucopolysaccharidosis VII dogs. Molecular therapy : the journal of the American Society of Gene Therapy 5:141-153.

Xu L, Mango RL, Sands MS, Haskins ME, Ellinwood NM, Ponder KP (2002b) Evaluation of pathological manifestations of disease in mucopolysaccharidosis VII mice after neonatal hepatic gene therapy. Molecular Therapy 6:745-758.

Yamada Y, Kato K, Sukegawa K, Tomatsu S, Fukuda S, Emura S, Kojima S, Matsuyama T, Sly WS, Kondo N, Orii T (1998) Treatment of MPS VII (Sly disease) by allogeneic BMT in a female with homozygous A619V mutation. Bone marrow transplantation 21:629-634.

Yamashita T, Chai HL, Teramoto S, Tsuji S, Shimazaki K, Muramatsu S-i, Kwak S (2013) Rescue of amyotrophic lateral sclerosis phenotype in a mouse model by intravenous AAV9-ADAR2delivery to motor neurons. EMBO Molecular Medicine 5:1710-1719.

Yang B, Li S, Wang H, Guo Y, Gessler DJ, Cao C, Su Q, Kramer J, Zhong L, Ahmed SS, Zhang H, He R, Desrosiers RC, Brown R, Xu Z, Gao G (2014) Global CNS Transduction of Adult Mice by Intravenously Delivered rAAVrh.8 and rAAVrh.10 and Nonhuman Primates by rAAVrh.10. Molecular therapy 22:1299-1309.

Ylä-Herttuala S (2012) Endgame: Glybera Finally Recommended for Approval as the First Gene Therapy Drug in the European Union. Molecular Therapy 20:1831-1832.

Zhang H, Yang B, Mu X, Ahmed SS, Su Q, He R, Wang H, Mueller C, Sena-Esteves M, Brown R, Xu Z, Gao G (2011) Several rAAV Vectors Efficiently Cross the Blood–brain Barrier and Transduce Neurons and Astrocytes in the Neonatal Mouse Central Nervous System. Molecular Therapy 19:1440-1448.

Zhang Y, Wang Y, Boado RJ, Pardridge WM (2007) Lysosomal Enzyme Replacement of the Brain with Intravenous Non-Viral Gene Transfer. Pharmaceutical Research 25:400-406.

Zinn E, Vandenberghe LH (2014) Adeno-associated virus: fit to serve. Current Opinion in Virology 8:90-97.

Zolotukhin S, Byrne BJ, Mason E, Zolotukhin I, Potter M, Chesnut K, Summerford C, Samulski RJ, Muzyczka N (1999) Recombinant adeno-associated virus purification using novel methods improves infectious titer and yield. Gene therapy 6:973-985.

2. WEB RESOURCES

Gene Therapy Clinical Trials Worldwide: www.abedia.com/wiley/

Clinical Trial Information for Study Participants & Doctors: www.clinicaltrials.com

UniQure – Glybera: www.uniqure.com/products/glybera

MPS Society UK – The Society for Mucopolysaccharide Diseases: www.mpssociety.org.uk

Orphanet Reports. Prevalence of rare diseases. Bibliographic data. May 2014: www.orpha.net/orphacom/cahiers/docs/GB/Prevalence_of_rare_diseases_by_alphabetical_list.pdf

U.S. Food and Drug Administration Home Page: www.fda.gov

European Medicines Agency: www.ema.europa.eu

RCSB Protein Data Bank – RSCB PDB – 3HN3 Structure Summary: www.rcsb.org/pdb/explore/explore.do?structureId=3HN3

Micro CT Laboratory – University of Calgary: www.ucalgary.ca/microct/

DrTummy: www.drtummy.com

Mouse Genome Informatics: www.informatics.jax.org

Viral Vector Production Unit (UPV): http://sct.uab.cat/upv

ANNEX

Citation: Molecular Therapy — Methods & Clinical Development (2014) **1,** 7; doi:10.1038/mtm.2013.7

www.nature.com/mtm

ARTICLE

Intrathecal administration of IGF-I by AAVrh10 improves sensory and motor deficits in a mouse model of diabetic neuropathy

Judit Homs[1], Gemma Pagès[1], Lorena Ariza[1], Caty Casas[2,3], Miguel Chillón[1,4], Xavier Navarro[2,3] and Assumpció Bosch[1]

Different adeno-associated virus (AAV) serotypes efficiently transduce neurons from central and peripheral nervous systems through various administration routes. Direct administration of the vectors to the cerebrospinal fluid (CSF) could be an efficient and safe strategy. Here, we show that lumbar puncture of a nonhuman AAV leads to wide and stable distribution of the vector along the spinal cord in adult mice. AAVrh10 efficiently and specifically infects neurons, both in dorsal root ganglia (60% total sensory neurons) and in the spinal cord (up to one-third of α-motor neurons). As a proof of concept, we demonstrate the efficacy of AAVrh10 in a mouse model of diabetic neuropathy, in which intrathecal delivery of the vector coding for insulin-like growth factor (IGF-I) favored the release of the therapeutic protein into the CSF through its expression by sensory and motor neurons. IGF-I–treated diabetic animals showed increased vascular endothelial growth factor expression, activation of Akt/PI3K pathway, and stimulated nerve regeneration and myelination in injured limbs. Moreover, we achieved restoration of nerve conduction velocities in both sensory and motor nerves by AAVrh10, whereas we reached only sensory nerve improvement with AAV1. Our results indicate that intrathecal injection of AAVrh10 is a promising tool to design gene therapy approaches for sensorimotor diseases.

Molecular Therapy — Methods & Clinical Development (2014) **1**, 7; doi:10.1038/mtm.2013.7; published online 15 January 2014

INTRODUCTION

The complications of diabetes represent the main volume in disability, reduced life expectancy, and economic cost associated with diabetes.[1] The most common and debilitating complication of diabetes is diabetic peripheral neuropathy (DPN), which affects 60–70% of patients and causes frequent hospitalization in diabetes.[2] Sensorimotor polyneuropathy is the most common form of DPN and can affect all types of nerve fibers. Abnormal sensory perception in diabetic patients includes loss of pain and temperature sensation, and burning skin and tenderness, initially affecting the feet and lower legs and later hands and arms. In more advanced stages, foot ulcers and neuropathic deformities may develop, eventually resulting in 40% of nontraumatic limb amputations. Axonal degeneration, nerve fiber loss, segmental demyelination, and remyelination are characteristic pathological features of human DPN.[3] Although intensive insulin therapy to control blood glucose reduces the incidence of new clinically detected neuropathy, diabetic patients still develop DPN.

Gene therapy strategies for treatment of chronic pain, genetic and acquired peripheral neuropathies like DPN, or accelerating peripheral nerve regeneration could be envisaged if efficient gene transfer to the peripheral nervous system (PNS) would be achieved. Viral vectors offer the possibility to specifically target different cell types in the PNS. We and others have demonstrated transduction of mouse and human Schwann cells in vitro[4] and in vivo in animal models of peripheral nerve trauma.[5,6] Herpes simplex virus–based vectors were shown to efficiently transduce sensory neurons when injected subcutaneously in animal models, which has lead to the initiation of a phase 1 clinical trial for pain treatment (for review, see ref. 7). Several serotypes of adeno-associated viruses (AAV) also infect sensory neurons in the dorsal root ganglia (DRG) through direct administration into the cerebrospinal fluid (CSF), via retrograde transport or by intravenous administration.[8–12]

Among the different AAV serotypes tested, AAVrh10, a nonhuman primate serotype, was proven to efficiently transduce neurons in the brain after intracranial administration, enabling a widespread diffusion, similar to AAV1 or AAV9.[13,14] Moreover, intravenous administration of AAVrh10 in neonatal mice crosses the blood–brain barrier and drives one of the most efficient transduction to the spinal cord and central nervous system compared to other AAV serotypes.[15,16]

With the aim to study if AAVrh10 vector is capable to efficiently deliver a therapeutic gene to sensory and motor neurons, we tested the biodistribution of this vector and compared it with AAV1, AAV2, and AAV8, following intraneural and intrathecal administration in adult mice. Here, we demonstrate that after lumbar delivery of the vectors into the CSF, the AAV vectors were widely distributed to

[1]Department of Biochemistry and Molecular Biology, Center of Animal Biotechnology and Gene Therapy (CBATEG), Universitat Autònoma de Barcelona, Bellaterra, Barcelona, Spain; [2]Department of Cell Biology, Physiology and Immunology, Institute of Neurosciences, Universitat Autònoma de Barcelona, Bellaterra, Barcelona, Spain; [3]Centro de Investigación Biomédica en Red sobre Enfermedades Neurodegenerativas (CIBERNED), Instituto de Salud Carlos III, Spain; [4]Institut Català de Recerca i Estudis Avançats (ICREA), Barcelona, Spain.
Correspondence: A Bosch (assumpcio.bosch@uab.es)
Received 6 November 2013; revised; accepted 7 November 2013;

the entire spinal cord, from lumbar to cervical segments. AAVrh10 efficiently infected neurons, both in DRG (near 60% of total sensory neurons) and in the spinal cord (up to 30% of motoneurons), while AAV1 was only able to transduce sensory neurons in the DRG. Finally, as a proof of concept, we demonstrated the efficiency of AAVrh10 in a mouse model of experimental diabetes, in which intrathecal delivery of AAVrh10 coding for insulin-like growth factor (IGF-I) was able to release the therapeutic protein into the CSF. In sensory and motor neurons of diabetic animals overexpressing IGF-I, we detected overexpression of vascular endothelial growth factor (VEGF) and activation of Akt/PI3K pathway as well as nerve regeneration and myelination in injured limbs. Moreover, we found increased nerve conduction velocity (NCV) in both sensory and motor nerves by AAVrh10-driven expression of IGF-I compared to green fluorescent protein (GFP)–treated mice, whereas only sensory nerve improvement was found using AAV1. These data demonstrate the potential of AAVrh10 for sensorimotor gene therapy.

RESULTS

AAVrh10 efficiently transduces sensory neurons in DRG

As a first approach to test AAVrh10 efficacy transducing sensory neurons, we delivered 1×10^{11} viral genomes (vg) into the CSF by lumbar puncture in the subarachnoid space, and it was compared to AAV1, AAV2, and AAV8. Animals were euthanized 3 weeks after administration, DRG sectioned, and GFP was quantified by direct fluorescent imaging. No transduction was obtained using AAV8, very small numbers of GFP-positive cells were counted with AAV2 (not shown), and the highest levels were achieved using AAV1 or AAVrh10. AAVrh10 tropism was characterized after intrathecal administration in the lumbar area by immunohistochemistry to specific neuronal markers. We quantified 13 ± 1.3% of transduced large neurons (NF-200 positive, Figure 1a–c) and 60 ± 3.2% of peripherin immunoreactivity (Figure 1d–f), showing GFP expression in lumbar ganglia (n = 3). Peripherin-positive neurons can be divided in calcitonin gene-related peptide or Ib4-positive nerons. Here, 29 ± 2.3% of calcitonin gene-related peptide positive colocalized with GFP (Figure 1g–i) and 11 ± 1.6% of IB4 neurons were also GFP positive (Figure 1j–l; n = 3). AAV1 transduced both large and small neurons but to a lower extent, and numbers were not quantified (Supplementary Figure S1a–f).

Although viral vectors were administered between the third and fourth lumbar vertebrae, once delivered in the intrathecal space, the virus was diluted in the CSF and could reach more proximal segments. Thus, we quantified GFP-expressing sensory neurons in lumbar, thoracic, and cervical DRG at week 1, 3, and 6 after virus administration (Figure 2a; Supplementary Figure S2). For AAV1, we detected stable transduction up to 6 weeks after injection only in lumbar DRG (Supplementary Figure S2; n = 3/time point). For AAVrh10, the highest level of transduction in the DRG was achieved at the injection area, that is the lumbar ganglia, where 56.9 ± 14.8% (n = 3 animals) of total DRG neurons showed GFP expression at 6 weeks (Figure 2a). Moderately lower levels of expression, although not significantly different, were quantified in the cervical area (36.1 ± 13.5%; n = 3 animals). However, in the thoracic segments, significantly lower numbers were detected, particularly 1 and 3 weeks after treatment, a phenomenon already described for AAV6.[10] AAVrh10-driven GFP expression was also evident along the axons of the transduced animals. Transversal sections of sciatic nerves showed around 50% of nerve fibers expressing GFP (Supplementary Figure S3a; n = 3 animals) that probably correspond to axons from infected nuclear bodies projecting to the hind limb. Moreover, direct intrasciatic injection

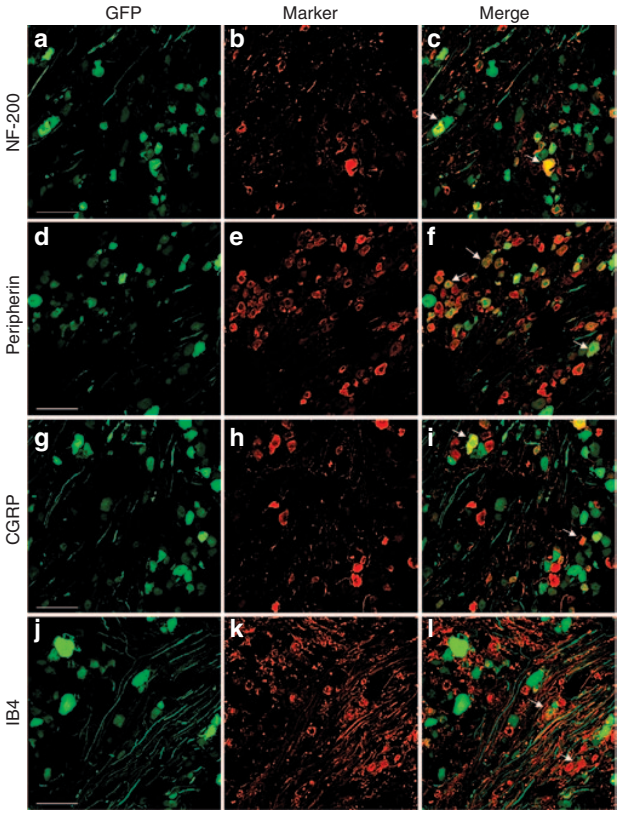

Figure 1 AAVrh10 transduction of dorsal root ganglia. (**a, d, g, j**) DRG sections from animals transduced with AAVrh10-GFP and euthanized at 3 weeks. (**b, e, h, k**) Immunohistochemistry with broad and specific markers of sensory neurons: (**b**) NF-200, (**e**) peripherin, (**h**) CGRP, and (**k**) IB4. GFP-positive sensory neurons merged with specific sensory markers (arrows, **c, f, i, l**). Scale bar = 81 µm. AAV, adeno-associated virus; DRG, dorsal root ganglia; GFP, green fluorescent protein.

of 9×10^{9} viral genomes of AAVrh10 coding for GFP targeted exclusively neurons and demonstrated its ability to be retrogradely transported to the neuronal bodies in the DRG (Supplementary Figure S3b; n = animals), as we have previously reported for AAV1 and AAV2 (ref. 6).

Intrathecal administration of AAVrh10 allows motor neuron transduction

Transduction of motor neuron after intrathecal administration of AAV9 was reported previously in mice, pigs, and nonhuman primates.[17–20] In lumbar spinal cord sections of AAVrh10-injected animals, we also observed widespread GFP expression in both dorsal and ventral areas (Supplementary Figure S4). In the white matter, we observed punctate signals, corresponding to the dorsal and ventral afferences entering the spinal cord (Supplementary Figure S4), but most importantly, at the dorsal and ventral gray matter, we also found cell bodies expressing GFP with a neuronal pattern (Figure 3). Immunohistochemical analysis with selective markers allowed us to characterize the transduced cell types. We did not detect transduction of astrocytes (glial fibrillary acidic protein–positive cells; Figure 3d–f,n) and microglia (Iba1 immunoreactivity; Figure 3j–l,p) and only very few oligodendrocytes (APC1-positive cells; Figure 3g–i,o and arrowhead in i). GFP-positive cell bodies colocalized mainly with choline acetyltransferase immunostaining, a specific

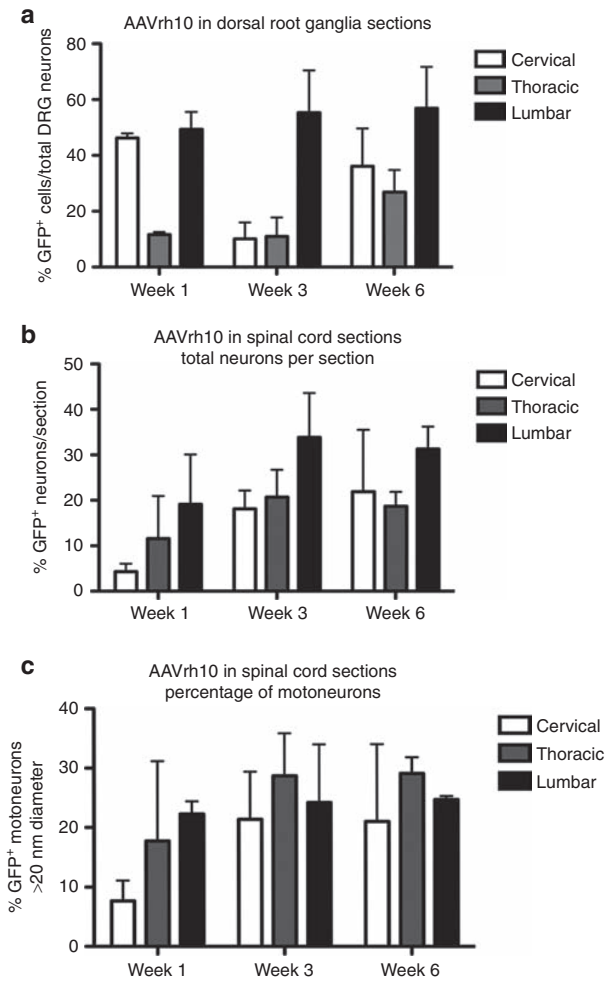

Figure 2 Quantification of GFP-positive sensory and motor neurons transduced by intrathecal AAVrh10. (**a**) Percentage of GFP-positive DRG neurons at different levels (lumbar, thoracic, and cervical) at 1, 3, and 6 weeks postinjection. (**b**) Number of GFP-positive neurons per section quantified at different segments of the ventral spinal cord (lumbar, thoracic, and cervical) after Nissl-positive colocalization. (**c**) Percentage of GFP-positive α-motoneurons quantified from **b** by size (>20 µm). Values are represented as the mean ± SEM ($n = 3$/group and time point). Statistically significant differences were observed by two-way ANOVA and Bonferroni *post hoc* tests in **a** ($P < 0.05$) at week 3 for lumbar versus thoracic and cervical numbers but not in **b** or **c**. AAV, adeno-associated virus; ANOVA, analysis of variance; DRG, dorsal root ganglia; GFP, green fluorescent protein.

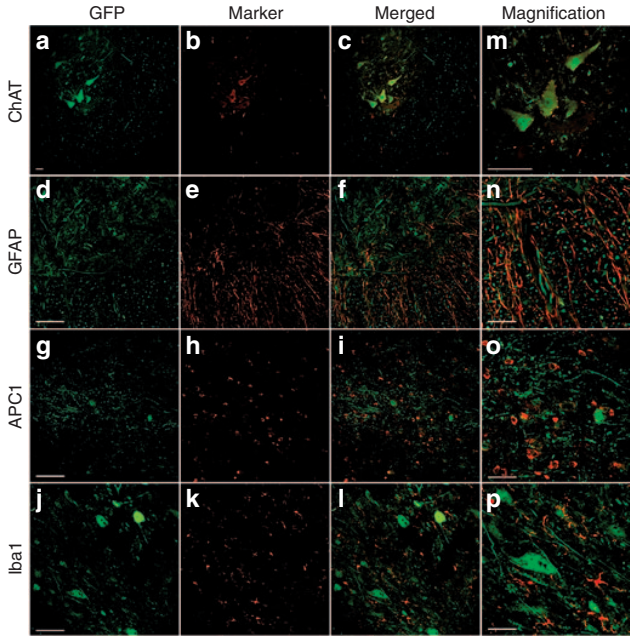

Figure 3 Tropism characterization of AAVrh10 in spinal cord after intrathecal administration of the vector. (**a, d, g, j**) GFP-transduced cells in the ventral horn of lumbar spinal cord (given in green). (**b, e, h, k**) Immunohistochemical analysis of spinal cord cross-sections with specific cell markers, (**b**) ChAT for motoneurons; (**e**) GFAP for astrocytes; (**h**) APC1 for oligodendrocytes; and (**k**) Iba1 for microglia (all given in red). (**c**) Merged images (**c, f, i, l**) showed restricted colocalization only between GFP and ChAT (**m**), except for one cell in **i** (arrowhead) colocalizing between APC1 and GFP. **a**–**l**, bar = 70 µm. Magnified merged images (**m, n, o, p**; scale bar = 31 µm). AAV, adeno-associated virus; ChAT, choline acetyltransferase; DRG, dorsal root ganglia; GFAP, glial fibrillary acidic protein; GFP, green fluorescent protein.

marker for cholinergic neurons (Figure 3a–c,m). We observed the strongest GFP signal in somatic motoneurons located in the ventral horn, of either big (>20 µm) or small size (<20 µm), and in either the medial or the lateral motor columns that send their axons to axial and limb muscles, respectively. Minor expression was detected in autonomic neurons located in the intermediolateral column in lamina VII at thoracic levels. We quantified the number of neurons in the ventral area of the spinal cord along the different spinal segments (cervical, thoracic, and lumbar; Figure 2b; $n = 3$ animals). At 3 weeks, we found near 40 neurons per section in the lumbar segments and around 20 neuronal somas in the thoracic and cervical segments without using immunohistochemistry against GFP. Importantly, one-third of α-motoneurons were transduced in all segments analyzed (Figure 2c). This demonstrates that AAVrh10-driven expression is stable over this period of time and that viruses diluted in the CSF were able to transduce sensory and spinal motor neurons in all the subdivisions of the spinal cord. Small interneurons expressing GFP as well as dorsal horn neurons were also observed, mainly in the lumbar region. Contrary to AAVrh10, AAV1-injected animals did not show GFP expression in the spinal cord (data not shown). In addition, we did not detect transduction of the meninges with any of the viruses used.

Motor and sensory neuron overexpression of IGF-I in a mouse model of DPN

As a proof of principle to test for the efficacy of AAVrh10 in treating diseases affecting both sensory and motor neurons, we used a mouse model of diabetic neuropathy by combining induction of diabetes by multiple low doses of streptozotocin with sciatic nerve crush. Four weeks after initiation of diabetes, male CD-1 mice were intrathecally injected with 1×10^{11} viral genomes of AAVrh10 or AAV1 coding for either IGF-I or GFP and submitted to sciatic nerve lesion on one leg to evaluate the regeneration delay that has been described in diabetic mice.[21,22] Electrophysiological studies were performed at 3 and 4 weeks postcrush (7 and 8 weeks after streptozotocin treatment) after which the animals were euthanized and samples processed for molecular analyses. Animals were monitored for weight and glycemia every 2 weeks (Supplementary Figure S5). All mice showed established hyperglycemia on the day of surgery without significant changes along the duration of the experiment (Supplementary Figure S5b,d). No statistically significant differences were observed between the four groups in body weight (Supplementary Figure S5a,c; Student's

t-test, $n = 10$ for GFP and 15 for IGF-I in AAVrh10-treated groups; $n = 7$ for GFP and 17 for IGF-I in AAV1-treated groups).

Electrophysiological studies showed evidences of peripheral neuropathy in the left intact hind limb of the diabetic mice that had significantly reduced motor and sensory NCV with respect to values of control mice. AAV vector injection did not induce further deterioration, and AAV-GFP mice had similar neuropathy as control noninjected diabetic mice (Table 1), despite variability between groups. Mice that received a vector for IGF-I expression showed less marked deterioration of peripheral nerve function during the month of follow-up that corresponding AAV-GFP mice. Mice with AAV1-IGF-I had significantly higher distal sensory NCV, whereas mice injected with AAVrh10-IGF-I had significantly higher amplitude of the sensory compound nerve action potential and proximal sensory NCV compared with their corresponding controls with vector encoding GFP (Table 1).

Regarding the regeneration capability, all the diabetic mice had slower rate of regeneration and reinnervation of motor and sensory targets after sciatic nerve lesion than control mice, as previously reported.[22] Administration of the AAV1-IGF-I did not produce any improvement of the regenerative capability evaluated by electrophysiological and functional methods. In contrast, mice injected with AAVrh10-IGF-I showed significantly higher motor and sensory NCV at 31 days postinjury (Table 2), suggestive of faster regeneration and maturation of the injured axons.

Four weeks after AAV injection and 8 weeks after induction of diabetes, animals were euthanized. IGF-I expression was demonstrated by immunohistochemistry in lumbar DRG and spinal cord in both AAV1- and AAVrh10-injected animals (Figure 4a,d, respectively). IGF-I immunohistochemistry in DRG differs from GFP expression shown in Figure 1 because IGF-I is a secreted protein, and as IGF-I receptor is also expressed in DRG cells,[23] it can be uptaken by other nontransduced neighboring cells, showing the global image of IGF-I signal in the DRG. Quantitative real-time PCR from lumbar DRG and ventral horn spinal cord also showed significant increase of IGF-I mRNA with both vectors compared to GFP (Figure 4b; $n = 5$–7/group; $^{**}P < 0.01$ and $^{***}P < 0.005$ by one-way analysis of variance and Tukey's multiple comparison test), correlating with immunohistochemistry images. Moreover, levels of IGF-I were also detected by enzyme-linked immunosorbent assay in the CSF of treated animals at the time of sacrifice, particularly for those injected with AAVrh10 (Figure 4c; $n = 3$/group; $^{*}P < 0.05$ by Student's *t*-test). AAV1-injected animals also showed increased IGF-I in CSF but not statistically significant from GFP-treated animals (Figure 4c). Increased IGF-I in sensory neurons probably activated Akt signaling pathway, as shown by phosphorylation of Akt compared to total Akt protein levels in AAVrh10 IGF-I and but not in GFP-injected mice (Figure 5a). IGF-I is capable to activate different signaling pathways and to promote cell survival as well as to regulate the expression of different trophic factors, VEGF being one among them. VEGF has been shown to be essential for neuronal survival, and its secretion and mRNA expression in many tissues is being induced by IGF-I. In Figure 5b, we show a significant increase in VEGF protein in lumbar DRG of IGF-I–injected animals, compared to GFP-injected mice. On the other hand, growth associated protein 43 (GAP-43) is overexpressed by neurons in the process of regeneration, and it is located in the growth cones of regenerating axons. We analyzed GAP-43 in regenerating sciatic nerves from animals injected with vectors expressing IGF-I or GFP at the time of injury. We detected a significant increase in GAP-43 mRNA in DRG and GAP-43 protein in sciatic nerve, 4 weeks after AAVrh10 IGF-I treatment (Figure 6a,b, respectively), correlating with the electrophysiological results and confirming a positive effect of IGF-I in the regeneration of injured nerves in diabetes. Levels of GAP-43 mRNA were also found increased in sciatic nerves of AAV1-injected animals but at lower levels than that in AAVrh10-injected animals. AAV1-mediated GAP-43 protein was not significantly increased in these animals (Supplementary Figure S6a,b).

Schwann cells play an important role in the regeneration process of PNS after injury. In this regard, Schwann cell survival, proliferation, motility, and myelination are crucial for a proper regeneration of the injured nerve, and all these processes can be promoted by IGF-I. We detected increased levels of PNS myelin proteins: myelin protein zero (P0), PMP22, myelin basic protein, and myelin-associated glycoprotein 4 weeks after injury in IGF-I–treated sciatic nerves (Figure 6c,d; Supplementary Figure S6c,d). Quantitative PCR of myelin proteins showed strongly increased mRNA levels in AAVrh10-injected animals and a similar tendency for AAV1-treated mice, although with lower levels. Myelin protein zero, accounting for 50% of PNS myelin proteins, was ten times enhanced in AAVrh10 IGF-I–injected animals and only four times in AAV1-injected mice, both of them being statistically significant ($P < 0.05$).

DISCUSSION

The goal of this study was to analyze the potential of AAV vectors for treating DPN. Even if DPN widely affects the PNS, restricted administration to the target tissue may be crucial, avoiding the use

Table 1 Results of electrophysiological tests performed in the intact hindlimb of diabetic mice at 7 and 8 weeks after induction of diabetes (3 and 4 weeks after intrathecal injection of viral vector in the AAV groups)

Treatment	*Control (n = 10)*		*AAV1-GFP (n = 10)*		*AAV1-IGF-I (n = 21)*		*AAVrh10-GFP (n = 7)*		*AAVrh10-IGF-I (n = 15)*	
Week diabetes	7	8	7	8	7	8	7	8	7	8
Plantar muscle										
CMAP (mV)	6.7 ± 0.4	6.5 ± 0.4	6.8 ± 0.4	6.3 ± 0.4	6.4 ± 0.3	6.3 ± 0.5	6.6 ± 0.9	6.3 ± 0.6	6.3 ± 0.3	5.9 ± 0.3
MNCV (m/s)	36.4 ± 1.2	34.8 ± 1.1	33.1 ± 0.8[c]	34.1 ± 1.1	38.8 ± 1.8	36.5 ± 0.6	36.7 ± 2.2	34.7 ± 2.1	41.3 ± 2.2	42.3 ± 2.2[c]
Digital nerve										
CNAP (μV)	29.4 ± 2.4	24.1 ± 1.1	31.9 ± 3.5	26.6 ± 2.2	32.2 ± 2.3	33.5 ± 2.7[c]	29.2 ± 3.0	20.0 ± 3.1	36.3 ± 3.0	31.2 ± 2.6[bc]
SNCVp (m/s)	36.5 ± 0.9	34.7 ± 0.9	36.9 ± 1.9	36.0 ± 1.8	39.9 ± 1.1	37.2 ± 1.0	42.6 ± 2.8[c]	39.2 ± 1.7[c]	44.1 ± 2.8[c]	46.7 ± 2.0[bc]
SNCVd (m/s)	29.2 ± 0.7	25.9 ± 0.7	29.1 ± 0.7	24.2 ± 0.8	32.0 ± 0.6[a]	28.7 ± 0.6[a]	28.1 ± 1.4	24.8 ± 0.9	28.6 ± 0.9	26.0 ± 0.6

Data are expressed as mean ± SEM. All CMAP and CNAP amplitudes are given for nerve stimulation at the sciatic notch.
CMAP, compound muscle action potential; CNAP, compound nerve action potential; MNCV, motor nerve conduction velocity; SNCV, sensory nerve conduction velocity; -d: distal nerve segment; -p: proximal nerve segment.
$P < 0.05$ versus [a]AAV1-GFP. [b]AAVrh10-GFP. [c]Control at the same time of follow-up. ANOVA with Bonferroni *post hoc* tests.

Table 2 Results of electrophysiological tests performed in the right hindlimb of diabetic ICR mice at 7 and 8 weeks after induction of diabetes, and 3 and 4 weeks after sciatic nerve crush (w.p.i.) and intrathecal injection of viral vector

Treatment	*AAV1-GFP (n = 9)*		*AAV1-IGF-I (n = 21)*		*AAVrh10-GFP (n = 7)*		*AAVrh10-IGF-I (n = 15)*	
w.p.i.	3	4	3	4	3	4	3	4
Ant tibialis muscle								
CMAP (mV)	12.5 ± 1.5	18.2 ± 1.8	12.6 ± 1.0	21.2 ± 1.1	14.0 ± 1.0	23.1 ± 1.6	14.7 ± 1.6	23.6 ± 2.5
Plantar muscle								
CMAP (mV)	0.54 ± 0.17	1.29 ± 0.34	0.41 ± 0.05	1.24 ± 0.21	0.63 ± 0.12	1.11 ± 0.32	0.64 ± 0.12	1.18 ± 0.18
MNCV (m/s)	11.3 ± 1.2	15.4 ± 0.8	11.3 ± 1.0	17.1 ± 1.1	10.4 ± 2.1	13.7 ± 0.7	16.1 ± 1.3[a]	18.8 ± 1.2[a]
Digital nerve								
CNAP (μV)	0.78 ± 0.44	3.43 ± 1.34	0.52 ± 0.29	3.10 ± 0.76	0 ± 0	2.60 ± 1.08	0.92 ± 0.64	3.67 ± 0.78
SNCVp (m/s)	15.3 ± 3.9	15.5 ± 1.0	16.4 ± 5.0	15.4 ± 1.4	—	21.2 ± 6.1	—	23.8 ± 1.3
SNCVd (m/s)	3.7 ± 0.5	7.3 ± 0.5	4.2 ± 0.8	7.4 ± 0.5	—	6.0 ± 0.7	—	10.0 ± 1.9[a]
Pinprick score	3.3 ± 0.5	5.8 ± 0.7	2.7 ± 0.3	5.3 ± 0.4	1.0 ± 0.0	4.0 ± 0.5	1.0 ± 0.2	5.1 ± 0.5

Data are expressed as mean ± SEM. All CMAP and CNAP amplitudes are given for nerve stimulation at the sciatic notch.
$P < 0.05$ versus [a]AAVrh10-GFP at the same time of follow-up. ANOVA with Bonferroni *post hoc* tests.
ANOVA, analysis of variance; CMAP, compound muscle action potential; CNAP, compound nerve action potential; MNCV, motor nerve conduction velocity; SNCV, sensory nerve conduction velocity; -d: distal nerve segment; -p: proximal nerve segment; w.p.i.: weeks post infection.

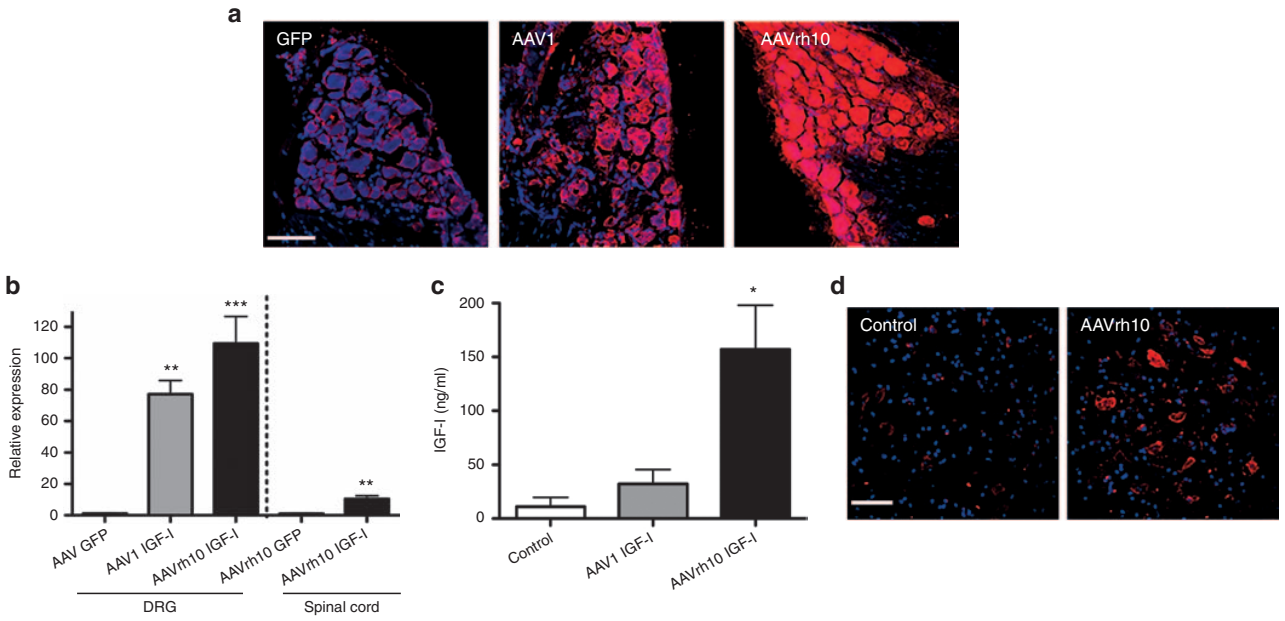

Figure 4 IGF-I expression driven by AAV1 or AAVrh10 is detected in sensory and motor neurons and secreted to the CSF of diabetic mice. IGF-I expression is demonstrated 4 weeks after intrathecal administration of AAV vectors. (**a**) IGF-I immunohistochemistry in DRG and (**d**) ventral spinal cord sections from the lumbar area. Confocal microscopy detected increased IGF-I staining in sensory and motor neuron-like morphology in mice injected with AAV1-IGF-I and AAVrh10 IGF-I compared to control animals injected AAV coding for GFP. Images were obtained sequentially under identical scanning conditions for each independent channel (red channel: IGF-I; blue channel: TO-PRO-3 to counterstain nuclei; $n = 2$). (**b**) Quantitative PCR from lumbar DRG and ventral horn of spinal cord showed significant increase of IGF-I with both vectors compared to GFP (one-way ANOVA and Tukey's multiple comparison test; $^{**}P < 0.01$; $^{***}P < 0.005$; $n = 5$–7/group). (**c**) IGF-I ELISA from CSF of treated animals obtained at the time of sacrifice ($n = 3$/group). Statistically significant numbers were obtained for AAVrh10-treated animals but not with AAV1, compared to nontreated control animals (Student's *t*-test, $^{*}P < 0.05$). **a**, bar = 160 μm **d**, bar = 73 μm. AAV, adeno-associated virus; ANOVA, analysis of variance; CSF, cerebrospinal fluid; ELISA, enzyme-linked immunosorbent assay; IGF, insulin-like growth factor.

of large doses of vector and the chance of expression of recombinant proteins in undesired tissues, leading to development of secondary effects or stimulation of the immune response against the virus or the therapeutic protein.[24,25] For this reason, we delivered AAV1 and AAVrh10 vectors to the CSF by lumbar puncture, a minimally invasive route that can be potentially performed in an outpatient setting, so to allow reaching sensory and motor neurons with minor exposure of peripheral tissues. Broad delivery to the PNS by targeting sensory and/or motor neurons is required to treat neuropathic pain, nerve trauma, or diseases-like DPN, Charcot–Marie–Tooth, amyotrophic lateral sclerosis, or spinal muscular atrophy.[26–28] Here, we demonstrate that AAVrh10 delivered by

lumbar puncture infects both sensory and motor neurons along the different segments of the spinal cord, with only significant differences in the relative percentage of neurons transduced between lumbar and thoracic DRG, but no differences were found between motoneurons or even between lumbar and cervical DRG. With only 10 µl of viruses, we achieved up to 60% of sensory neurons and 30% of motoneurons transduced. Moreover, in this work, we have used single-strand AAV as a platform, reported to be 20-fold less efficient compared to self-complementary AAVs, and we did not use immunohistochemistry to quantify GFP expression in transduced cells to avoid overestimation due to background, so we may have, in addition, ten times lower sensitivity when quantifying transduction levels.

Studies in larger animals are important to evaluate the potential of the therapeutic strategy. As a matter of fact, intramuscular AAV6 in nonhuman primates could target 50% motoneurons in 1-cm-long lumbar spinal cord segment.[29] Moreover, intravenous AAV9 was able to transduce motoneurons in adult cats up to 15% from lumbar to cervical segments, although peripheral tissues, including testis, were also labeled.[30] Recently, intrathecal administration of AAV9 in pigs and nonhuman primates demonstrated the capability of transducing sensory and motor neurons. However, most of transduced cells were astrocytes.[20,31,32] This is also in accordance with the preferential transduction of astrocytes after intravenous administration of this vector in adult mice.[33] Other serotypes, like AAV7, seem to be as efficient as AAV9 after intracisterna injection and targets both neurons and astrocytes.[19] Herein, we demonstrate AAVrh10-specific tropism for neurons in the spinal cord and DRG, similar to what was reported for the central nervous system,[14] but not for glial cells as found for AAV7 and AAV9, which may be an advantage because restricting cell type infection may decrease immunological response, although this needs to be analyzed.[20] In this regard, a high percentage of humans are seropositive for different AAV serotypes. In adults, anti-AAV2 antibodies are the most prevalent (up to 70% of healthy humans), followed by serotypes AAV5, AAV9, and AAV8.[34] Using a nonhuman AAV serotype in human gene therapy trials may have additional advantages compared to human serotypes like AAV9, since patients may not be preimmunized against this serotype, although cross-reaction between AAVrh10 and human AAV serotypes needs to be quantified.

As a proof of principle, we administered IGF-I as therapeutic gene in the mouse model of DPN. IGF-I provides trophic support to neurons of peripheral and central nervous systems. Through its tyrosine kinase receptor, IGF-I upregulates other neurotrophic factors including hypoxic-inducible factor 1α and VEGF.[35] Schwann cells express IGF-I receptors, and their activation promotes myelination[36] and protects Schwann cell dysfunction induced by high glucose in vitro.[37] Importantly, intrathecal daily delivery of IGF-I through an infusion pump in diabetic rats reversed slowing of motor and sensory conduction velocity as well as atrophy of myelinated sensory axons in peripheral nerve.[38] In fact, the therapeutic effect of growth factors was demonstrated for DPN by promoting neuronal survival, stimulating repair of peripheral nerve injury, or inducing nerve regeneration under diabetic conditions (for review, see ref. 39). For that reason, clinical trials using nerve growth factor, brain-derived neurotrophic factor, VEGF, and C-peptide were proposed, although without significant benefit so far.[40–43] Delivering factors continuously through gene therapy vectors may considerably improve the efficiency of these trials. Indeed, AAVrh10 vector may enable the long-term expression in sensory and motor neurons along the spinal cord without the risk of insertional mutagenesis.[44] Delivering nonsecreted proteins through this method could be an additional challenge since only those neurons expressing the transgene will be corrected.

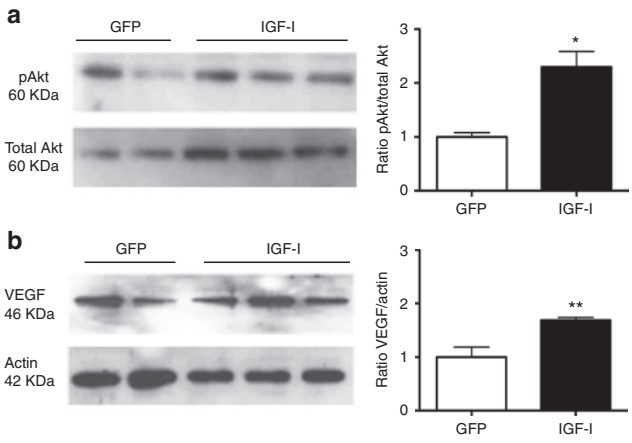

Figure 5 IGF-I signaling is enhanced in DRG of AAVrh10-treated diabetic mice. (**a**) Western blot showing phosphorylation of Ser473 Akt from DRG tissue extracts from animals injected with AAVrh10 coding for IGF-I or GFP. Total Akt was used to normalize protein levels. Western blots were scanned and represented as the ratio of phosphorylated Akt (pAkt) versus total Akt (mean ± SEM). Statistically significant differences were detected by Student's *t*-test (*$P < 0.01$; $n = 2$ for GFP; $n = 3$ for IGF-I). (**b**) DRG protein extracts were immunoblotted using anti-VEGF or actin antibodies. Densitometries show statistically significant increase of VEGF in AAVrh10IGF-I–treated DRGs (values are means ± SEM and represent ratio of VEGF normalized by actin levels from at least two blots; $n = 2$ for GFP-treated animals and $n = 5$ for IGF-I–treated animals; **$P < 0.01$ by Student's *t*-test). AAV, adeno-associated virus; DRG, dorsal root ganglia; GFP, green fluorescent protein; IGF, insulin-like growth factor; VEGF, vascular endothelial growth factor.

Unfortunately, animal models of diabetes do not reach the severity of human diabetic neuropathy. Animal nerves usually show relatively mild neurophysiological deficits and minor morphometric changes.[45,46] The lack of degenerative neuropathy in diabetic rodent models seems to be a consequence of the short life span of rodents or the physically shorter axons. Degenerative neuropathy is minimal even in larger animals like dogs or primates, with the exception of cats.[47] For this reason, we combined diabetes with nerve injury, because it is demonstrated that PNS regeneration is impaired in diabetic patients and animal models.[21,22] The results presented here demonstrate that IGF-I delivery using AAVrh10 achieves higher transduction to sensory neurons and, more importantly, to motoneurons, leading to higher levels of the therapeutic protein to both sensory and motor nerves, which is probably the cause of the higher expression of IGF-I downstream signaling pathway like myelin proteins or GAP-43 observed in our model. Altogether, these data demonstrate that IGF-I delivery through intrathecal injection to sensory neurons with AAV1 is able to achieve a modest improvement of the neuropathy but not of nerve regeneration after injury in diabetic mice, while when driven by AAVrh10, IGF-I is able to significantly accelerate regeneration and myelination of the peripheral nerve of diabetic animals, with particular effect to motor neurons. These improvements may be relevant in diabetic animal models of longer evolution, in which neuropathy is more severe, and in larger species in which axonal regeneration through longer nerves takes more time. Despite in our experimental design, we did not evaluate the effect of AAVrh10 coding for IGF-I on nerve regeneration without the effect of diabetes, our results suggest that intrathecal injection of AAVrh10 could be a promising tool to design gene therapy approaches for diseases affecting sensory and motor neurons, like DPN, as well as for peripheral nerve injury.

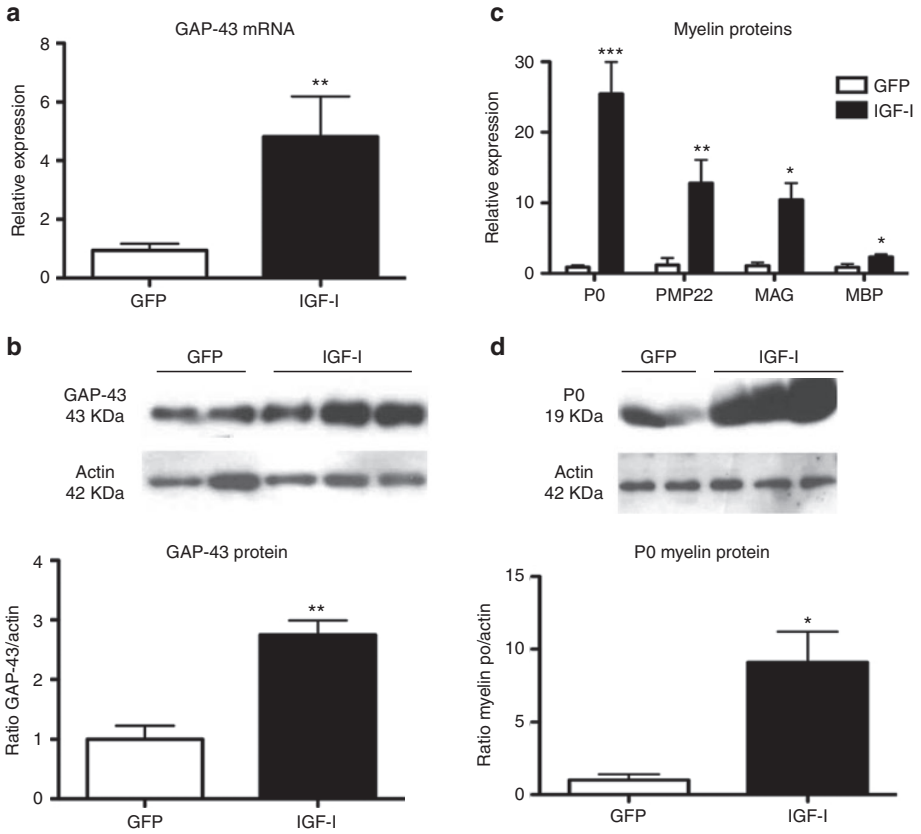

Figure 6 AAVrh10 coding for IGF-I promotes regeneration and myelin proteins expression in injured sciatic nerves of diabetic mice. Injured sciatic nerves and DRG from diabetic mice treated with AAVrh10 coding for GFP or IGF-I were dissected 4 weeks after treatment. Graphs represent means ± SEM (n = 3–5 animals). mRNA and protein of GAP-43, a marker for nerve regeneration, are significantly increased in IGF-I–treated animals as assessed by (**a**) quantitative PCR from DRG and (**b**) western blot from sciatic nerve protein extracts, where levels of GAP-43 were quantified and compared to actin. (**c**) Quantitative PCR from sciatic nerve shows increased mRNA for myelin proteins P0, PMP22, MAG, and MBP in animals that received IGF-I compared to GFP-treated mice. (**d**) Protein levels of myelin protein P0 analyzed by western blot corroborated quantitative PCR results. Student's t-tests show statistically significant results (***$P < 0.005$; **$P < 0.01$; *$P < 0.05$). AAV, adeno-associated virus; DRG, dorsal root ganglia; GAP, growth associated protein; GFP, green fluorescent protein; IGF, insulin-like growth factor; MBP, myelin basic protein.

MATERIALS AND METHODS

AAV vector construction, production, and titration

GFP cDNA was cloned into *Hind*III and *Nhe*I sites to the plasmid pAAV-CAG-polylinker-WPRE, containing the chicken β-actin promoter with the cytomegalovirus enhancer and the woodchuck hepatitis virus responsive element (WPRE). AAV2/1 and AAV2/rh10-CAG-GFP-WPRE were generated as previously described[48] by triple transfection in HEK 293-AAV cells (Stratagene, Carlsbad, CA) with branched polyethylenimine (PEI; Sigma, St Louis, MO) with the plasmid containing the inverted terminal repeats of AAV2, the AAV helper plasmid containing Rep2 and Cap for each serotype (kindly provided by JM Wilson, University of Pennsylvania, PA, USA) and the pXX6 plasmid containing helper adenoviral genes.[49] Vectors were purified by iodixanol gradients, after benzonase treatment[48] by the Vector Production Unit at Center of Animal Biotechnology and Gene Therapy (Universitat Autònoma de Barcelona).

Animals

Eight to twelve-week-old male Hsd:ICR (CD-1) (Harlan Laboratories, Indianapolis, IN) mice were used. Mice were fed *ad libitum* with a standard diet (2018S Teklad Global; Harlan Laboratories; 17% calories from fat) and kept under a light–dark cycle of 12 hours (lights on at 8:00 AM). To induce insulin-dependent diabetes, mice were given, on 5 consecutive days, an intraperitoneal injection of 45 mg/kg body weight of streptozotocin (dissolved in 0.1 mol/l citrate buffer, pH 4.5, immediately before administration). Diabetes was assessed by measuring blood glucose levels with a Glucometer Elite (Bayer, Leverkusen, Germany). Animal care and experimental procedures were approved by the Biosafety and the Animal and Human Experimentation Ethical Committees of the Universitat Autònoma de Barcelona.

Surgical procedures

Administration of viral vectors. Animals were anesthetized by intraperitoneal injection of ketamine (10 mg/kg of body weight; Imalgene 500; Rhône-Merieux, Lyon, France) and xylazine (1 mg/kg of body weight; Rompun; Bayer). Sciatic nerve injection and injury were described previously.[6] Three microliters of viral vectors were directly injected into the sciatic nerve using a 33-gauge needle and a Hamilton syringe connected to a Micropump (Micro4; World Precision Instruments, Sarasota, FL) at a rate of 400 nl/minute. Intrathecal administration was performed at the lumbar region. After lateral spine exposure, by paravertebral muscle dissection, local anesthesia with bupivacaine 0.5% (B.Braun, Melsungen, Germany) was applied. Ten microliters of viral vectors were slowly injected into the CSF through a 33-gauge needle and a Hamilton syringe between lumbar vertebrae L3 and L4. Appropriate access to the intrathecal space was confirmed by animal's tail movement. The needle remained in place at the injection site for one additional minute after which muscle and skin were sutured.

CSF extraction. Mice were deeply anesthetized and immobilized in stereotaxic appliance. An incision was made from the occipital region of the skull to the cervical region of the spine, and the posterior neck muscles were separated to access the arachnoid at the cisterna magna. Local anesthesia with bupivacaine was applied. An aspirator tube (Sigma-Aldrich) assembled to a microcapillary pipette was used to extract the CSF. A slight pressure was made with the microcapillary pipette on the arachnoid membrane to access

the cisterna magna. Then, 5 µl of CSF per mouse were withdrawn by aspiration. Animals were euthanized just after CSF extraction.

Sciatic nerve lesion. Under anesthesia as stated above, the right sciatic nerve was exposed at the mid-thigh and subjected to a crush lesion during 30 seconds for three times in succession with a Dumont #5 (World Precision Instruments, Sarasota, FL) forceps at a constant point, 42 mm from the tip of the third digit. The wound was then sutured by layers.

Functional tests

Nerve conduction studies were performed bilaterally in the sciatic nerve at two time points, 7 and 8 weeks after induction of diabetes, corresponding to 3 and 4 weeks following the surgical lesion on the right side.[22] With animals under anesthesia (pentobarbital 40 mg/kg intraperitoneally), the nerve was stimulated percutaneously through a pair of small needle electrodes placed first at the sciatic notch and then at the ankle. Rectangular electrical pulses (Grass S88) of 0.01 ms duration were applied up to 25% above the voltage that gave a maximal response. The compound muscle action potentials were recorded from the third interosseus plantar muscle and from the tibialis anterior muscle with microneedle electrodes. Similarly, the sensory compound nerve action potential was recorded by electrodes placed at the fourth toe near the digital nerves. All evoked action potentials were displayed on a storage oscilloscope (Tektronix 420, Beaverton, OR) at settings appropriate to measure the amplitude from baseline to peak and the latency to the onset of the recorded potentials. The NCV was calculated for each segment tested; motor NCV for the sciatic notch–ankle segment and sensory NCV for the proximal segment sciatic notch–ankle and for the distal segment ankle–digit. During electrophysiological tests, the animals were placed over a warm flat steamer controlled by a hot water circulating pump, and the hindpaw skin temperature was maintained above 32 °C. To reduce variability between sets, groups of mice receiving each AAV vector encoding for GFP and IGF-1 were studied in parallel and compared.

Quantitative real-time PCR

Sciatic nerves, DRG, and spinal cord were homogenized with Qiazol (Qiagen, Hilden, Germany) to obtain total RNA. Messenger RNA was retrotranscribed to cDNA (Omniscript RT Kit; Qiagen), and analysis of expression was performed by quantitative real-time PCR (Smart Cycler II; Cepheid, Sunnyvale, CA) with FastStart Sybrgreen Master (Roche Diagnostics, Basel, Switzerland). Primer sequences used: reference gene m36B4 (forward: ATGGGTACAAGCGCGTCCTG; reverse: AGCCGCAAATGCAGATGGAT); IGF-I (forward: GGACCAGAGACCCTTTGCGG; reverse: GTGCCCTCCGAATGCTGG AG); P0 (forward: TCTCAGGTCACGCTCTATGTC; reverse: CAGGTAGAAGAG CAACAGCAG); PMP22 (forward: CTCTTGTTGGGGATCCTGTTC; reverse: AA GGCGGATGTGGTACAGTTC); myelin basic protein (forward: GGTGCGCCC AAGCGGGGC; reverse: ACTTCTGGGGCAGGGAGCC); myelin-associated glycoprotein (forward: AGCACAGCGTCCTGGACATC; reverse: GGCCCAGCC AGCTCAGCTC); and GAP-43 (forward: AGCCTAAACAAGCCGATGTGCC; reverse: TTCGTCTACAGCGTCTTTCTCCTCC). Amplifications were performed as follows: heat inactivation (5 minutes, 95 °C, 1 cycle), followed by 40 cycles of 95 °C, 15 seconds; 58 °C (melting temperature for each pair of primers), 30 seconds; 72 °C, 30 seconds. Fluorescence detection of product was performed at the end of the PCR extension, and melting curves were analyzed by monitoring the continuous decrease in fluorescence of the SYBR Green signal. PCR products were verified for a single amplification product using melting curve analysis, and the molecular weight of each product was confirmed by agarose electrophoresis. Quantification relative to m36B4 controls was calculated using the Pfaffl method.[50]

Histology and immunological assays

Anesthetized animals were perfused with phosphate buffer, followed by 4% paraformaldehyde in phosphate buffer. Cryoprotected sciatic nerves, DRG, and spinal cord containing lumbar, thoracic, or cervical segments were embedded in Tissue-Tek Oct Compound (Miles, Elkhart, IN). Ten-micrometer-thick sections of sciatic nerves and DRG and 20-µm-thick sections of spinal cord and brain were blocked and incubated with primary antibodies overnight at 4 °C. For sciatic nerves and DRG, the antibodies used were: anti-PGP 9.5 (1:500; UltraClone, Isle of Wight, UK), anti-S100 (1:500; DakoCytomation, Glostrup, Denmark), anti-CRGP and anti-NF200 (1:400; Sigma-Aldrich), anti-peripherin (1:400; Millipore, Billerica, MA), and Isolectin IB4 (1:200; Millipore). Spinal cord sections were incubated with the following primary antibodies: anti-APC1 (1:400; Calbiochem, Merck KGaA, Darmstadt, Germany), anti-glial fibrillary acidic protein (1:500; DakoCytomation), anti-Iba1 (1:1,000; Wako Chemicals, Richmond, VA), anti–choline acetyltransferase (1:50; Millipore), and anti-IGF-I (1:100; Abcam, Cambridge, UK). Sections were then incubated with the following secondary antibodies: Alexa Fluor Goat Anti-rabbit 568, Alexa Fluor Goat Anti-mouse 568, and Alexa Fluor Rabit Anti-goat 568 (1:200; Invitrogen, Carlsbad, CA). Finally, sections were counterstained with Hoescht stain solution (Sigma-Aldrich) for nuclei labeling, and they were mounted in Gel Mount (Sigma-Aldrich). Fluorescence was detected with a laser-scanning confocal microscope (TCs SP2; Leica Microsystems, Heidelberg, Germany), and images taken for quantification. For DRG neuron counting, one every five sections was selected, and DRG neurons were identified as large, round cell bodies with large round nuclei, surrounded by satellite cells with small elongated nuclei, and counted by two independent researchers. At least five sections for each DRG were used. GFP was detected by direct fluorescence, without antibody enhancement.

For spinal cord neuron counting, 40 µm sections separated by 200 µm of each spinal cord were stained with Neurotrace red fluorescent Nissl (Molecular Probes, Eugene, OR) following manufacturer's instructions. GFP-positive cells localized in the ventral horn were counted, without antibody enhancement, along the spinal cord to estimate the number of ventral neurons transduced in each segment. For α-motoneuron counting, only choline acetyltransferase–positive neurons with diameters above 20 µm, with a prominent nucleolus and polygonal shape in the ventral horn were considered in Nissl-stained sections. Counting was performed by two different researchers, and data were pooled together.

Western blot. Sciatic nerves, DRGs, and spinal cord were sonicated and homogenized in RIA lysis buffer (50 mmol/l Tris–Cl pH 7.4, 150 mmol/l NaCl, 1 mmol/l ethylenediaminetetraacetic acid, 1% NP-40, and 0.25% sodium deoxycholate) and Complete Mini EDTA-free protease inhibitor cocktail tablets (Roche Diagnostics). Protein concentration was determined by BCA Protein Assay (Pierce, Rockford, IL), and 50 µg of proteins were separated on 10% sodium dodecyl sulfate–polyacrylamide gel electrophoresis gel (Bio-Rad, Hercules, CA). Polyvinylidene fluoride membranes were incubated with anti-VEGF (1:200; Abcam), anti-Akt-P (Ser473) (1:500; Cell Signaling Technology, Danvers, MA), anti-GAP-43 (1:500; Millipore) and anti-P0 (1:500; Abcam), and anti-rabbit conjugated to horseradish peroxidase (1:2,000; DakoCytomation) combined with western blotting detection reagent (ECL Plus; Amersham, Freiburg, Germany) according to the manufacturer's instructions. The same membranes were stripped and incubated with anti-actin (1:500; Sigma-Aldrich) and anti-total Akt (1:500; Cell Signaling Technology). Band pixel intensities were quantified by GeneSnap software for Gene Genius Bio Imaging System (Syngene, Cambridge, UK) and normalized by anti-actin levels in each line and by anti-total Akt levels for Akt-P samples.

Statistics

Values are represented as mean ± SEM. Statistical analyses using Student's *t*-test or one- and two-way analysis of variance with Bonferroni or Tukey *post hoc* tests were performed for each set of data. Differences were considered statistically significant if $P < 0.05$.

CONFLICT OF INTEREST

The authors declare no conflict of interest.

ACKNOWLEDGMENTS

We thank the Vector Production Unit at CBATEG (Universitat Autònoma de Barcelona) that was supported by the *Association Française contre les Myopathies* (AFM) for producing AAV vectors, James M. Wilson (University of Pennsylvania) for providing AAV1 and AAV10 RepCap plasmids, and Meritxell Puig and David Ramos (CBATEG, UAB) for technical assistance. J.H., G.P. and L.A. were recipients of predoctoral fellowships (J.H. from the AFM: AFM2008/13622AE; G.P. and L.A. from the Generalitat de Catalunya: 2009FI_B00219 and 2006FI00762, respectively). A.B. was a beneficiary of the Ramon y Cajal Program. This work was supported by the EU (Treat-NMD Network of Excellence, FP6), the Instituto de Salud Carlos III (PS09730 to A.B., ISCIII-PI10-00561 to M.C., TERCEL funds to X.N.), the Generalitat de Catalunya (SGR 2009-1300), the Marató TV3 (110432 to A.B. and C.C.) and the UAB (EME04-07).

REFERENCES

1 Whiting, DR, Guariguata, L, Weil, C and Shaw, J (2011). IDF diabetes atlas: global estimates of the prevalence of diabetes for 2011 and 2030. *Diabetes Res Clin Pract* **94**: 311–321.
2 Shaw, JE, de Courten, M, Boyko, EJ and Zimmet, PZ (1999). Impact of new diagnostic criteria for diabetes on different populations. *Diabetes Care* **22**: 762–766.
3 Dyck, P and Giannini, C (1999). Pathologic alterations in human diabetic polineuropathy. In: Dyck, P and Thomas, P (eds). *Diabetic Neuropathy, 2nd ed*. Saunders: Philadelphia. pp. 279–275.
4 Hu, Y, Leaver, SG, Plant, GW, Hendriks, WT, Niclou, SP, Verhaagen, J *et al*. (2005). Lentiviral-mediated transfer of CNTF to schwann cells within reconstructed peripheral nerve grafts enhances adult retinal ganglion cell survival and axonal regeneration. *Mol Ther* **11**: 906–915.
5 Hendriks, WT, Eggers, R, Verhaagen, J and Boer, GJ (2007). Gene transfer to the spinal cord neural scar with lentiviral vectors: predominant transgene expression in astrocytes but not in meningeal cells. *J Neurosci Res* **85**: 3041–3052.
6 Homs, J, Ariza, L, Pagès, G, Udina, E, Navarro, X, Chillón, M *et al*. (2011). Schwann cell targeting via intrasciatic injection of AAV8 as gene therapy strategy for peripheral nerve regeneration. *Gene Ther* **18**: 622–630.
7 Srinivasan, R, Fink, DJ and Glorioso, JC (2008). HSV vectors for gene therapy of chronic pain. *Curr Opin Mol Ther* **10**: 449–455.
8 Hollis, ER 2nd, Kadoya, K, Hirsch, M, Samulski, RJ and Tuszynski, MH (2008). Efficient retrograde neuronal transduction utilizing self-complementary AAV1. *Mol Ther* **16**: 296–301.
9 Storek, B, Reinhardt, M, Wang, C, Janssen, WG, Harder, NM, Banck, MS *et al*. (2008). Sensory neuron targeting by self-complementary AAV8 via lumbar puncture for chronic pain. *Proc Natl Acad Sci USA* **105**: 1055–1060.
10 Towne, C, Pertin, M, Beggah, AT, Aebischer, P and Decosterd, I (2009). Recombinant adeno-associated virus serotype 6 (rAAV2/6)-mediated gene transfer to nociceptive neurons through different routes of delivery. *Mol Pain* **5**: 52.
11 Mason, MR, Ehlert, EM, Eggers, R, Pool, CW, Hermening, S, Huseinovic, A *et al*. (2010). Comparison of AAV serotypes for gene delivery to dorsal root ganglion neurons. *Mol Ther* **18**: 715–724.
12 Zheng, H, Qiao, C, Wang, CH, Li, J, Li, J, Yuan, Z *et al*. (2010). Efficient retrograde transport of adeno-associated virus type 8 to spinal cord and dorsal root ganglion after vector delivery in muscle. *Hum Gene Ther* **21**: 87–97.
13 White, E, Bienemann, A, Sena-Esteves, M, Taylor, H, Bunnun, C, Castrique, E *et al*. (2011). Evaluation and optimization of the administration of recombinant adeno-associated viral vectors (serotypes 2/1, 2/2, 2/rh8, 2/9, and 2/rh10) by convection-enhanced delivery to the striatum. *Hum Gene Ther* **22**: 237–251.
14 Sondhi, D, Hackett, NR, Peterson, DA, Stratton, J, Baad, M, Travis, KM *et al*. (2007). Enhanced survival of the LINCL mouse following CLN2 gene transfer using the rh.10 rhesus macaque-derived adeno-associated virus vector. *Mol Ther* **15**: 481–491.
15 Zhang, H, Yang, B, Mu, X, Ahmed, SS, Su, Q, He, R *et al*. (2011). Several rAAV vectors efficiently cross the blood-brain barrier and transduce neurons and astrocytes in the neonatal mouse central nervous system. *Mol Ther* **19**: 1440–1448.
16 Hu, C, Busuttil, RW and Lipshutz, GS (2010). RH10 provides superior transgene expression in mice when compared with natural AAV serotypes for neonatal gene therapy. *J Gene Med* **12**: 766–778.
17 Federici, T, Taub, JS, Baum, GR, Gray, SJ, Grieger, JC, Matthews, KA *et al*. (2012). Robust spinal motor neuron transduction following intrathecal delivery of AAV9 in pigs. *Gene Ther* **19**: 852–859.
18 Snyder, BR, Gray, SJ, Quach, ET, Huang, JW, Leung, CH, Samulski, RJ *et al*. (2011). Comparison of adeno-associated viral vector serotypes for spinal cord and motor neuron gene delivery. *Hum Gene Ther* **22**: 1129–1135.
19 Samaranch, L, Salegio, EA, San Sebastian, W, Kells, AP, Bringas, JR, Forsayeth, J *et al*. (2013). Strong cortical and spinal cord transduction after AAV7 and AAV9 delivery into the cerebrospinal fluid of nonhuman primates. *Hum Gene Ther* **24**: 526–532.
20 Gray, SJ, Nagabhushan Kalburgi, S, McCown, TJ and Jude Samulski, R (2013). Global CNS gene delivery and evasion of anti-AAV-neutralizing antibodies by intrathecal AAV administration in non-human primates. *Gene Ther* **20**: 450–459.
21 Kennedy, JM and Zochodne, DW (2000). The regenerative deficit of peripheral nerves in experimental diabetes: its extent, timing and possible mechanisms. *Brain* **123** (Pt 10): 2118–2129.
22 Homs, J, Ariza, L, Pagès, G, Verdú, E, Casals, L, Udina, E *et al*. (2011). Comparative study of peripheral neuropathy and nerve regeneration in NOD and ICR diabetic mice. *J Peripher Nerv Syst* **16**: 213–227.
23 Craner, MJ, Klein, JP, Black, JA and Waxman, SG (2002). Preferential expression of IGF-I in small DRG neurons and down-regulation following injury. *Neuroreport* **13**: 1649–1652.
24 Franco, LM, Sun, B, Yang, X, Bird, A, Zhang, H, Schneider, A *et al*. (2005). Evasion of immune responses to introduced human acid alpha-glucosidase by liver-restricted expression in glycogen storage disease type II. *Mol Ther* **12**: 876–884.
25 Wang, L, Dobrzynski, E, Schlachterman, A, Cao, O and Herzog, RW (2005). Systemic protein delivery by muscle-gene transfer is limited by a local immune response. *Blood* **105**: 4226–4234.
26 Bevan, AK, Hutchinson, KR, Foust, KD, Braun, L, McGovern, VL, Schmelzer, L *et al*. (2010). Early heart failure in the SMNDelta7 model of spinal muscular atrophy and correction by postnatal scAAV9-SMN delivery. *Hum Mol Genet* **19**: 3895–3905.
27 Foust, KD, Wang, X, McGovern, VL, Braun, L, Bevan, AK, Haidet, AM *et al*. (2010). Rescue of the spinal muscular atrophy phenotype in a mouse model by early postnatal delivery of SMN. *Nat Biotechnol* **28**: 271–274.
28 Dominguez, E, Marais, T, Chatauret, N, Benkhelifa-Ziyyat, S, Duque, S, Ravassard, P *et al*. (2011). Intravenous scAAV9 delivery of a codon-optimized SMN1 sequence rescues SMA mice. *Hum Mol Genet* **20**: 681–693.
29 Towne, C, Schneider, BL, Kieran, D, Redmond, DE Jr and Aebischer, P (2010). Efficient transduction of non-human primate motor neurons after intramuscular delivery of recombinant AAV serotype 6. *Gene Ther* **17**: 141–146.
30 Duque, S, Joussemet, B, Riviere, C, Marais, T, Dubreil, L, Douar, AM *et al*. (2009). Intravenous administration of self-complementary AAV9 enables transgene delivery to adult motor neurons. *Mol Ther* **17**: 1187–1196.
31 Bevan, AK, Duque, S, Foust, KD, Morales, PR, Braun, L, Schmelzer, L *et al*. (2011). Systemic gene delivery in large species for targeting spinal cord, brain, and peripheral tissues for pediatric disorders. *Mol Ther* **19**: 1971–1980.
32 Samaranch, L, Salegio, EA, San Sebastian, W, Kells, AP, Foust, KD, Bringas, JR *et al*. (2012). Adeno-associated virus serotype 9 transduction in the central nervous system of nonhuman primates. *Hum Gene Ther* **23**: 382–389.
33 Foust, KD, Nurre, E, Montgomery, CL, Hernandez, A, Chan, CM and Kaspar, BK (2009). Intravascular AAV9 preferentially targets neonatal neurons and adult astrocytes. *Nat Biotechnol* **27**: 59–65.
34 Boutin, S, Monteilhet, V, Veron, P, Leborgne, C, Benveniste, O, Montus, MF *et al*. (2010). Prevalence of serum IgG and neutralizing factors against adeno-associated virus (AAV) types 1, 2, 5, 6, 8, and 9 in the healthy population: implications for gene therapy using AAV vectors. *Hum Gene Ther* **21**: 704–712.
35 Fukuda, R, Hirota, K, Fan, F, Jung, YD, Ellis, LM and Semenza, GL (2002). Insulin-like growth factor 1 induces hypoxia-inducible factor 1-mediated vascular endothelial growth factor expression, which is dependent on MAP kinase and phosphatidylinositol 3-kinase signaling in colon cancer cells. *J Biol Chem* **277**: 38205–38211.
36 Mason, JL, Xuan, S, Dragatsis, I, Efstratiadis, A and Goldman, JE (2003). Insulin-like growth factor (IGF) signaling through type 1 IGF receptor plays an important role in remyelination. *J Neurosci* **23**: 7710–7718.
37 Delaney, CL, Russell, JW, Cheng, HL and Feldman, EL (2001). Insulin-like growth factor-I and over-expression of Bcl-xL prevent glucose-mediated apoptosis in Schwann cells. *J Neuropathol Exp Neurol* **60**: 147–160.
38 Brussee, V, Cunningham, FA and Zochodne, DW (2004). Direct insulin signaling of neurons reverses diabetic neuropathy. *Diabetes* **53**: 1824–1830.
39 Leinninger, GM, Vincent, AM and Feldman, EL (2004). The role of growth factors in diabetic peripheral neuropathy. *J Peripher Nerv Syst* **9**: 26–53.
40 Apfel, SC, Schwartz, S, Adornato, BT, Freeman, R, Biton, V, Rendell, M *et al*. (2000). Efficacy and safety of recombinant human nerve growth factor in patients with diabetic polyneuropathy: a randomized controlled trial. rhNGF Clinical Investigator Group. *JAMA* **284**: 2215–2221.
41 Isner, JM, Ropper, A and Hirst, K (2001). VEGF gene transfer for diabetic neuropathy. *Hum Gene Ther* **12**: 1593–1594.
42 Wellmer, A, Misra, VP, Sharief, MK, Kopelman, PG and Anand, P (2001). A double-blind placebo-controlled clinical trial of recombinant human brain-derived neurotrophic factor (rhBDNF) in diabetic polyneuropathy. *J Peripher Nerv Syst* **6**: 204–210.
43 Ekberg, K, Brismar, T, Johansson, BL, Lindström, P, Juntti-Berggren, L, Norrby, A *et al*. (2007). C-Peptide replacement therapy and sensory nerve function in type 1 diabetic neuropathy. *Diabetes Care* **30**: 71–76.
44 Li, H, Malani, N, Hamilton, SR, Schlachterman, A, Bussadori, G, Edmonson, SE *et al*. (2011). Assessing the potential for AAV vector genotoxicity in a murine model. *Blood* **117**: 3311–3319.
45 Sharma, A and Thomas, P (1987). Animal model: pathology and pathophysiology. In: Dyck, P, Thomas, P, Asbury, A, Winegrad, A and Porte, D Jr (eds). *Diabetic Neuropathy, 1st ed*. Saunders: Philadelphia. pp. 237–252.
46 Wright, A and Nukada, H (1994). Sciatic nerve morphology and morphometry in mature rats with streptozocin-induced diabetes. *Acta Neuropathol* **88**: 571–578.
47 Mizisin, AP, Nelson, RW, Sturges, BK, Vernau, KM, Lecouteur, RA, Williams, DC *et al*. (2007). Comparable myelinated nerve pathology in feline and human diabetes mellitus. *Acta Neuropathol* **113**: 431–442.
48 Zolotukhin, S, Byrne, BJ, Mason, E, Zolotukhin, I, Potter, M, Chesnut, K *et al*. (1999). Recombinant adeno-associated virus purification using novel methods improves infectious titer and yield. *Gene Ther* **6**: 973–985.
49 Xiao, X, Li, J and Samulski, RJ (1998). Production of high-titer recombinant adeno-associated virus vectors in the absence of helper adenovirus. *J Virol* **72**: 2224–2232.
50 Pfaffl, MW (2001). A new mathematical model for relative quantification in real-time RT-PCR. *Nucleic Acids Res* **29**: e45.

Supplementary Information accompanies this paper on the *Molecular Therapy—Methods & Clinical Development* website (http://www.nature.com/mtm)

HUMAN GENE THERAPY 25:199–211 (March 2014)

DOI: 10.1089/hum.2013.152

Central Nervous System Delivery of Helper-Dependent Canine Adenovirus Corrects Neuropathology and Behavior in Mucopolysaccharidosis Type VII Mice

Lorena Ariza,[1] Lydia Giménez-Llort,[2,*] Aurélie Cubizolle,[3,*] Gemma Pagès,[1] Belén García-Lareu,[1] Nicolas Serratrice,[3] Dan Cots,[1] Rosemary Thwaite,[1] Miguel Chillón,[1,4] Eric J. Kremer,[3] and Assumpció Bosch[1]

Abstract

Canine adenovirus type 2 vectors (CAV-2) are promising tools to treat global central nervous system (CNS) disorders because of their preferential transduction of neurons and efficient retrograde axonal transport. Here we tested the potential of a helper-dependent CAV-2 vector expressing β-glucuronidase (HD-RIGIE) in a mouse model of mucopolysaccharidosis type VII (MPS VII), a lysosomal storage disease caused by deficiency in β-glucuronidase activity. MPS VII leads to glycosaminoglycan accumulation into enlarged vesicles in peripheral tissues and the CNS, resulting in peripheral and neuronal dysfunction. After intracranial administration of HD-RIGIE, we show long-term expression of β-glucuronidase that led to correction of neuropathology around the injection site and in distal areas. This phenotypic correction correlated with a decrease in secondary-elevated lysosomal enzyme activity and glycosaminoglycan levels, consistent with global biochemical correction. Moreover, HD-RIGIE-treated mice show significant cognitive improvement. Thus, injections of HD-CAV-2 vectors in the brain allow a global and sustained expression and may have implications for brain therapy in patients with lysosomal storage disease.

Introduction

Mucopolysaccharidosis type VII (MPS VII or Sly Syndrome) is an autosomal recessive disease that belongs to a group of lysosomal storage disorders (LSD), referred to collectively as mucopolysaccharidoses (MPS), caused by the loss of function of one of several lysosomal enzymes. MPS VII is caused by a deficiency in β-glucuronidase (βgluc) activity (EC 3.2.1.31), a lysosomal hydrolase involved in the stepwise degradation of glucuronic acid-containing glycosaminoglycans (GAGs) dermatan sulfate, heparan sulfate, and chondroitin sulfate (Vogler *et al.*, 1994). Lysosomal enzymes are essentially ubiquitously expressed; thus, multiple organs are impaired because of cells accumulating undegraded substrates. MPS VII patients display a range of clinical variability, from the most severe with *hydrops fetalis* to an attenuated phenotype with late onset and almost normal intelligence (Muenzer, 2011). The features of MPS VII include coarse facies, hydrocephaly, and multiple skeletal abnormalities. Affected individuals also frequently develop hepatosplenomegaly, heart valve abnormalities, developmental delay, and progressive intellectual disability (Shipley *et al.*, 1993). The MPS VII mouse has been extensively used as a model of the human LSD as it shares clinical, biochemical, and pathological symptoms, including growth retardation (Birkenmeier *et al.*, 1989; Vogler *et al.*, 1998). Thus, MPS VII mouse is a useful tool for the evaluation of the effectiveness of experimental therapies for MPS VII disorders.

Among the treatments tested for MPS VII, bone marrow transplants, particularly in neonatal mice, can correct widespread lysosomal storage of MPS VII mice in bone, bone marrow, visceral organs, and brain; increase the lifespan to approach that found in normal mice; and correct cardiac abnormalities (Soper *et al.*, 2001; Schuldt *et al.*, 2004). Another therapeutic approach for peripheral LSD symptoms is enzyme replacement therapy (ERT). ERT has improved pathologies in patients with Gaucher disease (Grabowski *et al.*, 1998), Fabry

[1]Center of Animal Biotechnology and Gene Therapy and Department of Biochemistry and Molecular Biology, and [2]Institute of Neuroscience and Department of Psychiatry and Forensic Medicine, School of Medicine, Universitat Autònoma de Barcelona, 08193 Bellaterra, Barcelona, Spain.
[3]Institut de Génétique Moléculaire de Montpellier, Université de Montpellier 1 & 2, 34293 Montpellier, France.
[4]Institut Català de Recerca i Estudis Avançats, 08193 Barcelona, Spain.
*These two authors contributed equally to this work.

disease (Eng *et al.*, 2001; Wilcox *et al.*, 2004), Pompe disease (Thurberg *et al.*, 2006), MPS I (Kakkis *et al.*, 2001), MPS II (Muenzer, 2011), and MPS VI (Harmatz *et al.*, 2006). For MPS VII, data from animal models (O'Connor *et al.*, 1998; LeBowitz *et al.*, 2004) have supported the approval of a phase 1/2 clinical trial (NCT01856218). However, this approach is limited by the permeability of the blood–brain barrier (BBB). As many LSD, including MPS VII, affect the central nervous system (CNS), a strategy that can cross the BBB is necessary.

One approach to address long-term CNS therapy is gene transfer via viral vectors that confer stable and long-term correction. This could provide sustained therapy if a sufficient level of enzyme was secreted in the brain. We and others have demonstrated the potential of different vectors in correcting neuronal pathologies in MPS II (Cardone *et al.*, 2006), MPS IIIA and B (Cressant *et al.*, 2004; Langford-Smith *et al.*, 2012), and MPS VII mice (Bosch *et al.*, 2000a,b; Liu *et al.*, 2007) as well as in larger animal models for the disease (Ciron *et al.*, 2006; Ellinwood *et al.*, 2011). However, clinically relevant gene therapy using common human pathogens as vectors may be complicated by the high incidence of preexisting humoral and cellular immunity (Chirmule *et al.*, 1999; Perreau *et al.*, 2007a).

Human adenoviral vectors induce both innate and adaptive immune responses that trigger the elimination of transgene expression in a relatively short term. Helper-dependent (HD) adenovirus can circumvent the immune response once reaching the nucleus, although they could have been previously neutralized by antiadenovirus antibodies (reviewed by Lowenstein *et al.*, 2007). Canine adenovirus type 2 (CAdV2, or commonly referred to as CAV-2) vectors preferentially transduce neurons, and retrograde axonal transport is efficient, leading to expression of the transgene in many areas of the brain after a single injection (Soudais *et al.*, 2001; Salinas *et al.*, 2009). Compared with human adenovirus serotype 5 vectors, CAV-2 vectors induce a low level of innate response and do not activate the human complement pathways (Keriel *et al.*, 2006; Perreau *et al.*, 2007b). In addition, limited presence and titers of neutralizing antibodies against CAV-2 are found in the human population (Kremer *et al.*, 2000; Perreau and Kremer, 2005). In addition, HD-CAV-2 vectors lead to long-term transgene expression in rodents (Soudais *et al.*, 2004), and have a cloning capacity of $\sim$30 kb. This is an advantage compared with adeno-associated viral (AAV) vectors, as it allows the possibility of modulating therapeutic genes with large, endogenous, or inducible promoters and/or regulatory sequences.

The aim of this study was to test the therapeutic efficacy of intrastriatal injection of an HD-CAV-2 vector expressing βgluc (HD-RIGIE) in MPS VII mice. We achieved global, long-term correction in MPS VII mouse brains with bilateral striatal injections of HD-RIGIE. We show recovery of biochemical and neuropathological abnormalities throughout the forebrain and midbrain, which led to significant cognitive improvement.

Materials and Methods

Animals

We used a tolerant mouse model for MPS VII (Sly *et al.*, 2001) developed from the original βgluc-deficient mouse (Levy *et al.*, 1996). Heterozygous ($Gus^{mps/+}$) mice, kindly provided by Dr. William S. Sly (St. Louis University School of Medicine, St. Louis, MO), were bred and mutants were identified at 1 month of age by the absence of βgluc activity from tail clip homogenates. Animal care and experimental procedures were performed in accordance with 86/609/EEC regarding the care and use of animals for experimental procedures and were approved by the Biosafety and the Ethics Committees of the Universitat Autònoma de Barcelona.

First-generation CAV-2 vectors

E1-deleted CAVGFP has been previously described (Kremer *et al.*, 2000). Vector particles were produced in canine E1 *trans*-complementing cells (DKZeo), originally derived from the canine kidney cell line DK (ATCC CRL6247) (Kremer *et al.*, 2000). Virus from the supernatant were concentrated by precipitation with ammonium sulfate (Schagen *et al.*, 2000) and pooled with the cellular fraction to maximize recovery. This pool was purified using two CsCl density ultracentrifugation steps and CsCl was removed by size exclusion chromatography using PD-10 columns (GE Healthcare), and the virus was stored in 10% glycerol phosphate-buffered saline. Titers were 1.44×10^{12} physical particles (pp)/ml with a pp to infectious particle (ip) ratio of 4:1.

Production of HD-RIGIE and HD-GFP vectors

HD-RIGIE expressed the human *GUSB* cDNA and GFP under the control of a Rous sarcoma virus promoter. The RIGIE cassette (RSV-IVS-*GUSB*-IRES-EGFP) was generated using classic molecular biology techniques. The human GUSB cDNA was a gift from William Sly (University of St Louis). *Asc*I/*Not*I-digested pHD-RIGIE or pHD-GFP were transfected into 5×10^6 DKZeo cells using 18 μl of Turbofect (Fermentas, Thermo Scientific) for 10 μg of linearized DNA/10 cm plate. The cells were infected with 100 pp of helper vector/cell. GFP^+ cells were collected by flow cytometry 24 hr post-transfection, re-plated, and lysed by three freeze–thaw cycles 20 hr later. Cells were sorted after transfection until at least 2×10^6 of GFP^+ cells were isolated. The cleared lysates were then incubated on a fresh monolayer of DKZeo cells using helper vector JBΔ5. Twenty-four hours postinfection, GFP^+ cells were sorted by flow cytometry, replated, and lysed by three freeze–thaw cycles 20 hr later. The cleared lysate was used for amplification until 3×10^7 GFP^+ cells were obtained. At each amplification step, DKZeo cells were coinfected with 100 pp/cell of helper vector. Finally, the last amplification occurred in $\sim8\times10^8$ DKCre cells without adding helper vector. JBΔ5 contains a loxP-flanked packaging domain and an RSV-lacZ expression cassette (Soudais *et al.*, 2001, 2004). When propagated in DKCre cells, an $\sim$900 bp fragment containing the packaging domain and part of the RSV promoter was excised (floxed), and the resulting 32.3 kb vector was rendered packaging deficient (Soudais *et al.*, 2004). The helper vector retained a minimal part of the RSV promoter, which promoted *lacZ* expression. To test the level of helper contamination in HD vector preparations, β-galactosidase activity was assayed by X-gal staining. HD-RIGIE was purified by triple banding on CsCl density gradients: an initial step gradient of 1.25 and 1.45 g/ml, and then two self-forming isopycnic gradients using 1.32 g/ml CsCl as previously described (Soudais *et al.*, 2004). The purified stock was stored at -80°C in phosphate-buffered saline (PBS)/10% glycerol.

Physical particles titers were determined by OD at 260 nm and quantitative polymerase chain reaction (qPCR) and were found to be $\sim 1.3 \times 10^{12}$ pp/ml. HD-RIGIE ip were determined by GFP expression. Combined, the pp/ip ratio was 60:1. Because of the relatively low level of GFP from the combination of the weak RSV promoter and IRES in DK cells, this ratio likely overestimates the pp-to-ip ratio. As assayed by X-gal staining and qPCR, helper vector contamination varied between preparations from <1% to ~10%.

Animal studies

Intracranial injections. Mice were anesthetized by intraperitoneal injection of ketamine (10 mg/kg of body weight; Imalgene 500; Rhône-Merieux) and xylazine (1 mg/kg of body weight; Rompun; Bayer) and mounted onto a stereotactic frame (David Kopf Instruments). The skull was exposed by a small incision. A small burr hole was made 1 mm caudal and 1.5 mm lateral to bregma. Three microliters of the vector preparation was loaded into a Hamilton syringe mounted to the stereotactic frame. The tip of the needle was inserted into the striatum 3.0 mm in depth from the skull surface in heterozygous mice and 2.6 mm in mutant mice, and 2 μl of HD-RIGIE, corresponding to 2×10^9 pp, was delivered with an ultramicropump (World Precision Instruments) at a rate of 0.5 μl/min. The needle was slowly withdrawn after an additional 5 min. Mock-injected control animals were injected in the same coordinates with 2 μl of PBS.

Transient immunosuppression. Cyclophosphamide (CFA; Sigma) was diluted in PBS and administered intraperitoneally at 50 mg/kg of body weight every 2 days, from day −3 to day + 13, considering day 0 as the intracranial injection time, as a modification of the treatment defined by Cao *et al.* (2011).

Behavioral tests

A standardized set of experimental procedures (abbreviated SHIRPA, Giménez-Holt *et al.*, 2002) were used to characterize the phenotype of treated mice. Observation of undisturbed behavior in the home-cage was followed by assessment of fluorimeter tasks.

Rod tests. Motor coordination and equilibrium were assessed by the distance covered and the latency to fall off a horizontal wood rod (1.3 cm diameter) and a wire rod (1 cm diameter) on two consecutive 20 sec trials.

Hanger test. Prehensility and motor coordination were measured as the distance covered on the *wire hang test*, where the animals were allowed to cling (2 mm diameter, 40 cm long) with their forepaws for two trials of 5 sec and a third 60 sec trial. Muscle strength was measured as the time until falling off the wire in the 60 sec trial. All the apparatus were suspended 40 cm above a padded table.

Tertiary screen was designed tailored to neuropsychiatric-like deficits, assessing spontaneous exploratory behavior, anxiety-like behaviors, and cognition in a series of tests involving different degrees of complexity.

Corner test. Neophobia was recorded in a new home-cage by the horizontal (*n* of visited corners) and vertical (*n* and latency of rearings) activity during a period of 30 sec.

Open-field test. Exploratory activity and anxiety-like behaviors were evaluated for 5 min by means of horizontal (crossings of 5×5 cm) and vertical (rearings) locomotor activities recorded for each minute of the test.

T-maze. The spontaneous exploratory behavior was tested in a T-shaped maze (arms, length 25 cm). Animals were placed inside the vertical arm of the maze facing the end wall. The performance was evaluated by determining the time elapsed until the animal crossed (four-paw criteria) the intersection of the three arms.

Spatial learning and memory in a 2-day water maze. On day 1, animals were trained to criterion (90% escaping under 60 sec) in a series of cued visible platform trials (7 cm diameter, 1 cm above the water surface, position indicated by a visible 5×8 cm striped flag, 20 min intertrial time) in a pool (Intex Recreation; 91 cm diameter, 40 cm deep, 25°C opaque water). This required four platform trials (CUE1–CUE4). The last visible platform trial of any animal was considered to be its posthabituation baseline and was designated CUE4 (cued visible platform trial 4). Mice that failed to find the platform within 90 sec were manually guided to the platform and placed on it for 5–10 sec, the same period as successful animals. Twenty-four hours after the last cued platform trial, animals were tested in a series of four hidden platform trials (PT1–PT4, 20 min apart). In these place-learning tasks, the hidden platform (1.5 cm below the water surface) was located in a new position, opposite the one used for cue learning. Escape latencies were measured with a stopwatch.

Biochemical assays

Detection of lysosomal enzyme activities in tissue extracts. Deeply anesthetized animals were euthanized. The cerebrum was removed and sliced into 2-mm-thick slices using a mouse brain slicer (Zivic Instruments) and stored at −80°C. Tissues were homogenized in lysis buffer (25 m*M* Tris, 75 m*M* NaCl [pH 7.5]; both from Sigma) and centrifuged at $12{,}000 \times g$ for 10 min at 4°C. Ten micrograms of each slice was assayed in a fluorimeter Wallac 1420 Victor3 (Perkin Elmer) for βgluc or β-hexosaminidase activity using 10 m*M* 4-methylumbelliferyl-β-D-glucuronide (Sigma) or 0.01 m*M* 4-methylumbelliferyl-N-acetyl-β-D-glucosaminide (Sigma) as substrate, respectively.

Detection of βgluc activity in tissue sections. Animals were anesthetized and perfused with 4% paraformaldehyde, and brains were removed and postfixed. After cryoprotection with 30% sucrose, tissues were embedded in O.C.T. Tissue Tek compound (Miles Scientific) and cut into 10-μm-thick sagittal or coronal sections. Sections were incubated for 4 hr at 37°C with 0.004% hexazotized pararosaniline in 0.25 m*M* naphtol-AS-BI-β-D-glucuronide (Sigma).

For volumetric estimation of βgluc extension, 100-μm-thick coronal sections were cut at 4°C after 5 hr postfixation with 4% paraformaldehyde using a vibratome (Leica). The whole cerebrum was sectioned, and one in every five sections was stained for βgluc activity. Transduction volume was estimated based on the number of slides positive for β-gluc.

GAG quantification. Twenty milligrams of each 2-mm-thick slice was homogenized in papain extraction reagent at 65°C for 3 hr. GAG content was determined using the Blyscan Sulfated Glycosaminoglycan Assay (Biocolor).

Histology and immunological assays

Ten-micrometer-thick cryosections were obtained as described above. Sections were blocked with 2% bovine serum albumin and incubated with rabbit anti-Iba1 (1:500; Wako Chemicals GmbH) or NeuN (1:200; Chemicon, Millipore) overnight at 4°C. Goat antirabbit Alexa Fluor 568 as a secondary antibody (1:200; Molecular Probes) and a Hoechst solution to stain the nuclei (Sigma) were used. To quantify cortical microglia, $Iba1^+$ cells from different sections around the injected area were counted and normalized by the total number of cells counterstained with Hoechst.

Histopathology. About 100-μm-thick coronal brain sections were postfixed with 4% paraformaldehyde and 1% glutaraldehyde and then with 1% osmium tetroxide, and finally embedded in Epon (all reagents from Sigma). One-micrometer-thick sections were cut and stained with toluidine blue for 30 sec. Histological sections were evaluated morphologically by light microscopy. Sections were further examined, and 200 cells per section and brain structure were counted for each animal to evaluate the percentage of cells without or with very small cytoplasmic vacuoles.

Quantitative polymerase chain reaction

Genomic DNA was obtained from 2-mm-thick brain slices with 0.1 mg/ml of proteinase K (Roche Diagnostics), followed by phenol/chloroform extraction. HD-RIGIE genome copy numbers were measured by qPCR using the Bio-Rad CFX Manager (Bio-Rad Laboratories) and SYBR green PCR (Bio-Rad Laboratories). Briefly, vector sequences and mouse genomic cyclophilin (as reference gene) sequences were simultaneously amplified, and each sample was expressed in terms of its cyclophilin content. The results (vector genome copy number per cell, viral genomes [vg]/cell) were expressed as *n*-fold differences in the transgene sequence copy number relative to the cyclophilin gene copy number (number of vg copies for 2N genome). Samples were considered eligible for the study if the cyclophilin sequence C_t values were <26 and were scored vector-negative if the transgene sequence C_t value was >35. Thermal cycling conditions comprised an initial denaturing step at 95°C for 3 min, followed by 40 cycles at 95°C for 10 sec, 58°C for 10 sec, and 72°C for 30 sec. Each sample was analyzed in duplicate. Nucleotide sequences of primers are available on request.

Statistics

Values are represented as mean ± SEM. Statistical analyses using Student's *t*-test or one- and two-way ANOVA with *post-hoc* tests were performed for each data set. Repeated-measures ANOVA with a two-factorial design T × G (T = effect of time; G = effect of group) was used for behavioral tests, followed by *post-hoc* Duncan's test. Differences were considered statistically significant if $p < 0.05$.

Results and Discussion

Microglia activation prevents HD-CAV-2 expression in the mouse brain

CAV-2 can be retrogradely transported to different areas of the brain after a single injection into the striatum (Soudais *et al.*, 2004). Thus, although MPS VII causes global CNS pathology, we asked if a single injection exclusively in the striatum of 8–10-week-old MPS VII mice with 2×10^9 pp of HD-RIGIE could be of therapeutic efficacy. Animals were euthanized 1 and 6 weeks after the injection. Brains were sectioned into six 2-mm-thick slices, rostral to caudal, as represented in Fig. 1a. GFP expression was observed 1 week postinjection at the injection area and in more distal regions of the brain such as the substantia nigra, containing neurons from the nigrostriatal pathway and projecting their axons to the striatum (Fig. 1b), indicating that CAV-2 vectors maintain retrograde transport in MPS VII brains. Animals euthanized at 1 week posttreatment showed the presence of viral DNA in four of the six slices in the injected hemisphere, with a maximum of 16.83 ± 4.41 vg/cell in S2, corresponding to the injection area. We also observed the presence of viral DNA in the contralateral hemisphere although at lower levels, which may be caused by retrogradely transported virus or to leakage of the vector in the cerebrospinal fluid that may lead to the infection of cells in the choroid plexus or in the ependyma around the ventricles, mainly contained in S2 (Supplementary Fig. S1; Supplementary Data are available online at www.liebertpub.com/hum). No DNA was detected in S5 and S6, slices containing the cerebellum and brainstem. However, no GFP expression was observed in the animals euthanized 5 weeks later, neither βgluc activity (data not shown), correlating with the disappearance of vg in these slices (Fig. 1c).

Delivery of Ad vectors into the CNS induces dose-dependent innate immune responses in the form of acute inflammation, including microglial activation, macrophage recruitment, and T-cell infiltration (Thomas *et al.*, 2001). Consequently, we detected Iba1-positive cells, a marker of microglia, in the brains of animals injected with CAV-2 vector and euthanized 1 week later, correlating with the presence of CAV-2 vg and GFP expression, as seen at the injection area (Fig. 1d) and at the substantia nigra (not shown). Quantification of this signal showed stronger Iba1 staining with first-generation CAV-2 vector than with HD vector at both times analyzed, consistent with a reduction in the immune reaction elicited by HD adenovirus (Fig. 1e). In animals euthanized 6 weeks after injection of HD-RIGIE, mild activation was present only at the injection point, nonstatistically different from brains injected with PBS or noninjected (Fig. 1e). Thus, in contrast to results seen in rats and other mouse strains (Soudais *et al.*, 2004; Sotak *et al.*, 2005), in our hands, E1-deleted and HD-CAV-2 vectors led to short-term transgene expression associated with Iba1 expression. Although HD-Ad vectors do not express viral antigens, innate inflammatory responses to high doses of Ad could trigger elimination of transduced cells even using HD vectors (Muhammad *et al*., 2012). Moreover, acute toxicity provoked by viral capsid proteins or residual helper vector could also elicit an immune response that could eliminate the transduced cells. Furthermore, in addition to viral proteins, immune responses may have occurred against GFP,

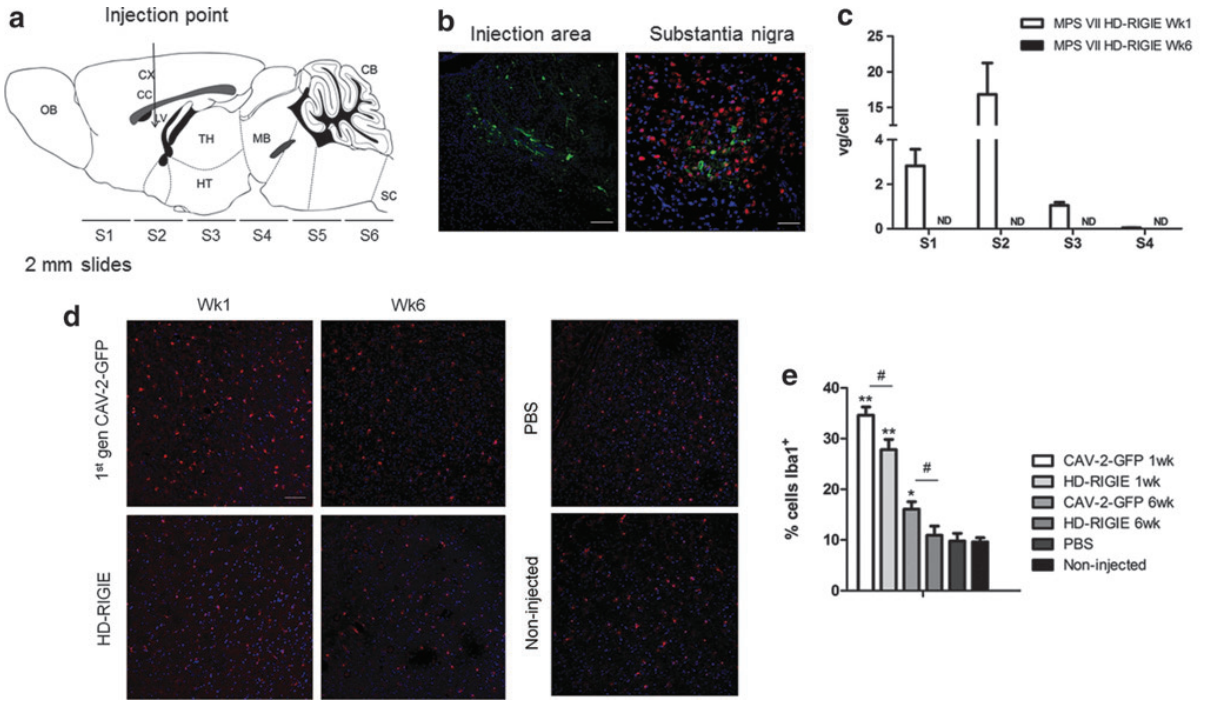

FIG. 1. Immune response avoids long-term expression of HD-CAV-2 vectors in CNS **(a)** Mouse brain diagram showing the coordinates used for the administration of HD-RIGIE, and the 2-mm-thick slices analyzed (S1–S6). CB, cerebellum; CC, corpus callosum; CX, cerebral cortex; HT, hypothalamus; LV, lateral ventricle; MB, midbrain; OB, olfactory bulb; SC, spinal cord; TH, thalamus. **(b)** Representative pictures of MPS VII mice injected with HD-RIGIE 1 week earlier: on the left image GFP expression at the injection point (scale bar = 100 μm), and at the substantia nigra on the right image (scale bar = 50 μm). Nuclei counterstaining was with Hoechst (blue) and neurons with NeuN (red). **(c)** Viral genomes per cell were quantified by qPCR in 2-mm-thick slices of brains injected with HD-RIGIE 1 and 6 weeks later. Disappearance of viral genomes at 6 weeks was observed (ND, not detected). **(d)** Microglia activation is identified by Iba1 staining (red) at the injection area 1 and 6 weeks after administration (left panel) of CAVGFP (up) and HD-RIGIE (down). Nuclei were counterstained with Hoechst (blue). The right panel shows Iba1 staining in animals injected with PBS or noninjected, as a control. Scale bar = 100 μm. **(e)** Percentage of Iba1$^+$ cells/field in the different animals injected. Data are mean ± SEM, $n = 2$ animals euthanized at Wk1 and $n = 5$ animals euthanized at Wk6 postinjection; $^*p < 0.05$, $^{**}p < 0.01$ comparing noninjected with vector-injected animals; $^{\#}p < 0.05$ comparing CAVGFP and HD-RIGIE at the same time points. CAV-2, canine adenovirus type 2 vectors; CNS, central nervous system; HD-RIGIE, helper-dependent CAV-2 vector expressing β-glucuronidase; PBS, phosphate-buffered saline; qPCR, quantitative polymerase chain reaction; Wk, week.

used in this proof-of-principle study as a marker to identify transduced cells. Clearly, a clinical-grade vector would not have a GFP expression cassette.

Because GAG and ganglioside accumulation are associated with chronic CNS inflammation, and the response to viral vector varies between genus, species, and even strains, we transiently immunosuppressed the animals with 50 mg/kg CFA (Supplementary Fig. S2), previously used to reduce inflammation and neutralizing antibody formation (Cao *et al.*, 2011). Iba1 immunohistochemistry in the HD-RIGIE-injected and transiently immunosuppressed mice showed no activation compared with control mice (Fig. 2a). More importantly, βgluc activity was detected in brain slices from MPS VII mice injected with HD-RIGIE 6 weeks earlier (Fig. 2b). Thus, 50 mg/kg of CFA treatment was followed for the rest of the experiments. CFA is widely used to treat autoimmune diseases, to prevent rejection after allograft organ transplantation and to suppress antibody formation (Moore *et al.*, 2006). Probably other transitory immunosuppressants such as cyclosporine A could have also worked in our model. However, the clinical relevance of this treatable inflammatory response in mice is unknown because mice and humans have notably different reactions in many cases (Seok *et al.*, 2013).

Lysosomal enzyme activities in HD-RIGIE-injected MPS VII mice

On the basis of these results, a group of 8–10-week-old animals was injected bilaterally in the striata (Fig. 1a). Control littermates (heterozygous and mutant mice) were mock injected with the same volume of PBS and treated with CFA at the same time and dose. Mice were euthanized at 6 and 16 weeks, and βgluc activity was assayed using *in situ* coloration by incubating slices with hexazotized pararosaniline in 0.25 m*M* naphtol-AS-BI-β-D-glucuronide in 100-μm-thick sections, one in every 5 sections, along the whole brain. This is an insensitive assay that stains βgluc activity in red. βgluc activity was not detected in PBS-treated or heterozygous mice, showing the low sensitivity of

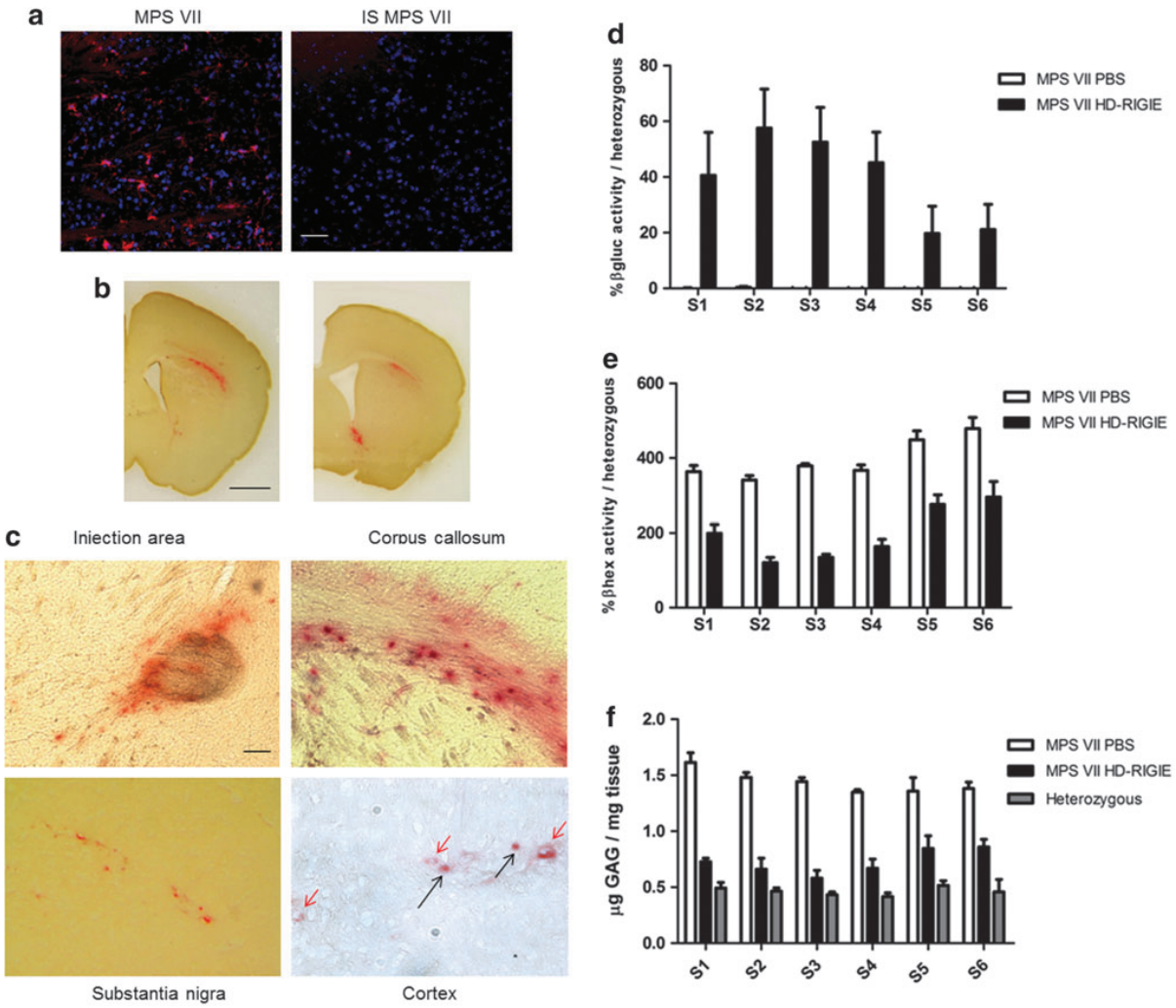

FIG. 2. Lysosomal enzyme activity and GAG accumulation analysis 6 weeks postinjection. **(a)** Iba1 staining (red) in immunocompetent (left image) or transiently immunosuppressed MPS VII mice with 50 mg/kg of cyclophosphamide (right image) show lack of activated microglia after HD-RIGIE administration (scale bar = 50 μm; nuclei were counterstained with Hoechst [blue]). βgluc activity (red) in **(b)** 100-μm-thick (scale bar = 1 mm) and **(c)** 10-μm-thick brain slices at the injection area and other distal areas such as corpus callosum, substantia nigra, and cortex; red and black arrows indicate endothelial cells and cortical neurons, respectively, identified by morphology in cortex cryosections (scale bar = 100 μm). βgluc activity **(d)**, secondary elevation of lysosomal enzyme β-hexosaminidase **(e)**, and GAG accumulation **(f)** in 2-mm-thick slice homogenates from MPS VII mice injected with PBS or HD-RIGIE and compared with βgluc activity in heterozygous mice ($p < 0.01$ for βgluc; $p < 0.01$ in S5 and S6 for βhex; $p < 0.01$ in S5 and S6 for GAG). No statistically significant differences were seen among heterozygous and HD-RIGIE-treated mice in slices spanning between S1 and S4. Data are mean ± SEM; $n = 7$ for each experimental group.

the assay. In HD-RIGIE-treated MPS VII mice, we detected βgluc activity in striatum, several areas of the cortex, corpus callosum, substantia nigra, and around ventricles (Fig. 2b and c), consistent with the efficient retrograde transport described for CAV-2 vectors (Soudais *et al.*, 2001; Salinas *et al.*, 2009). The majority of transduced cells had morphology suggesting that they were neurons. We also detected cells underlying blood vessels, consistent with endothelial cell morphology (Fig. 2c). Overall, based on this assay, we estimated a transduction area with a diameter of 4 mm around the injection area.

The brain of some of these animals ($n = 7$ for each group) was sliced into 2-mm-thick sections, as described in Fig. 1a, and protein extracts were prepared. For each slice, we measured βgluc and β-hexosaminidase (βhex) activity using a more sensitive fluorimetric assay. In several MPS diseases, βhex activity is elevated when another lysosomal enzyme activity is missing, likely because of transcription factor EB (TFEB) (Sardiello *et al.*, 2009). Data were plotted as the percentage of activity of each enzyme compared with heterozygous mouse levels, which have a normal phenotype (Fig. 2d and e). This MPS VII mouse model was created to

be tolerant for human βgluc, by expressing a mutant inactive form of human βgluc, although protein levels are almost undetectable in most tissues (Sly *et al.*, 2001). Notably, βgluc activity in heterozygous mice is 80% of the wild-type animals (data not shown). As seen in Fig. 2d, no βgluc activity was detected in mock-treated MPS VII mice. By contrast, HD-RIGIE-treated mice showed near 50% of the βgluc activity found in heterozygous animals from slice 1 to 4, with the maximum at the injection area (S2) (up to 57.55% ± 14.02%) and around 20% in S5 and S6, corresponding to cerebellum and brainstem ($p < 0.01$). Equally relevant, we found a significant decrease in the secondary elevation of βhex in all brain areas, consistent with the biochemical correction of βgluc deficiency (Fig. 2e). βhex activity reached heterozygous levels (120.79% ± 14.015% and 120.228% ± 12.857% of heterozygous mice) in S2 and S3, respectively. We found an inverse correlation between βgluc and βhex activities in all sections. Notably, there was not a significant difference between HD-RIGIE-treated and heterozygous mice for slices S1–S4. Therefore, by administering HD-RIGIE into the striatum, we could detect CAV-2 vg and transgene activity throughout the cerebrum, which led to global protein transfer in the brain.

In MPS VII mice euthanized 16 weeks post-HD-RIGIE injection, we also found βgluc activity ($n = 4$ for each group) in tissue sections of brains for a total of 4 mm (Fig. 3a). Similar to animals analyzed 6 weeks post-HD-RIGIE injection, enzyme activity detected by fluorimetry in protein homogenates of 2-mm-thick slices showed a high level of transduction, with βgluc activity found in all the slices, spanning the whole brain. HD-RIGIE-injected mice expressed 40–65% of heterozygous activity from slices S1 to S4. The maximum activity was observed near the injection point in S2 and S3, with 63.8% ± 2.75% and 60.86% ± 4.88% of the activity of heterozygous animals, respectively (Fig. 3b). Activities around 20% were also detected in the slices corresponding to cerebellum and brainstem (S5 and S6), and no enzyme activity was detected in the MPS VII animals injected with PBS (Fig. 3b).

βhex activity showed similar pattern as in animals analyzed at 6 weeks postinjection and inversely correlated to the amount of βgluc observed in each slice. While MPS VII mice treated with PBS had around 400% of heterozygous activity, HD-RIGIE-injected MPS VII mice showed correction in S1, S5, and S6, and were not significantly different from heterozygous mice in S2, S3, and S4 (Fig. 3c).

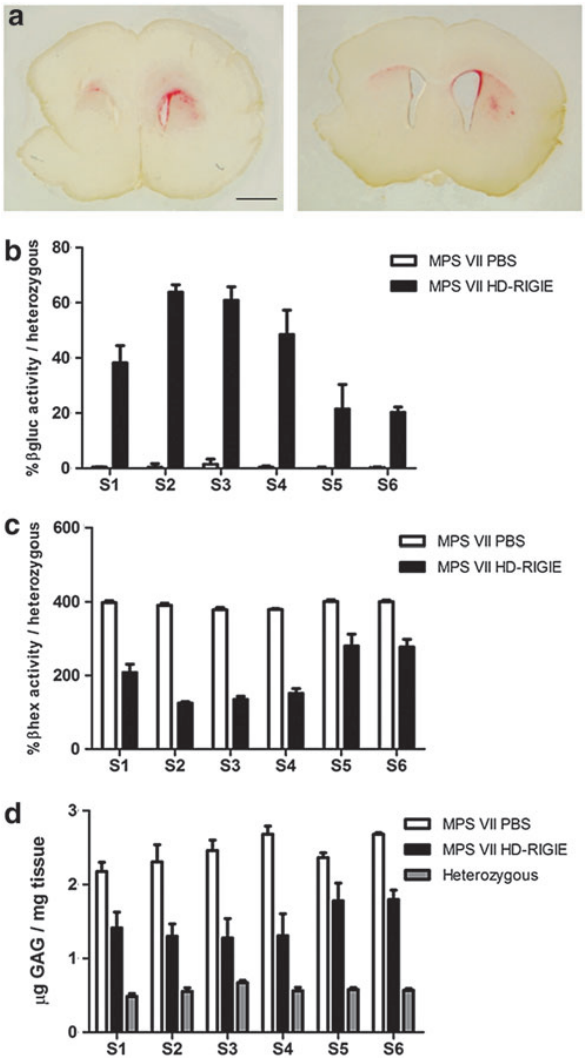

FIG. 3. Lysosomal enzyme activity and GAG accumulation analysis 16 weeks after the treatment. βgluc activity in **(a)** 100-μm-thick slices (red; scale bar = 1 mm) and **(b)** 2-mm-thick slice homogenates, **(c)** secondary elevation of β-hexosaminidase activity, and **(d)** GAG accumulation in 2-mm-thick slice homogenate slices in MPS VII mice injected with PBS or HD-RIGIE compared with heterozygous mice ($p < 0.01$ for βgluc; $p < 0.01$ in S1, S5, and S6 for βhex; and $p < 0.01$ for GAG). Data are mean ± SEM; $n = 4$ for each experimental group.

GAG accumulation in MPS VII-treated mouse brain extracts

MPS VII is characterized by the inability to degrade glucuronic acid-containing GAG. GAG quantification was used to evaluate the therapeutic effect of the HD-RIGIE treatment at 6 and 16 weeks post-HD-RIGIE injection. We reduced GAG accumulation in all sections of the brain, consistent with increased βgluc and reduced βhex activities observed in Figs. 2 and 3. Mice were treated around 8–10 weeks of age and were analyzed 6 or 16 weeks later, that is, when they reached 3.5 or nearly 6 months of age. In the first experimental group, MPS VII animals had GAG levels near 1.5 μg/mg of tissue in all the slices of the brain, threefold more than heterozygous mice. Animals injected with HD-RIGIE showed no statistically significant differences in GAG levels between S1 and S4 compared with heterozygous mice and a 40% reduction in S5 and S6 compared with the same slices of MPS VII-PBS mice ($p < 0.01$) (Fig. 2f).

MPS VII mice analyzed at 6 months showed greater GAG accumulation in all the slices, with levels reaching values of 2.7 μg/mg of tissue, fivefold higher than heterozygous mice. GAG quantification in MPS VII-HD-RIGIE mice showed a 50% decrease in S2, S3, and S4 and between 30% and 40% in S1, S5, and S6 compared with nontreated mutant mice (Fig. 3d). Although there were still statistically significant

differences between HD-RIGIE-treated and heterozygous animals in S2 and S3 slices ($p < 0.01$), this reduction was greater at 6 months of age, when the pathology of the disease was much more severe and these animals were at the end of their life expectancy.

Correction of pathology in the HD-RIGIE-injected mouse brain

We evaluated brain pathology in treated animals 6 and 16 weeks postinjection in semi-thin sections from the cortex, striatum, and meninges around injection point (S2), cortex and striatum at S3 and S4 levels, and hippocampus.

Representative images of the different brain regions from animals euthanized 6 weeks postinjection showed a significant correction of neurons, and glial cells, which presented with greater distended lysosomal morphology in all areas analyzed (Fig. 4). More than 90% of the cells in the injection area and between 83% and 89% in more distal regions showed no, few, or minuscule vacuoles, compared with large vacuoles in nontreated MPS VII animals (Table 1). An additional group of animals received HD-RIGIE only in one hemisphere. Six weeks after treatment, contralateral hemispheres showed also correction in S2, mainly in striatum and cortex (Supplementary Fig. S3). Therefore, even when injecting in a single hemisphere, there was evidence of vg and lysosomal correction in the contralateral hemisphere (Supplementary Figs. S1 and S3). Although we cannot discard transport in the CSF and transduction of perivascular cells in this hemisphere via HD-RIGIE leakage from the injected area, the most plausible explanation would be via axonal transport of the vector and/or βgluc.

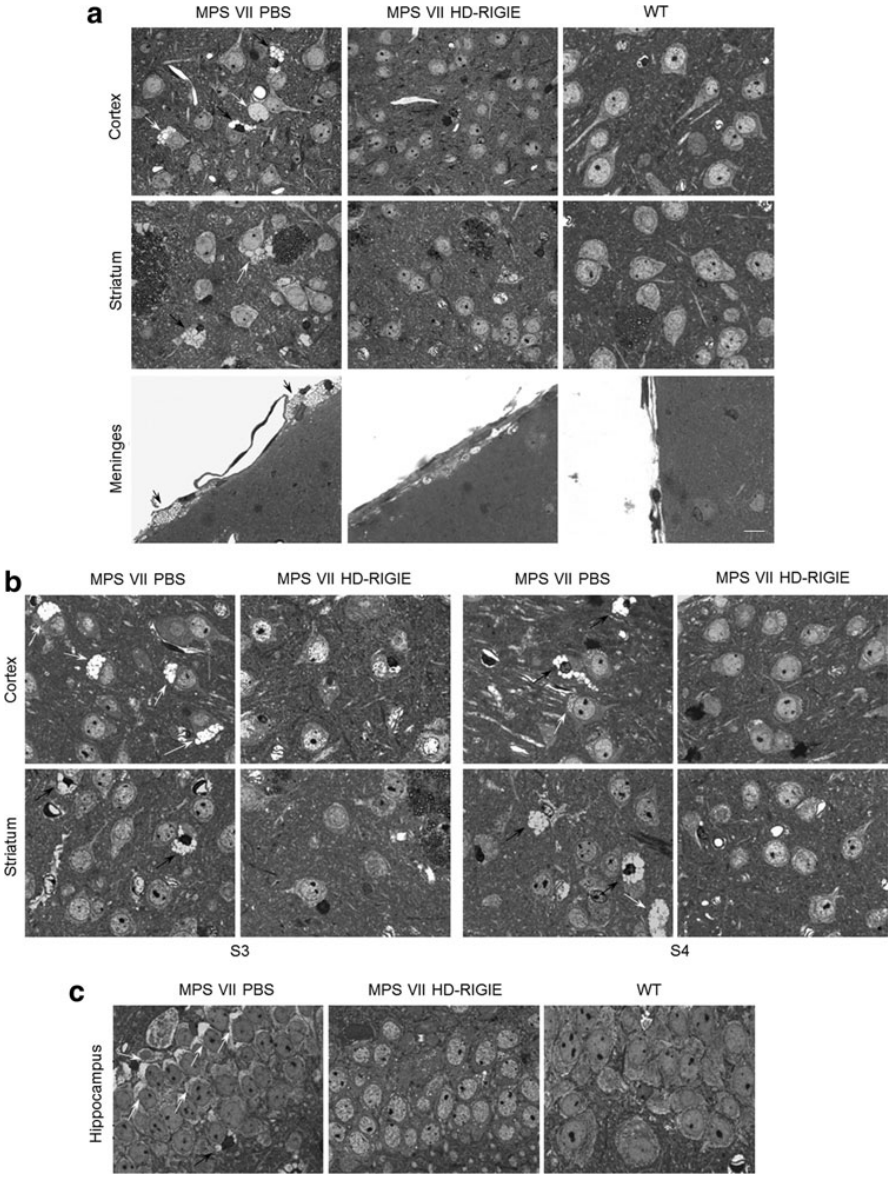

FIG. 4. Histopathological studies 6 weeks postinjection. Semi-thin sections of different brain areas surrounding the injection point were stained with toluidine blue to highlight the enlargement of vacuoles containing lysosomal storage material as seen in PBS-treated MPS VII mice. Representative images from **(a)** cortex, striatum, and meninges in MPS VII PBS (left), MPS VII HD-RIGIE (middle), and WT mice (right) at injection area, and at more distal areas **(b)**, slices in S3 (left panel) and S4 (right panel), and **(c)** hippocampus. HD-RIGIE-treated mice show a pattern similar to WT animals in all tissues analyzed. Quantification of corrected cells is described in Table 1. Scale bar = 20 μm. Black and white arrows indicate vesicle accumulation in glial cells and neurons, respectively.

TABLE 1. PERCENTAGE OF CORRECTED CELLS PRESENT IN CENTRAL NERVOUS SYSTEM STRUCTURES QUANTIFIED IN HISTOPATHOLOGICAL IMAGES FROM ANIMALS TREATED WITH HD-RIGIE AND ANALYZED AFTER 6 OR 16 WEEKS

	Injection area		*Distal regions*				
	Cortex (%)	*Striatum (%)*	*Cortex (S3) (%)*	*Striatum (S3) (%)*	*Cortex (S4) (%)*	*Striatum (S4) (%)*	*Hippocampus (%)*
HD-RIGIE 6wk	90 ± 5	95 ± 3	86 ± 5	89 ± 4	83 ± 9	85 ± 10	88 ± 6
HD-RIGIE 16wk	94 ± 3	96 ± 2	90 ± 6	91 ± 5	88 ± 7	90 ± 5	85 ± 9

HD-RIGIE, helper-dependent CAV-2 vector expressing β-glucuronidase; wk, week.
Data are mean ± SEM. Three fields of each animal and area were counted. S3 and S4 correspond to the slides represented in Fig. 1a.

Consistent with the biochemical correction, histopathology of proximal and distal areas to the injection point showed a significant reduction of enlarged lysosomes in neurons and glial cells in mice euthanized 16 weeks post-HD-RIGIE injection (Fig. 5). We also quantified the percentage of cells with recovered phenotype in animals treated 16 weeks earlier, and we found between 90% and 96% in the injection area and higher than 85% in more distal regions (Table 1).

Together, these data demonstrated that HD-RIGIE therapy led to stable transgene expression at least for 16 weeks

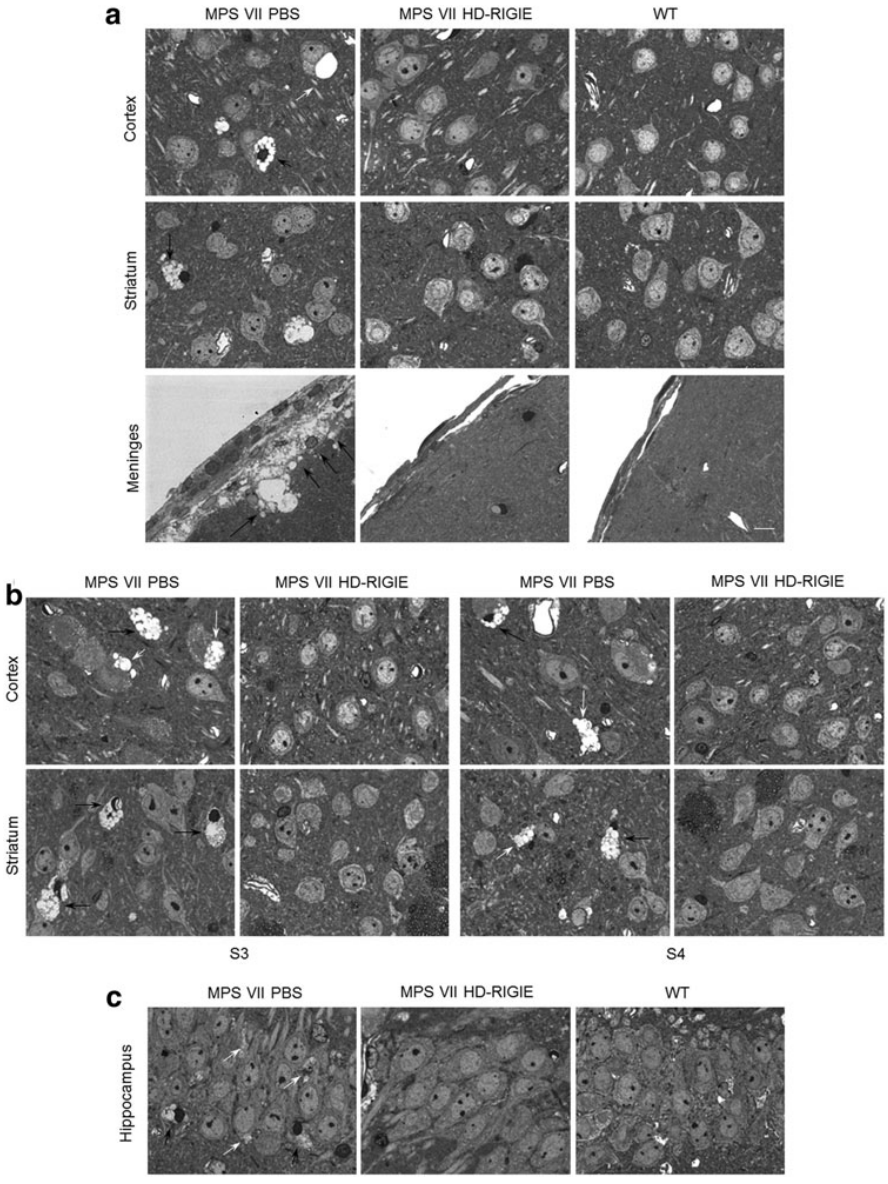

FIG. 5. Histopathological studies 16 weeks postinjection. Representative images from **(a)** cortex, striatum, and meninges in MPS VII PBS (left), MPS VII HD-RIGIE (middle), and WT mice (right) at injection area, and at more distal areas **(b)**, slices in S3 (left panel) and S4 (right panel), and **(c)** hippocampus. HD-RIGIE-treated mice show a pattern similar to WT animals in all tissues analyzed. Quantification of corrected cells is described in Table 1. Scale bar = 20 μm. Black and white arrows indicate vesicle accumulation in glial cells and neurons, respectively.

throughout the mid- and the forebrain of MPS VII mice after bilateral striatal injections and that unilateral injection improved MPS VII pathology in the contralateral hemisphere.

HD-RIGIE reverses MPS VII-associated cognitive deficits

In MPS VII mice, progressive impairment in peripheral tissues and in the CNS causes behavioral alterations. Although MPS VII is a multisystem disease, our aim was to test the suitability of HD-CAV-2 in treating a global neurodegenerative disease. We analyzed the behavior of treated mice, mainly using animals treated for 6 weeks, because the poor overall physical condition of 6-month-old animals, at the end of their life, precluded interpretation of the results. This physical impairment may also contribute to the reduction in behavioral performances reported at different ages (Liu *et al.*, 2005; Chen *et al.*, 2012). For that reason, we chose tests with conditions and degree of difficulty to provide convergent validity (Gimenez-Llort *et al.*, 2002, 2007).

We evaluated spontaneous behavior and sensorimotor functions, behavioral and psychological symptoms (locomotor and exploratory activity, anxious-like behaviors), as well as cognition (learning and memory). Impairment of some muscle and lower motor neuron functions was found when MPS VII animals were assessed in the two-rod and hanger tests (Fig. 6a) ($p < 0.001$). MPS VII mice showed the poorest coordination and prehensility and lower muscular strength ($p < 0.05$), whereas equilibrium was normal. HD-RIGIE treatment restored coordination and improved prehensility (both, $p < 0.05$) but did not modify muscular strength. Not surprisingly, this suggests that some functions depending on somatic development will require systemic or a long-term treatment from early developmental stages (O'Connor *et al.*, 1998).

Classical unconditioned tests such as the corner test (Fig. 6b), the T-maze test (Fig. 6c), and open-field test (Fig. 6d–f) involving different levels of anxiogenic conditions indicated reduced horizontal and vertical locomotor activities. Severe problems to interact with the environment were also evident by reduced exploration (Fig. 6d and e) (Time, T, $p < 0.01$; Time × Group, T × G, $p < 0.05$; Group, G, $p < 0.001$). HD-RIGIE treatment reversed the reduced activity in the corner test (Fig. 6b; Corners and Rearings, $p < 0.001$), freezing episodes ($p < 0.001$), forward locomotion ($p < 0.001$), the delay in the onset of vertical exploratory behaviors ($p < 0.05$), and the total vertical activity ($p < 0.001$).

In the T-maze for spontaneous alternation, MPS VII animals showed the poorest performance with a significant delay in the consecution of the behavioral events (Fig. 6c; latency to get started and to reach the intersection, both $p < 0.05$). Only 43% completed the test, while investing more time (exploratory efficiency, $p < 0.01$) and committing more errors ($p < 0.01$). HD-RIGIE treatment increased the incidence to 86%, corrected the delay to reach the intersection ($p < 0.05$), and reduced the number of errors ($p < 0.05$), although it did not modify the exploratory efficiency.

Assessment of spatial learning and memory in the 2-day water maze demonstrated that MPS VII mice had the poorest total cognitive capacity and deficits in the learning acquisition process as well as in both short- and long-term memories. Although all groups showed a similar acquisition curve of the simple cued-learning task (Fig. 6g; T, $p <$,0.001), MPS VII mice had the poorest total cognitive capacity ($p < 0.05$) and final outcome, as shown by their baseline performance in the last visible platform trial ($p < 0.05$), which was restored to heterozygous levels by HD-RIGIE treatment.

Place learning (PT) is a more difficult task because the platform is hidden and its location changed. Heterozygous animals spent more time in the platform's prior location, but once it was found, they efficiently remembered it. In contrast, the behavior of MPS VII during the first PT trial (PT1) was similar to their first contact with the maze (CUE1). Moreover, the overall cognitive ability of MPS VII mice to solve the tasks was lower (Fig. 6h; $p < 0.01$), and long- and short-term memory was impaired (Fig. 6i; PT1-CUE4, $p < 0.05$; and Fig. 6i; PT1-PT4, $p < 0.01$, respectively) as compared with heterozygous and MPS VII HD-RIGIE mice (both, $p < 0.05$). HD-RIGIE treatment rescued the cognitive deficits (Fig. 6g–i) and, most importantly, the total learning and memory capacities (Fig. 6h).

Our experimental design shows that reduction in behavioral performances was mostly caused by a reduced exploratory activity, has a strong influence of novelty, and is limited by the cognitive capacity of the animal to confront the situation. Such deficiencies were more clearly shown in the time course of the performances and were improved, and even corrected, by HD-RIGIE treatment. Finally, the cognitive impairment of MPS VII mice was severe, as not only short- and long-term learning and memory processes but also the strategies to solve the tasks and the cognitive capacity, itself, were compromised. Cognitive dysfunction worsened with the difficulty (hidden PT), and their cognitive plasticity did not benefit from previous experience. In contrast, heterozygous animals remembered the prior location of the platform and insisted on searching for it. Place task learning also evidenced impairment in short-term memory and deficits in the total learning capacity of MPS VII as compared with heterozygous mice. However, the major findings are that HD-RIGIE treatment completely rescued the cognitive deficits, mostly in short-term memory, and the total learning and memory capacities.

Notably, this is the first study in which elevated enzyme levels in brain, reduction of lysosomal storage, and reversal of cognitive deficits have been observed after intracranial injection of a HD-CAV-2 vector in a mouse model of disease. Previous experiments with HD adenoviral vectors had demonstrated their potential in the treatment of gliomas after direct tumor injection (Muhammad *et al.*, 2012) and in animal models for different diseases after intravenous injection (Dimmock *et al.*, 2011; Crane *et al.*, 2012). Recently, HD-CAV-2 vector was injected in the CNS of a mouse model of MPS IIIA, but although discrete long-term transgene expression was obtained, only 9% reduction of storage material was achieved at the injection point and no cognitive reversion was described (Lau *et al.*, 2012). One significant difference was the transient immunosuppression in the MPS VII animals to achieve robust, long-term transgene expression in this study. However, immune response is dose dependent. The low transgene expression obtained in MPS IIIA animals may allow the escape of the immune response, but it is not sufficient to elicit a significant therapeutic effect in the MPS IIIA model. Similarly, Dindot *et al.* (2011) achieved long-term expression after intrathecal administration of

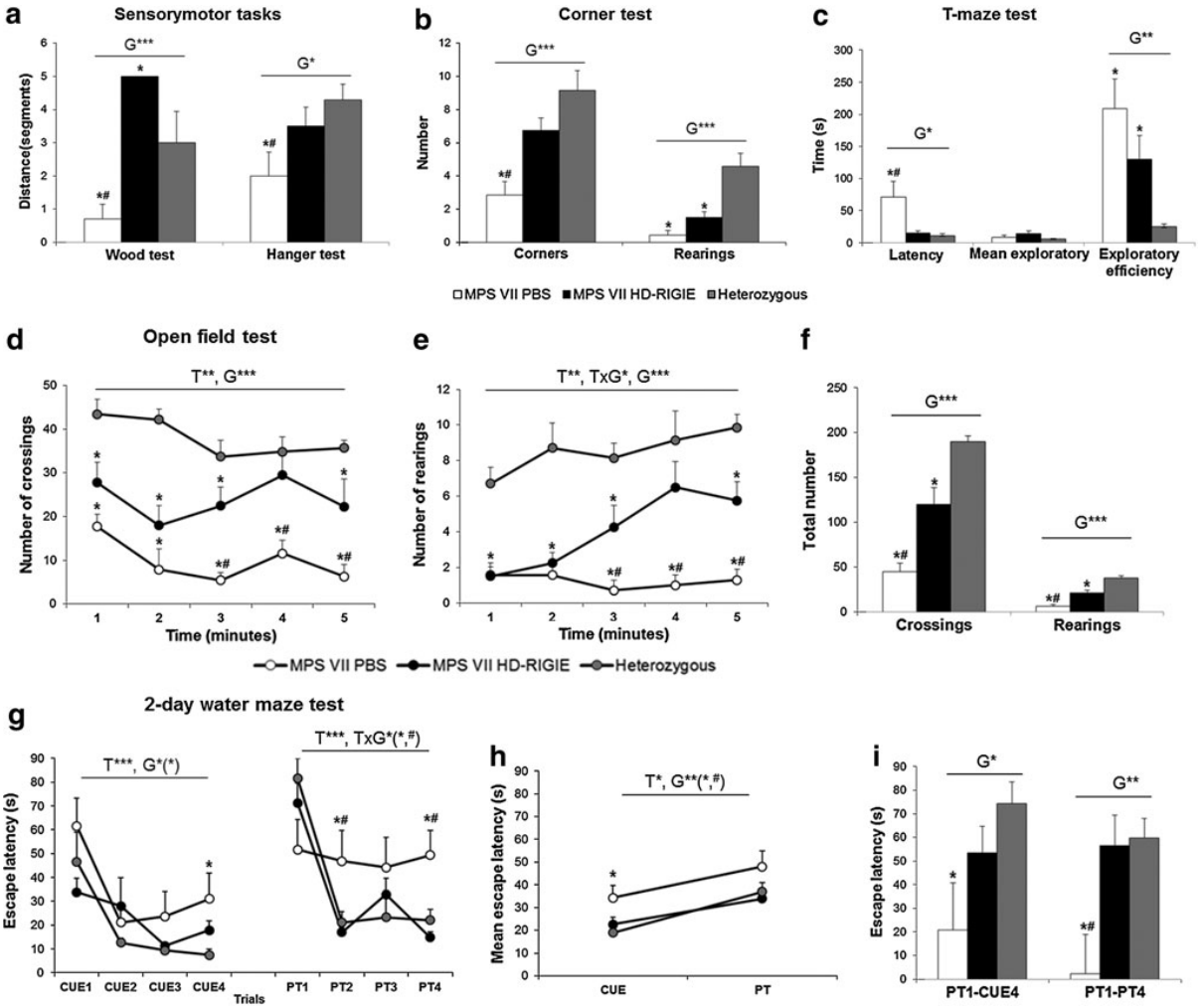

FIG. 6. Behavioral effects of HD-RIGIE in MPS VII mice. **(a)** Sensorimotor tasks. HD-RIGIE treatment allowed complete restoration of coordination in the wood test, while prehensility in the hanger test, measured as the latency to fall, was improved by the treatment. **(b)** Corner test. MPS VII mice showed reduction of total horizontal (crossings) and vertical (rearings) activities, which were significantly improved by HD-RIGIE treatment. **(c)** T-maze test. HD-RIGIE treatment completely corrected the increased latency to reach the intersection of the maze and improved the overall capacity to solve the paradigm (exploratory efficiency) but did not modify the mean exploratory time in the arms. **(d–f)** Open-field test. HD-RIGIE corrected the reduction of horizontal and vertical activity exhibited in the open-field test, as shown by the temporal course of the behavior (**d**, crossings 1–5; **e**, rearings 1–5) and the accumulated counts (**f**). **(g)** Two-day water maze. Acquisition curves. Latency to find the visible (CUE1–CUE4) and hidden (PT1–PT4) platform in a 2-day water maze for mice. Decrease of escape latencies through the cue-learning task was similar between the groups, but MPS VII showed the poorest baseline performance in the last visible platform trial. In the reversal place-learning task, the MPS VII mice showed significantly worse escape latencies as compared with the good acquisition shown by HET and MPS VII-treated mice. **(h)** Long-term memory. Mean escape latency in the cue- and place-learning tasks. All the groups showed significantly higher mean escape latencies when the platform was hidden as compared with the previous task. However, MPS VII mice showed a worse long-term performance as compared with HET and treatment with HD-RIGIE restored this deficit. **(i)** Long-term and short-term memories. Long-term memory deficits observed by means of the differences in the escape latency after the 24 hr interval (PT1–CUE4) were lacking in HD-RIGIE-treated animals. Short-term memory deficits observed in the place-learning task (PT1–PT4) were reversed in HD-RIGIE-treated animals. Data are mean ± SEM; $*p<0.05$, $**p<0.01$, $***p<0.001$ comparing HET with the other two MPS groups; $^{\#}p<0.05$ comparing MPS VII PBS with MPS VII HD-RIGIE. T, time; G, group; T × G, time × group; $n=7$ for each group.

human HD adenovirus coding for GFP in a wild-type mouse. The authors administered 2.5×10^9 pp/mouse into the 40 μl volume that constitutes the mouse CSF. Here we injected a similar amount of pp but concentrated into a single injection in the brain parenchyma that may certainly lead to a higher local immune response as demonstrated by Iba1 immunohistochemistry (Fig. 1).

In summary, we have shown that intrastriatal injection of HD-RIGIE resulted in stable expression of βgluc in the brains of MPS VII mice, inducing correction in the brain of

these animals. These findings are relevant to the treatment of neurological abnormalities in humans with lysosomal storage diseases and may also be possibly used in neurodegenerative disorders, although it would be necessary to assess the vector performance in large animal models of the disease.

Acknowledgments

We thank the Vector Production Unit at Center of Animal Biotechnology and Gene Therapy (CBATEG; Universitat Autònoma de Barcelona), which was supported by the Association Française contre les Myopathies, for producing CAVGFP, and Meritxell Puig, David Ramos, and Angel Vázquez (CBATEG) for technical assistance. We are indebted to Laia Acarin (Universitat Autònoma de Barcelona) for help with Iba1 immunohistochemistry. We thank the Montpellier RIO imaging and, in particular, Miriam Boyer-Clavel for help with flow cytometry.

G.P. and B.G.-L. were recipients of predoctoral fellowships (G.P. from the Generalitat de Catalunya [2009FI_B00219] and B.G.-L. from the Ministerio de Educación [EDU/3445/2011]). E.J.K. is an Inserm fellow. Funding was provided by the European Commission through European Community's 7th Framework Program (FP7/2007–2013; Grant 222992, BrainCAV to E.J.K. and A.B.), the Region Languedoc Roussillon (ARPE and CTP 115277 to E.J.K.) and AGAUR (2009 CTP 00030) to M.C., the Fondation de France (Grant #2008005416), Vaincre les Maladies Lysosomales, and the E-RARE 2009 program (project CAV-4-MPS funded by E-RARE to E.J.K. and to A.B. [Instituto de Salud Carlos III-PS0902674]).

Author Disclosure Statement

No competing financial interests exist.

References

Birkenmeier, E.H., Davisson, M.T., Beamer, W.G., *et al.* (1989). Murine mucopolysaccharidosis type VII. Characterization of a mouse with beta-glucuronidase deficiency. J. Clin. Invest. 83, 1258–1266.

Bosch, A., Perret, E., Desmaris, N., and Heard, J.M. (2000a). Long-term and significant correction of brain lesions in adult mucopolysaccharidosis type VII mice using recombinant AAV vectors. Mol. Ther. 1, 63–70.

Bosch, A., Perret, E., Desmaris, N., *et al.* (2000b). Reversal of pathology in the entire brain of mucopolysaccharidosis type VII mice after lentivirus-mediated gene transfer. Hum. Gene Ther. 11, 1139–1150.

Cao, H., Yang, T., Li, X.F., *et al.* (2011). Readministration of helper-dependent adenoviral vectors to mouse airway mediated via transient immunosuppression. Gene Ther. 18, 173–181.

Cardone, M., Polito, V.A., Pepe, S., *et al.* (2006). Correction of Hunter syndrome in the MPSII mouse model by AAV2/8-mediated gene delivery. Hum. Mol. Genet. 15, 1225–1236.

Chen, Y.H., Claflin, K., Geoghegan, J.C., and Davidson, B.L. (2012). Sialic acid deposition impairs the utility of AAV9, but not peptide-modified AAVs for brain gene therapy in a mouse model of lysosomal storage disease. Mol. Ther. 20, 1393–1399.

Chirmule, N., Propert, K., Magosin, S., *et al.* (1999). Immune responses to adenovirus and adeno-associated virus in humans. Gene Ther. 6, 1574–1583.

Ciron, C., Desmaris, N., Colle, M.A., *et al.* (2006). Gene therapy of the brain in the dog model of Hurler's syndrome. Ann. Neurol. 60, 204–213.

Crane, B., Luo, X., Demaster, A., *et al.* (2012). Rescue administration of a helper-dependent adenovirus vector with long-term efficacy in dogs with glycogen storage disease type Ia. Gene Ther. 19, 443–452.

Cressant, A., Desmaris, N., Verot, L., *et al.* (2004). Improved behavior and neuropathology in the mouse model of Sanfilippo type IIIB disease after adeno-associated virus-mediated gene transfer in the striatum. J. Neurosci. 24, 10229–10239.

Dimmock, D., Brunetti-Pierri, N., Palmer, D.J., *et al.* (2011). Correction of hyperbilirubinemia in gunn rats using clinically relevant low doses of helper-dependent adenoviral vectors. Hum. Gene Ther. 22, 483–488.

Dindot, S., Piccolo, P., Grove, N., *et al.* (2011). Intrathecal injection of helper-dependent adenoviral vectors results in long-term transgene expression in neuroependymal cells and neurons. Hum. Gene Ther. 22, 745–751.

Ellinwood, N.M., Ausseil, J., Desmaris, N., *et al.* (2011). Safe, efficient, and reproducible gene therapy of the brain in the dog models of Sanfilippo and Hurler syndromes. Mol. Ther. 19, 251–259.

Eng, C.M., Guffon, N., Wilcox, W.R., *et al.* (2001). Safety and efficacy of recombinant human alpha-galactosidase A—replacement therapy in Fabry's disease. N. Engl. J. Med. 345, 9–16.

Gimenez-Llort, L., Fernandez-Teruel, A., Escorihuela, R.M., *et al.* (2002). Mice lacking the adenosine A1 receptor are anxious and aggressive, but are normal learners with reduced muscle strength and survival rate. Eur. J. Neurosci. 16, 547–550.

Gimenez-Llort, L., Blazquez, G., Canete, T., *et al.* (2007). Modeling behavioral and neuronal symptoms of Alzheimer's disease in mice: a role for intraneuronal amyloid. Neurosci. Biobehav. Rev. 31, 125–147.

Grabowski, G.A., Leslie, N., and Wenstrup, R. (1998). Enzyme therapy for Gaucher disease: the first 5 years. Blood Rev. 12, 115–133.

Harmatz, P., Giugliani, R., Schwartz, I., *et al.* (2006). Enzyme replacement therapy for mucopolysaccharidosis VI: a phase 3, randomized, double-blind, placebo-controlled, multinational study of recombinant human N-acetylgalactosamine 4-sulfatase (recombinant human arylsulfatase B or rhASB) and follow-on, open-label extension study. J. Pediatr. 148, 533–539.

Kakkis, E.D., Muenzer, J., Tiller, G.E., *et al.* (2001). Enzyme-replacement therapy in mucopolysaccharidosis I. N. Engl. J. Med. 344, 182–188.

Keriel, A., Rene, C., Galer, C., *et al.* (2006). Canine adenovirus vectors for lung-directed gene transfer: efficacy, immune response, and duration of transgene expression using helper-dependent vectors. J. Virol. 80, 1487–1496.

Kremer, E.J., Boutin, S., Chillon, M., and Danos, O. (2000). Canine adenovirus vectors: an alternative for adenovirus-mediated gene transfer. J. Virol. 74, 505–512.

Langford-Smith, A., Wilkinson, F.L., Langford-Smith, K.J., *et al.* (2012). Hematopoietic stem cell and gene therapy corrects primary neuropathology and behavior in mucopolysaccharidosis IIIA mice. Mol. Ther. 20, 1610–1621.

Lau, A.A., Rozaklis, T., Ibanes, S., *et al.* (2012). Helper-dependent canine adenovirus vector-mediated transgene expression in a neurodegenerative lysosomal storage disorder. Gene 491, 53–57.

LeBowitz, J.H., Grubb, J.H., Maga, J.A., *et al.* (2004). Glycosylation-independent targeting enhances enzyme delivery to lysosomes and decreases storage in mucopolysaccharidosis type VII mice. Proc. Natl. Acad. Sci. USA 101, 3083–3088.

Levy, B., Galvin, N., Vogler, C., *et al.* (1996). Neuropathology of murine mucopolysaccharidosis type VII. Acta Neuropathol. 92, 562–568.

Liu, G., Martins, I., Wemmie, J.A., *et al.* (2005). Functional correction of CNS phenotypes in a lysosomal storage disease model using adeno-associated virus type 4 vectors. J. Neurosci. 25, 9321–9327.

Liu, G., Chen, Y.H., He, X., *et al.* (2007). Adeno-associated virus type 5 reduces learning deficits and restores glutamate receptor subunit levels in MPS VII mice CNS. Mol. Ther. 15, 242–247.

Lowenstein, P.R., Mandel, R.J., Xiong, W.D., *et al.* (2007). Immune responses to adenovirus and adeno-associated vectors used for gene therapy of brain diseases: the role of immunological synapses in understanding the cell biology of neuroimmune interactions. Curr. Gene Ther. 7, 347–360.

Moore, D.J., Markmann, J.F., and Deng, S. (2006). Avenues for immunomodulation and graft protection by gene therapy in transplantation. Transpl. Int. 19, 435–445.

Muenzer, J. (2011). Overview of the mucopolysaccharidoses. Rheumatology (Oxford) 50 Suppl. 5, v4–v12.

Muhammad, A.K., Xiong, W., Puntel, M., *et al.* (2012). Safety profile of gutless adenovirus vectors delivered into the normal brain parenchyma: implications for a glioma phase 1 clinical trial. Hum. Gene Ther. Methods 23, 271–284.

O'Connor, L.H., Erway, L.C., Vogler, C.A., *et al.* (1998). Enzyme replacement therapy for murine mucopolysaccharidosis type VII leads to improvements in behavior and auditory function. J. Clin. Invest. 101, 1394–1400.

Perreau, M., and Kremer, E.J. (2005). Frequency, proliferation, and activation of human memory T cells induced by a non-human adenovirus. J. Virol. 79, 14595–14605.

Perreau, M., Guerin, M.C., Drouet, C., and Kremer, E.J. (2007a). Interactions between human plasma components and a xenogenic adenovirus vector: reduced immunogenicity during gene transfer. Mol. Ther. 15, 1998–2007.

Perreau, M., Mennechet, F., Serratrice, N., *et al.* (2007b). Contrasting effects of human, canine, and hybrid adenovirus vectors on the phenotypical and functional maturation of human dendritic cells: implications for clinical efficacy. J. Virol. 81, 3272–3284.

Salinas, S., Bilsland, L.G., Henaff, D., *et al.* (2009). CAR-associated vesicular transport of an adenovirus in motor neuron axons. PLoS Pathog. 5, e1000442.

Sardiello, M., Palmieri, M., di Ronza, A., *et al.* (2009). A gene network regulating lysosomal biogenesis and function. Science 325, 473–477.

Schagen, F.H., Rademaker, H.J., Rabelink, M.J., *et al.* (2000). Ammonium sulphate precipitation of recombinant adenovirus from culture medium: an easy method to increase the total virus yield. Gene Ther. 7, 1570–1574.

Schuldt, A.J., Hampton, T.J., Chu, V., *et al.* (2004). Electrocardiographic and other cardiac anomalies in beta-glucuronidase-null mice corrected by nonablative neonatal marrow transplantation. Proc. Natl. Acad. Sci. USA 101, 603–608.

Seok, J., Warren, H.S., Cuenca, A.G., *et al.* (2013). Genomic responses in mouse models poorly mimic human inflammatory diseases. Proc. Natl. Acad. Sci. USA 110, 3507–3512.

Shipley, J.M., Klinkenberg, M., Wu, B.M., *et al.* (1993). Mutational analysis of a patient with mucopolysaccharidosis type VII, and identification of pseudogenes. Am. J. Hum. Genet. 52, 517–526.

Sly, W.S., Vogler, C., Grubb, J.H., *et al.* (2001). Active site mutant transgene confers tolerance to human beta-glucuronidase without affecting the phenotype of MPS VII mice. Proc. Natl. Acad. Sci. USA 98, 2205–2210.

Soper, B.W., Lessard, M.D., Vogler, C.A., *et al.* (2001). Nonablative neonatal marrow transplantation attenuates functional and physical defects of beta-glucuronidase deficiency. Blood 97, 1498–1504.

Sotak, B.N., Hnasko, T.S., Robinson, S., *et al.* (2005). Dysregulation of dopamine signaling in the dorsal striatum inhibits feeding. Brain Res. 1061, 88–96.

Soudais, C., Laplace-Builhe, C., Kissa, K., and Kremer, E.J. (2001). Preferential transduction of neurons by canine adenovirus vectors and their efficient retrograde transport *in vivo*. FASEB J. 15, 2283–2285.

Soudais, C., Skander, N., and Kremer, E.J. (2004). Long-term *in vivo* transduction of neurons throughout the rat CNS using novel helper-dependent CAV-2 vectors. FASEB J. 18, 391–393.

Thomas, C.E., Birkett, D., Anozie, I., *et al.* (2001). Acute direct adenoviral vector cytotoxicity and chronic, but not acute, inflammatory responses correlate with decreased vector-mediated transgene expression in the brain. Mol. Ther. 3, 36–46.

Thurberg, B.L., Lynch Maloney, C., Vaccaro, C., *et al.* (2006). Characterization of pre- and post-treatment pathology after enzyme replacement therapy for Pompe disease. Lab. Invest. 86, 1208–1220.

Vogler, C., Levy, B., Kyle, J.W., *et al.* (1994). Mucopolysaccharidosis VII: postmortem biochemical and pathological findings in a young adult with beta-glucuronidase deficiency. Mod. Pathol. 7, 132–137.

Vogler, C., Sands, M.S., Galvin, N., *et al.* (1998). Murine mucopolysaccharidosis type VII: the impact of therapies on the clinical course and pathology in a murine model of lysosomal storage disease. J. Inherit. Metab. Dis. 21, 575–586.

Wilcox, W.R., Banikazemi, M., Guffon, N., *et al.* (2004). Long-term safety and efficacy of enzyme replacement therapy for Fabry disease. Am. J. Hum. Genet. 75, 65–74.

Address correspondence to:
Dr. Assumpció Bosch
CBATEG, Edifici H
Campus Universitat Autònoma de Barcelona
08193 Bellaterra, Barcelona
Spain

E-mail: assumpcio.bosch@uab.es

Received for publication August 6, 2013;
accepted after revision November 19, 2013.

Published online: December 3, 2013.

Gene Therapy (2014), 1–6

www.nature.com/gt

SHORT COMMUNICATION

AAVrh.10 immunogenicity in mice and humans. Relevance of antibody cross-reactivity in human gene therapy

R Thwaite[1], G Pagès[1], M Chillón[1,2] and A Bosch[1]

Simian adeno-associated virus (AAV) serotype rh.10 is a promising gene therapy tool, achieving safe, sustained transgene expression in the nervous system, lung, liver and heart in animal models. To date, preexisting immunity in humans has not been confirmed, though exposure is unexpected. We compared the humoral immune response with serotypes AAVrh.10 and AAV9 in mice, and AAVrh.10, AAV9 and AAV2 in 100 healthy humans. Mice, injected-intravenously, raised significantly more anti-AAV9 than anti-AAVrh.10 IgG (immunoglobulins), and sera demonstrated greater neutralizing capacity, correspondingly. Antibody cross-binding studies in mice showed negligible cross-recognition between AAVrh.10, AAV9 and AAV2. In humans, IgG prevalence against the most common human serotype, AAV2, was 72%; AAV9, 47% and AAVrh.10, a surprising, 59%. Yet, neutralizing-antibody seroprevalences were 71% for AAV2, 18% for AAV9 and 21% for AAVrh.10. Thus, most anti-AAV9 and anti-AAVrh.10 IgG were nonneutralizing. Indeed, sera generally neutralized AAV2 more strongly than AAVrh.10. Further, all samples neutralizing AAVrh.10 or AAV9 also neutralized AAV2, suggesting antibody cross-recognition. This contrasts with the results in mice, and highlights the complexity of tailoring gene therapy to minimize the immune response in humans, when multiple-mixed infections during a lifetime evoke a broad repertoire of preexisting antibodies capable of cross reacting with non-human serotypes.

Gene Therapy advance online publication, 20 November 2014; doi:10.1038/gt.2014.103

INTRODUCTION

Adeno-associated virus (AAV) vectors do not provoke a strong innate immune response as dendritic cells are poorly transduced. Consequently, markers of innate immunity tend not to be upregulated, though evidence is growing, concerning their relevance to the outcome of AAV-mediated gene transfer.[1] More overtly problematic is the challenge posed by preexisting anti-AAV antibodies present in patients' serum before therapy. These arise with prior exposure, given AAVs are widespread in humans (reviewed by Calcedo and Wilson[2]). In addition, generation of antibodies and T-cell responses against the transgene product, particularly a foreign protein, may depend on the AAV serotype and its capacity to infect antigen-presenting cells.[3–5] Thus, selecting the appropriate viral capsid is critical when planning a therapeutic approach using AAV vectors, since it determines tropism[6] and has major implications regarding the host immune response.

We focus on AAVrh.10, a rhesus macaque serotype,[7] hypothesizing that humans are less likely to be exposed, hence preexisting antibodies should be minimal. Recombinant AAVrh.10 shows promise for gene therapy. It stably-transduces neurons and to a lesser extent oligodendrocytes, after intracranial or intrathecal administration, demonstrating capacity to revert different central- and peripheral-nervous system pathologies in mouse models such as late-infantile neuronal ceroid lipofuscinosis,[8] metachromatic leukodystrophy,[9] diabetic neuropathy,[10] and amyotrophic lateral sclerosis[11] among other diseases. Recently rAAVrh.10 was approved for two clinical trials to treat late-infantile neuronal lipofuscinosis (NCT01161576) and Sanfilippo Type A syndrome.[12] Furthermore, intravenous administration of AAVrh.10 efficiently transduces liver, heart and dorsal root ganglia and reverses cardiomyopathy in a mouse model of Friedreich's ataxia.[13]

Several studies report the prevalence of neutralizing antibodies (NAbs) against AAV serotypes 1, 2, 5, 6, 7, 8, 9 and the capsid hybrid rh32.33.[14,15] However, no data on preexisting antibodies to AAVrh.10 in the general human population, nor on the immunogenicity of AAVrh.10 among serotypes have been reported. Here we show the humoral immune response to AAVrh.10 is significantly weaker than AAV9 in mice. Yet, in humans, immunoglobulin G (IgG) prevalence against AAVrh.10 is greater than against AAV9. However, these immunoglobulins are a mixed population of NAbs and non-NAbs. Further characterization suggests cross-reactivity with abundant-preexisting antibodies raised against AAV2.

RESULTS AND DISCUSSION

We previously demonstrated serotype-dependent differences in the titers of NAbs generated after intrasciatic administration in mice. Three weeks post injection of AAV1, 2 or 8, AAV8-transduced animals had the lowest titers.[16] In addition, using AAVrh.10, we have observed less NAbs were raised after intrathecal injection to mice compared with AAV serotypes 1, 8 and 9 (unpublished data). Here, we compared the immunogenicity of AAVrh.10 and AAV9 in mice first by quantifying the total anti-AAV IgG raised 3 weeks after intravenous injection of either virus, and then testing the sera's capacity to neutralize the virus using a luciferase reporter. We chose AAV9 for comparison as it crosses the blood-brain barrier and is therefore a popular candidate for efficient central

[1]Department of Biochemistry and Molecular Biology, Center of Animal Biotechnology and Gene Therapy (CBATEG), Universitat Autònoma de Barcelona, Bellaterra, Barcelona, Spain and [2]Institut Català de Recerca i Estudis Avançats (ICREA), Barcelona, Spain. Correspondence: Dr A Bosch, Department of Biochemistry and Molecular Biology, Center of Animal Biotechnology and Gene Therapy (CBATEG), Universitat Autònoma de Barcelona, Edifici H, Bellaterra 08193, Barcelona, Spain.
E-mail: assumpcio.bosch@uab.es
Received 5 June 2014; revised 7 October 2014; accepted 10 October 2014

nervous system gene delivery to treat neurological diseases with somatic involvement, such as lysosomal storage diseases.[17,18]

Figure 1a, shows that all the animals injected with AAV9 ($n=9$) raised more anti-AAV IgG than the animals injected with AAVrh.10 ($n=8$). Mean total IgG of each group (AAV9 = 2659 ± 326 μg ml^{-1} and AAVrh.10 = 692 ± 97 μg ml^{-1}) was significantly different ($P<0.05$). Note, in normal-mouse sera the typical IgG concentration range is 0.7–5 mg ml^{-1}.[19] Thus, our quantification of the anti-AAV IgG subpopulation is physiologically compatible. Figure 1b demonstrates that sera with antibodies raised against AAV9 are more neutralizing than with antibodies against AAVrh.10. The percentage of infection-inhibition dropped significantly for AAVrh.10 over a series of serum dilutions, whereas for AAV9 it remained nearly 100% throughout. The mean percentage of infection-inhibition, comparing AAVrh.10 and AAV9, at 1:200 serum dilution is seen in Figure 1c which may be directly compared with anti-AAV IgG (Figure 1a). Pearson-correlation analysis showed a significant positive-correlation between IgG and NAbs (0.776, $P=0.0002$, $n=17$). Supplementary Figure 1 shows similar correlation with green fluorescent protein as a reporter gene, using sera from mice injected with various AAV serotypes, (0.852, $P=0.0004$, $n=12$).

When choosing a vector for gene therapy, immunogenicity (here referring to the capacity to raise NAbs) is a relevant consideration. The presence of NAbs does not necessarily preclude-successful transduction, provided that a critical threshold is not reached or depending on the tissue transduced or the administration route. In this vein, persistent expression of the transgene in both mice and non-human primates was achieved after administering AAVrh.10 interpleurally despite sustained presence of NAbs in the sera.[20] This was also observed for AAV9 delivered intrathecally to non-human primates,[21] although these results are controversial;[22] as NAbs in the sera prevented transduction after intravenous administration.[21,22] Our results indicate, regarding the raising of NAbs in mice, AAVrh.10 is a more favorable choice of vector than AAV9, evoking fewer antibodies in the context studied.

We also performed antibody cross-binding studies in mice *via* indirect enzyme linked immunosorbant assay, using sera with IgG raised against either AAVrh.10, 9 or 2, to see if these antibodies would bind to the viral capsid of other serotypes. Table 1 shows that antibody binding to other capsids was negligible, results resembling naive control levels in all cases, indicating the absence of significant cross-reactivity of IgG against these three AAVs in mice. This is not strain specific, as we obtained similar results with C57bl/6 mice with AAV2 (data not shown). Lack of serological cross-reactivity across certain serotypes in serum raised against AAVs in animal models has been previously reported.[8,23] Nevertheless, there is relatively high homology between the VP1-capsid protein among AAVs and recent reports show capsid antibodies to different AAV serotypes bind common regions.[24,25] Indeed to reduce such problems, directed evolution[26] or other

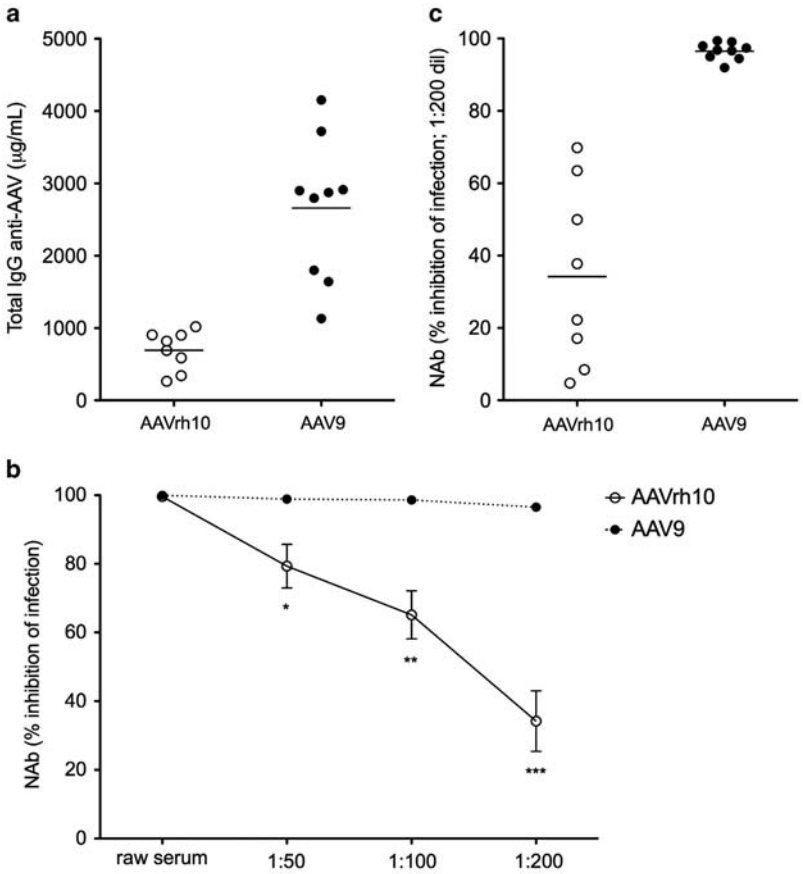

Figure 1. AAV9 is more immunogenic than AAVrh.10 in mice. Sera from 6–8 week-old mice, 21 days post-intravenous injection of 1x10^{11} vg ml^{-1} of either AAV9 ($n=9$) or AAVrh.10 ($n=8$) in a total volume of 150 μl, comparing (**a**) total anti-AAV IgG μg ml^{-1} determined by indirect enzyme linked immunosorbant assay, '—' denotes the mean; (**b**) Neutralizing antibodies (NAbs) expressed as percentage of inhibition of adeno-associated virus (AAV) infection of HEK293 cells by the sera over a dilution range from 0 to 1:200, determined using luciferase reporter. Two-tailed *t*-tests: *$P<0.05$, **$P<0.01$, ***$P<0.001$; and (**c**) scatter plot of NAb data at 1:200 dilution from (**b**), '—' denotes the mean. All samples in A, B and C were tested in duplicates.

Table 1. Anti-AAV IgG to AAVrh.10, 9 and 2 do not cross-react in mice

Sera from mice injected with AAV	*Mean OD*	*% Binding to capsid*	*Anti-AAV IgG (μg ml^{-1})*	*Mean OD*	*% Binding to capsid*	*Anti-AAV IgG (μg ml^{-1})*	*Mean OD*	*% Binding to capsid*	*Anti-AAV IgG (μg ml^{-1})*
AAVrh10	*Anti-AAVrh.10*			*Anti-AAV9*			*Anti-AAV2*		
Animal 1	0.338 ± 0.017	100	1444 ± 54	0.004 ± 0.001	1.2	91 ± 8	0.014 ± 0.003	4.1	203 ± 22
Animal 2	0.328 ± 0.020	100	1412 ± 63	0.021 ± 0.004	6.4	262 ± 28	0.006 ± 0.004	1.8	112 ± 49
Animal 3	0.394 ± 0.023	100	1624 ± 75	0.007 ± 0.000	1.8	139 ± 0	0.002 ± 0.003	0.5	55 ± 44
Animal 4	0.347 ± 0.018	100	1471 ± 56	0.005 ± 0.003	1.4	101 ± 38	0.004 ± 0.003	1.2	89 ± 45
AAV9	*Anti-AAVrh.10*			*Anti-AAV9*			*Anti-AAV2*		
Animal 1	0.007 ± 0.003	1.4	135 ± 36	0.508 ± 0.013	100	2005 ± 48	0.005 ± 0.006	1.0	91 ± 80
Animal 2	0.009 ± 0.001	1.1	161 ± 11	0.855 ± 0.013	100	2588 ± n/a	0.005 ± 0.003	0.6	107 ± 44
Animal 3	0.008 ± 0.000	1.5	150 ± 0	0.528 ± 0.018	100	2076 ± 63	0.003 ± 0.001	0.6	81 ± 18
Animal 4	0.006 ± 0.001	1.1	120 ± 7	0.526 ± 0.001	100	2068 ± 2	0.004 ± 0.001	0.8	91 ± 8
AAV2	*Anti-AAVrh.10*			*Anti-AAV9*			*Anti-AAV2*		
Animal 1	0.003 ± 0.001	0.5	73 ± 10	0.002 ± 0.001	0.3	47 ± 36	0.644 ± 0.016	100	2523 ± 65
Animal 2	0.005 ± 0.001	1.0	106 ± 7	0.001 ± 0.001	0.2	24 ± 13	0.519 ± 0.006	100	2043 ± 20
Animal 3	0.003 ± 0.001	1.0	68 ± 31	0.001 ± 0.001	0.3	12 ± 0	0.309 ± 0.001	100	1351 ± 2
Animal 4	0.008 ± 0.003	1.5	147 ± 34	0.004 ± 0.000	0.7	99 ± 0	0.548 ± 0.001	100	2148 ± 2
Naive control	0.014 ± 0.006	4.0	199 ± 49	0.010 ± 0.006	1.7	162 ± 63	0.005 ± 0.003	1.0	101 ± 38

Abbreviations: AAV, adeno-associated virus; IgG, immunoglobulin G; OD, optical density; n/a = not available: one duplicate out of standard curve range. Percentage binding to capsid normalized from OD. Percentage binding for control OD calculated using pooled mean OD of four animals at 100% binding for each viral capsid. Results are means of duplicates ± s.e.m.

capsid-engineering methods[27] are being explored to design AAV-gene therapy vectors with greater resistance to NAbs.

The human scenario concerning preexisting antibodies to AAVs is far more complex, as exposure to wild types, particularly AAV2, is common. At 3 years of age, over 20% of children already have NAbs against AAV2.[28] However, we hypothesized humans would not have been exposed to a simian serotype, and would therefore not harbor NAbs against AAVrh.10. With AAVrh.10 and AAV9, we included AAV2 in the study as the most common human serotype, and to compare with other published results. In our sample of 100 healthy human adults from Catalonia, Spain, the seroprevalence of anti-AAV IgG was 72% for anti-AAV2, 47% for anti-AAV9 and a surprising 59% for anti-AAVrh.10, whereas 28% of donors were negative for IgG against any of the viruses (Figure 2a). The results for AAV2 and 9 are highly consistent with the seroprevalences in France,[14] 72% and 47%, respectively. Concerning NAbs, 71% of our serum samples neutralized AAV2, 18% AAV9 and 21% AAVrh.10 at the lowest serum dilution used (1:20; Figure 2b). Hence, many serum samples with anti-AAV9 and anti-AAVrh.10 IgG were nonneutralizing, particularly those low for anti-AAVrh.10 IgG. However, all these sera neutralized AAV2. Other authors also reported a drop between the percentage of donors with anti-AAV IgG and those with neutralizing capacity for the same virus; particularly evident for AAV5, AAV8 and, to a lesser extent, AAV9.[14] We found no effect of sex (Mann–Whitney tests) or age (Spearman correlation) in the results for IgG or NAbs for any of the viruses.

A feasible explanation for our results is that we are witnessing cross-reactivity between serotypes.[14,28] It is noteworthy that the 21 sera which neutralized AAVrh.10 had significantly higher IgG against AAV2 than against AAVrh.10 (paired *t*-test, $P < 0.001$) and consequently, all neutralized AAV2 more strongly than AAVrh.10 (Table 2). In addition, sera neutralizing AAV9 had significantly more IgG against AAV2 than AAV9 (Table 2; paired *t*-test, $P < 0.05$). Note, not all AAVrh.10-positive sera neutralized AAV9 or *vice-versa* and a paired *t*-test on those sera which neutralized both viruses was statistically nonsignificant for both IgG and NAb, though a few sera were very high for anti-AAV9 IgG. To characterize this further, we undertook profiling studies comparing neutralizing capacity for the three viruses over several serum dilutions. Figure 2c shows, in all cases analyzed, AAVrh.10 was never the virus that was most strongly inhibited by NAbs.

These results suggest antibody cross-recognition particularly from antibodies raised against AAV2. Indeed, almost all sera containing anti-AAV2 IgG (98.6%) neutralized this virus, indicating that these are highly specific antibodies, while only 38.3 and 35.6% of the sera containing anti-AAV9 and anti-AAVrh.10 IgG, respectively, were neutralizing (comparing Figures 2a and b). This suggests that the latter are not specific antibodies and could have been raised against AAV2 but recognize epitopes present in the AAVrh.10 capsid *via* homology with other serotypes. However, we cannot discard that our *in vitro* assay has limited sensitivity as previously described[29] and optimized *in vivo* assays are needed to confirm the results.

Along these lines, we highlight recent results from epitope mapping of naturally occurring antibodies to AAV2, 5, 8 and 9 in sheep, showing that animals harbor antibodies to both unique and common capsid epitopes.[25] Interestingly, since the antibodies detected recognized surface and internal or buried-capsid peptides, the authors premise that immunity is raised to intact capsids, as well as, to capsid epitopes revealed after proteolysis. This multiplies the potential repertoire of preexisting antibodies in species where natural infection occurs.

Our results stress several key considerations for AAV vector choice in gene therapy. First, serotypes differ in their propensity to raise antibodies, exemplified by AAVrh.10 being less immunogenic than AAV9 in mice. Second, the vector immune response in mice may not predict the response in humans as seen in our cross-binding studies. Finally, the serological response to an AAV is of much greater breadth in humans, beyond the immune response raised by a single vector administration. This is probably because of multiple, mixed exposure to AAVs during a lifetime, as well as, concomitant molecular evolution of the virus.[15] This combination of factors stimulates a broad repertoire of preexisting antibodies, both neutralizing and nonneutralizing, with differing affinity to capsids of other serotypes. Thus, despite promising results so far, the simian origin of AAVrh.10 does not guarantee safe passage from preexisting antibodies for use in human gene therapy, as there may be cross-reactivity with anti-human AAV antibodies. This is particularly evident for human sero-positivity to AAV2, which might be used as a flag for potential reactivity to other serotypes.

MATERIALS AND METHODS

Injection of mice with AAVs

Antibodies were raised against the capsid of AAV serotypes by injecting 6–8 week-old naive ICR (imprinting control region) male

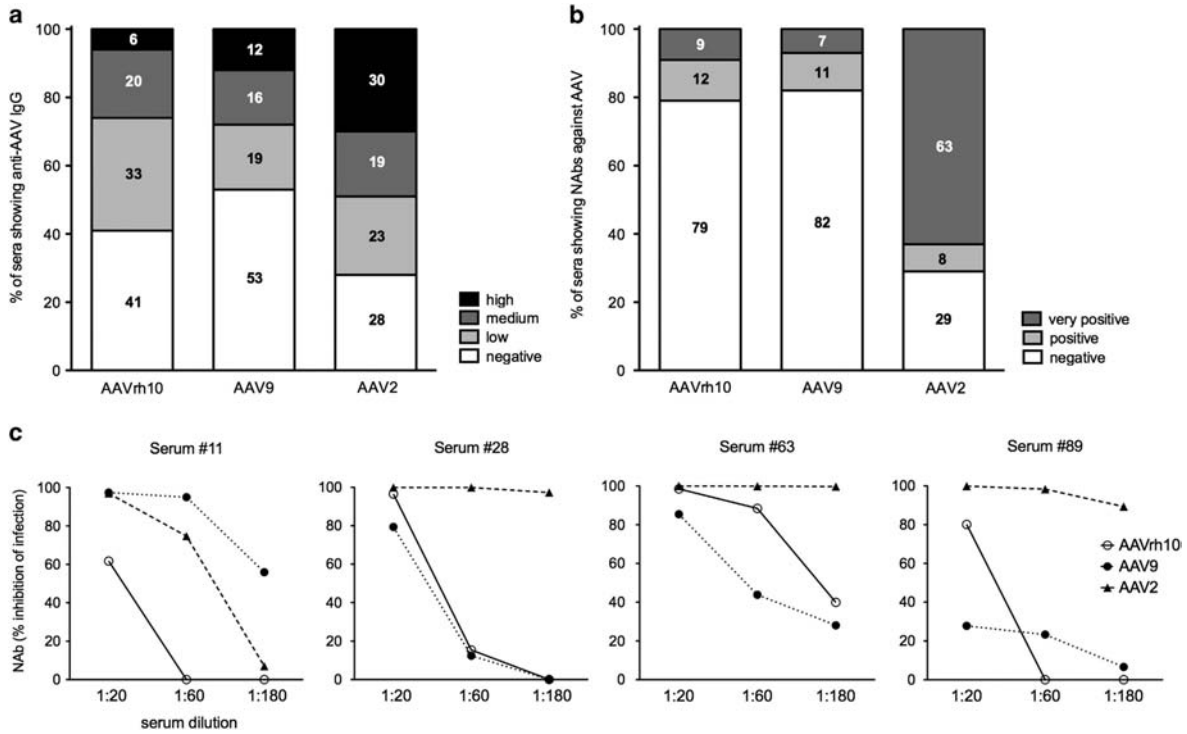

Figure 2. Pre-existing immunity to AAV serotypes rh.10, 9 and 2 in healthy human sera from Catalonia, Spain ($n = 100$). (**a**) Distribution percentage of donors with titers of anti-AAV immunoglobulin G (IgG) determined by indirect enzyme linked immunosorbant assay. Titers classified using optical density (OD) at 450 nm: high (OD > 1.600), medium (OD ⩽ 1.600 and > 1.000), low (OD ⩽ 1.000 to negative cut-off) and negative when OD readings were similarly low over a range of dilutions in duplicate (1:20, 1:60, 1:180). Negative cut-off was the mean OD value for 25 such samples, +3 s.d. (**b**) Distribution percentage of donors with titers of NAbs against each AAV, according to, if serum dilutions of 1:20 inhibited vector transduction by ⩾ 90%, very positive; ⩾ 50 and < 90%, positive; or < 50%, negative. All samples were tested in duplicates using a luciferase reporter. (**c**) Neutralization profiles of sera from four donors (#11, 28, 63 and 89) showing percentage inhibition of adeno-associated virus (AAV) infection of HEK293 cells by the sera at 1:20, 1:60 and 1:180 dilutions in duplicate using a luciferase reporter.

mice intravenously in the tail vein with $1x10^{11}$ vg ml^{-1} of AAV9, AAVrh.10 or AAV2 coding for green fluorescent protein in a total volume of 150 µl, plus one phosphate-buffered saline-injected control. Animals were killed 3 weeks post injection for serum collection. All experimental procedures were approved by the Universitat Autònoma de Barcelona (UAB) Animal Experimentation Committee.

Human serum samples

Serum samples from 100 healthy adult donors were obtained from the Catalan 'Banc de Sang i Teixits' (BST), approved by the Human and Animal Experimentation Ethics Committee (UAB), the Clinical Investigation Ethics Committee at Vall d'Hebron Hospital and the Scientific Committee of the BST Biobank.

AAV vector production

AAV vectors were produced by the Viral Production Unit, UAB (VPU) (http://sct.uab.cat/upv), following standard operating procedures.[30] Briefly, HEK293AAV cells (Stratagene, Carlsbad, CA, USA) were co-transfected with pXX6 providing helper virus functions; pRep2CapX packaging plasmid expressing the *rep* gene of AAV2 and the *cap* genes of either AAV2, AAV9 or AAVrh.10 (provided by Dr JM Wilson, University of Pennsylvania), and pAAV-ITR containing luciferase or green fluorescent protein as reporter genes driven by the cytomegalovirus (CMV) promoter between AAV2 ITRs. Recombinant vectors were clarified after benzonase treatment (50 U ml^{-1}, Novagen, Madison, WI, USA) and polyethylene glycol (PEG 8000, Sigma, St Louis, MO, USA) precipitation. Viruses were then purified on an iodixanol density gradient (Optiprep, Axis-Shield, Oslo, Norway).[31] Viral genomes per ml (vg ml^{-1}) were quantified by picogreen (Invitrogen, Carlsbad, CA, USA; M Chillon, manuscript submitted). Strictly speaking, recombinant AAVs are classified as pseudotypes, while distinct wild-type AAVs are serotypes. However, for the sake of simplicity we shall use serotype to refer to both recombinant and wild type throughout the text.

Total anti-AAV IgG in human and mouse sera

Indirect enzyme linked immunosorbant assays were set up on the basis of previously published reports.[14,32] Maxisorp microwell plates (Nunc A/S, Roskilde, Denmark) were coated with $1x10^9$ vg per well of virus. For the standard curve (mice only), mouse IgG (Sigma-Aldrich, St Louis, MO, USA) was coated in serial dilutions. Secondary antibodies were conjugated with peroxidase (rabbit anti-human IgG (wholemolecule)-peroxidase (Sigma A8792, Sigma-Aldrich) for humans; and ECL sheep anti-mouse IgG, horseradish peroxidase-linked species-specific whole antibody (GE Healthcare (NA931), Little Chalfont, UK; for mice). Detection was *via* 3,3′,5,5′tetramethylbenzidine (TMB) substrate reagent (BD biosciences, Franklin Lakes, NJ, USA). Absorbance was measured at 450 nm in a Bio-tek power wave reader linked to KC4 software program version 3.3 (BioTek, Winooski, VT, USA).

Results were expressed as OD readings related to serum dilutions (humans), or as total IgG anti-AAV in µg ml^{-1} for mice. For humans, individuals were considered negative for IgG antibodies against the AAV of interest when OD readings were similarly low over a range of dilutions (1:20, 1:60, 1:180). A cut-off OD for negative samples was determined, taking the mean OD value for a minimum of 25 such samples, +3 s.d. (cut-off

Table 2. Co-prevalence of neutralizing antibodies to AAVs rh.10, 9 and 2 and their abundance (optical density in enzyme linked immunosorbant assay) for the 21 human serum samples (from $n = 100$) neutralizing AAVrh.10

Human serum #	*Neutralizes AAVrh.10*	*% Inhibition of AAVrh10*[a]	*Anti-AAVrh. 10 IgG*[a]	*Neutralizes AAV9*	*% Inhibition of AAV9*[b]	*Anti-AAV9 IgG*[b]	*Neutralizes AAV2*	*% Inhibition of AAV2*[c]	*Anti-AAV2 IgG*[c]
1	Pos	75	1.013 ± 0.020	Pos	56	0.896 ± 0.045	V pos	98	1.896 ± 0.030
11	Pos	62	1.116 ± 0.059	V pos	97	2.011 ± 0.004	V pos	97	1.138 ± 0.065
15	V pos	98	1.535 ± 0.008	V pos	99	1.918 ± 0.011	V pos	98	1.881 ± 0.005
16	Pos	78	0.904 ± 0.011	Neg	< 50	0.534 ± 0.054	V pos	100	1.406 ± 0.009
25	Pos	89	1.122 ± 0.024	Neg	< 50	0.676 ± 0.010	V pos	98	1.830 ± 0.022
26	V pos	98	1.847 ± 0.147	V pos	99	1.885 ± 0.086	V pos	100	1.728 ± 0.098
28	V pos	97	1.452 ± 0.033	Pos	79	1.236 ± 0.030	V pos	100	1.812 ± 0.001
29	Pos	63	1.027 ± 0.028	Neg	< 50	0.512 ± 0.006	V pos	100	1.822 ± 0.023
32	Pos	74	1.030 ± 0.023	Neg	< 50	0.420 ± 0.011	V pos	100	1.773 ± 0.018
39	Pos	87	1.191 ± 0.046	Neg	< 50	0.871 ± 0.047	V pos	98	1.976 ± 0.028
53	V pos	97	1.157 ± 0.023	V pos	95	1.698 ± 0.066	V pos	100	2.016 ± 0.018
54	Pos	58	0.828 ± 0.001	Pos	57	1.035 ± 0.004	V pos	100	1.494 ± 0.044
63	V pos	99	1.888 ± 0.028	Pos	85	1.485 ± 0.001	V pos	100	1.942 ± 0.078
65	Pos	88	1.562 ± 0.045	V pos	99	2.318 ± 0.178	V pos	95	1.494 ± 0.045
67	V pos	98	1.652 ± 0.092	V pos	97	1.009 ± 0.115	V pos	100	2.016 ± 0.059
69	Pos	65	1.264 ± 0.021	Pos	70	0.587 ± 0.008	V pos	100	1.567 ± 0.040
76	V pos	97	1.361 ± 0.037	Neg	< 50	0.315 ± 0.011	V pos	100	1.905 ± 0.136
87	V pos	98	1.365 ± 0.033	V pos	96	1.419 ± 0.022	V pos	98	2.075 ± 0.009
89	Pos	80	1.680 ± 0.030	Neg	< 50	0.450 ± 0.001	V pos	100	1.562 ± 0.009
94	Pos	77	1.261 ± 0.016	Pos	59	0.563 ± 0.054	V pos	98	1.962 ± 0.014
99	V pos	97	1.603 ± 0.020	Pos	57	1.459 ± 0.045	V pos	98	1.982 ± 0.003
33 (control)	Neg		0.179 ± 0.001	Neg		0.218 ± 0.004	V pos		1.375 ± 0.050
20 (baseline)	Neg		0.160 ± 0.006	Neg		0.101 ± 0.001	Neg		0.161 ± 0.018

Abbreviations: v pos = very positive > 90% inhibition of transduction, pos = positive 50–90% inhibition, neg = negative < 50% inhibition. Results are means of duplicates ± s.e.m. Neutralization assays at 1:20 dilution. Paired *t*-test for equivalence of means: [a]$P < 0.001$ anti-AAVrh.10 versus anti-AAV2, [b]$P > 0.05$ anti-AAVrh.10 versus anti-AAV9 (positive samples only), [c]$P < 0.05$ anti-AAV9 (positive samples only) versus anti-AAV2.

AAVrh.10 = 0.575, AAV9 = 0.665 and AAV2 = 0.471). IgG titer based on the OD was established as: high = OD > 1.600, med = OD ⩽ 1.600 and > 1.000, and low = ⩽1.000 to the cut-off (See Supplementary Figure 2 for examples).

Anti-AAV IgG cross-binding to different viral capsids

We performed enzyme linked immunosorbant assays, as described above, using sera from AAV9, AAVrh.10 and AAV2-intravenously injected mice (four animals per group) and naive serum as a control. Sera were tested in duplicate for antibodies to the capsid of the injected virus and to the uninjected AAV9, AAVrh.10 and/or AAV2 capsid, as appropriate. OD reading at 450 nm was considered as 100% binding (maximum OD) for sera containing IgG binding to the same AAV capsid that the antibodies were raised against. OD readings for binding to other capsids were expressed as a percentage of the maximum OD signal. ODs for naive serum were consistently negligible for all capsids that were tested.

AAV neutralizing assays

Serum from heat-inactivated human serum samples or mouse sera (non-heat inactivated) was serially diluted with infection medium (Dulbecco's modified Eagle's medium+2% f*etal bovine serum*+1% PenStrep, PAA; (GE Healthcare, Buckinghamshire, UK)), incubated for 30 min at 37 °C with virus to then infect HEK293QB cells (QBiogene, Lachine, QC, Canada; 20,000 cells/well) at $1x10^9$ vg per well for AAV9 and AAVrh.10, and $2x10^7$ vg per well for AAV2 to achieve similar transduction as determined by titration. Vector-transgene expression was quantified after 48 h, lysing the cells according to manufacturer's instructions (Pierce Firefly Luciferase Flash Assay kit (ThermoFisher Scientific, Waltham, MA, USA)). Luminescence was read in VICTOR3 (PerkinElmer, Waltham, MA, USA). Transduction efficiency was expressed as luminescence, normalized by amount of protein per well (Pierce BCA Protein Assay kit, (ThermoFisher Scientific)), giving final values of luminescence per µg protein. Serum samples were considered positive for NAbs if they inhibited reporter gene expression by > 50% compared with the maximum signal (average of three maximum values for negative sera, considered 100% transduction). If inhibition was > 90% the serum was considered very positive.

Statistical analysis

Data analysis was performed with IBM SPSS statistics software (Armonk, NY, USA). Values are expressed as mean ± s.e.m. Differences between mean values were compared using two-tailed *t*-tests and one tailed paired *t*-tests, with $P < 0.05$ considered statistically significant.

CONFLICT OF INTEREST

The authors declare no conflict of interest.

ACKNOWLEDGEMENTS

We thank the Vector Production Unit at CBATEG (Universitat Autònoma de Barcelona) for producing AAV vectors, the LLEB (UAB) for the luminescence measurements, Dr James M. Wilson (University of Pennsylvania) for providing AAV9 and AAVrh.10 RepCap plasmids and Dr Lorena Ariza (CBATEG, UAB) for experimental advice. We are also grateful to the Catalan Banc de Sang i Teixits (BST) for the human samples. GP was recipient of predoctoral fellowship from the Generalitat de Catalunya (2009FI_B00219). This work was supported by the Generalitat de Catalunya (2014 SGR 1354), the Instituto de Salud Carlos III (PS09720) and the Marató TV3 (110432) to AB.

REFERENCES

1 Mingozzi F, High KA. Immune responses to AAV vectors: overcoming barriers to successful gene therapy. *Blood* 2013; **122**: 23–36.
2 Calcedo R, Wilson JM. Humoral immune response to AAV. *Front Immunol* 2013; **4**: 341.
3 Mays LE, Vandenberghe LH, Xiao R, Bell P, Nam HJ, Agbandje-McKenna M *et al.* Adeno-associated virus capsid structure drives CD4-dependent CD8+ T cell response to vector encoded proteins. *J Immunol* 2009; **182**: 6051–6060.

4 Ciesielska A, Hadaczek P, Mittermeyer G, Zhou S, Wright JF, Bankiewicz KS *et al.* Cerebral infusion of AAV9 vector-encoding non-self proteins can elicit cell-mediated immune responses. *Mol Ther* 2013; **21**: 158–166.
5 Samaranch L, San Sebastian W, Kells AP, Salegio EA, Heller G, Bringas JR *et al.* AAV9-mediated expression of a non-self protein in nonhuman primate central nervous system triggers widespread neuroinflammation driven by antigen-presenting cell transduction. *Mol Ther* 2014; **22**: 329–337.
6 Grieger JC, Samulski RJ. Adeno-associated virus vectorology, manufacturing, and clinical applications. *Methods Enzymol* 2012; **507**: 229–254.
7 Gao G, Alvira MR, Somanathan S, Lu Y, Vandenberghe LH, Rux JJ *et al.* Adeno-associated viruses undergo substantial evolution in primates during natural infections. *Proc Natl Acad Sci USA* 2003; **100**: 6081–6086.
8 Sondhi D, Hackett NR, Peterson DA, Stratton J, Baad M, Travis KM *et al.* Enhanced survival of the LINCL mouse following CLN2 gene transfer using the rh.10 rhesus macaque-derived adeno-associated virus vector. *Mol Ther* 2007; **15**: 481–491.
9 Piguet F, Sondhi D, Piraud M, Fouquet F, Hackett NR, Ahouansou O *et al.* Correction of brain oligodendrocytes by AAVrh.10 intracerebral gene therapy in metachromatic leukodystrophy mice. *Hum Gene Ther* 2012; **23**: 903–914.
10 Homs J, Pages G, Ariza L, Casas C, Chillon M, Navarro X *et al.* Intrathecal administration of IGF-I by AAVrh10 improves sensory and motor deficits in a mouse model of diabetic neuropathy. *Mol Ther Method Clin Dev* 2014; **1**: 7.
11 Wang H, Yang B, Qiu L, Yang C, Kramer J, Su Q *et al.* Widespread spinal cord transduction by intrathecal injection of rAAV delivers efficacious RNAi therapy for amyotrophic lateral sclerosis. *Hum Mol Genet* 2014; **23**: 668–681.
12 Tardieu M, Zerah M, Husson B, de Bournonville S, Deiva K, Adamsbaum C *et al.* Intracerebral administration of adeno-associated viral vector serotype rh.10 carrying human SGSH and SUMF1 cDNAs in children with mucopolysaccharidosis type IIIA disease: results of a phase I/II trial. *Hum Gene Ther* 2014; **25**: 506–516.
13 Perdomini M, Belbellaa B, Monassier L, Reutenauer L, Messaddeq N, Cartier N *et al.* Prevention and reversal of severe mitochondrial cardiomyopathy by gene therapy in a mouse model of Friedreich's ataxia. *Nat Med* 2014; **20**: 542–547.
14 Boutin S, Monteilhet V, Veron P, Leborgne C, Benveniste O, Montus MF *et al.* Prevalence of serum IgG and neutralizing factors against adeno-associated virus (AAV) types 1, 2, 5, 6, 8, and 9 in the healthy population: implications for gene therapy using AAV vectors. *Hum Gene Ther* 2010; **21**: 704–712.
15 Calcedo R, Vandenberghe LH, Gao G, Lin J, Wilson JM. Worldwide epidemiology of neutralizing antibodies to adeno-associated viruses. *J Infect Dis* 2009; **199**: 381–390.
16 Homs J, Ariza L, Pages G, Udina E, Navarro X, Chillon M *et al.* Schwann cell targeting via intrasciatic injection of AAV8 as gene therapy strategy for peripheral nerve regeneration. *Gene Ther* 2011; **18**: 622–630.
17 Foust KD, Nurre E, Montgomery CL, Hernandez A, Chan CM, Kaspar BK. Intravascular AAV9 preferentially targets neonatal neurons and adult astrocytes. *Nat Biotechnol* 2009; **27**: 59–65.
18 Duque S, Joussemet B, Riviere C, Marais T, Dubreil L, Douar AM *et al.* Intravenous administration of self-complementary AAV9 enables transgene delivery to adult motor neurons. *Mol Ther* 2009; **17**: 1187–1196.
19 Lieberman R, Stiffel C, Asofsky R, Mouton D, Biozzi G, Benacerraf B. Genetic factors controlling anti-sheep erythrocyte antibody response and immunoglobulin synthesis in backcross and F2 progeny of mice genetically selected for 'high' or 'low' antibody synthesis. *J Exp Med* 1972; **136**: 790–798.
20 Chiuchiolo MJ, Kaminsky SM, Sondhi D, Hackett NR, Rosenberg JB, Frenk EZ *et al.* Intrapleural administration of an AAVrh.10 vector coding for human alpha1-antitrypsin for the treatment of alpha1-antitrypsin deficiency. *Human gene therapy. Clin Dev* 2013; **24**: 161–173.
21 Gray SJ, Nagabhushan Kalburgi S, McCown TJ, Jude Samulski R. Global CNS gene delivery and evasion of anti-AAV-neutralizing antibodies by intrathecal AAV administration in non-human primates. *Gene Ther* 2013; **20**: 450–459.
22 Samaranch L, Salegio EA, San Sebastian W, Kells AP, Foust KD, Bringas JR *et al.* Adeno-associated virus serotype 9 transduction in the central nervous system of nonhuman primates. *Hum Gene Ther* 2012; **23**: 382–389.
23 Riviere C, Danos O, Douar AM. Long-term expression and repeated administration of AAV type 1, 2 and 5 vectors in skeletal muscle of immunocompetent adult mice. *Gene Ther* 2006; **13**: 1300–1308.
24 Gurda BL, DiMattia MA, Miller EB, Bennett A, McKenna R, Weichert WS *et al.* Capsid antibodies to different adeno-associated virus serotypes bind common regions. *J Virol* 2013; **87**: 9111–9124.
25 Tellez J, Van Vliet K, Tseng YS, Finn JD, Tschernia N, Almeida-Porada G *et al.* Characterization of naturally-occurring humoral immunity to AAV in sheep. *PLoS One* 2013; **8**: e75142.
26 Bartel M, Schaffer D, Buning H. Enhancing the clinical potential of AAV vectors by capsid engineering to evade pre-existing immunity. *Front Microbiol* 2011; **2**: 204.
27 Louis Jeune V, Joergensen JA, Hajjar RJ, Weber T. Pre-existing anti-adeno-associated virus antibodies as a challenge in AAV gene therapy. *Hum Gene Ther Methods* 2013; **24**: 59–67.
28 Calcedo R, Morizono H, Wang L, McCarter R, He J, Jones D *et al.* Adeno-associated virus antibody profiles in newborns, children, and adolescents. *Clin Vaccine Immunol* 2011; **18**: 1586–1588.
29 Wang L, Calcedo R, Wang H, Bell P, Grant R, Vandenberghe LH *et al.* The pleiotropic effects of natural AAV infections on liver-directed gene transfer in macaques. *Mol Ther* 2010; **18**: 126–134.
30 Zolotukhin S. Production of recombinant adeno-associated virus vectors. *Hum Gene Ther* 2005; **16**: 551–557.
31 Zolotukhin S, Byrne BJ, Mason E, Zolotukhin I, Potter M, Chesnut K *et al.* Recombinant adeno-associated virus purification using novel methods improves infectious titer and yield. *Gene Ther* 1999; **6**: 973–985.
32 Treleaven CM, Tamsett TJ, Bu J, Fidler JA, Sardi SP, Hurlbut GD *et al.* Gene transfer to the CNS is efficacious in immune-primed mice harboring physiologically relevant titers of anti-AAV antibodies. *Mol Ther* 2012; **20**: 1713–1723.

Supplementary Information accompanies this paper on Gene Therapy website (http://www.nature.com/gt)